UNIVERSITY OF CRETE
DEPARTMENT OF MATERIALS
SCIENCE AND TECHNOLOGY

pH-responsive Microgels: Polyelectrolyte, Homopolymer and Polyampholyte Mix and Core-Shell Particles

Master Thesis of
Konstantinos Emm. Christodoulakis

Supervisor:
Assistant Professor Maria Vamvakaki

FOUNDATION FOR RESEARCH AND TECHNOLOGY-HELLAS
INSTITUTE OF ELECTRONIC STRUCTURE AND LASER

HERAKLION, OCTOBER 2008

Περίληψη

Σκοπός της εργασίας μας είναι η σύνθεση και ο χαρακτηρισμός μικροπηκτωμάτων που αποκρίνονται σε μεταβολές του pH. Στην παρούσα εργασία συνθέσαμε μικροπηκτώματα που βασίζονται στο μεθακρυλικό 2-(διαιθυλαμινο)αιθυλεστέρα (DEA) ή στο μεθακρυλικό οξύ (MAA) χρησιμοποιώντας τη μέθοδο πολυμερισμού γαλακτώματος. Η στερική σταθεροποίηση των σωματιδίων επιτεύχθηκε με τη χρήση του μεθακρυλικού εστέρα της πολυ(αιθυλενογλυκόλης) ως σταθεροποιητή. Τα μικροπηκτώματα του PMAA συντέθηκαν χρησιμοποιώντας τον υδρόφοβο μεθακρυλικό *tert*-βουτυλεστέρα (*t*-BuMA) ως μονομερές. Μετά τη σύνθεση, τα μικροπηκτώματα του P(*t*-BuMA) αποπροστατεύτηκαν, με όξινη υδρόλυση, δίνοντας τα μικροπηκτώματα του PMAA. Τα παραπάνω μικροπηκτώματα διογκώνονται αντιστρεπτά στο νερό με απλή ρύθμιση του pH του διαλύματος ή του βαθμού ιοντισμού των μονάδων του μονομερούς. Συγκεκριμένα, τα μικροπηκτώματα του PDEA διογκώνονται σε χαμηλές τιμές pH, λόγω του ιοντισμού των αμινομάδων του DEA, ενώ με αύξηση του pH οι αμινομάδες αποφορτίζονται και το σωματίδιο γίνεται υδρόφοβο και συρρικνώνεται. Αντίστοιχα, τα μικροπηκτώματα του PMAA διογκώνονται σε υψηλές τιμές pH λόγω του ιοντισμού των καρβοξυλομάδων ενώ σε χαμηλές τιμές pH οι όξινες ομάδες αποφορτίζονται και τα μικροπηκτώματα συρρικνώνονται. Οι πειραματικές σταθερές διάστασης, pK_a, των μικροπηκτωμάτων υπολογίστηκαν από τις καμπύλες τιτλοδότησης των μικροπηκτωμάτων.Η επίδραση του pH στο μέγεθος των σωματιδίων μελετήθηκε με δυναμική σκέδαση φωτός σαν συνάρτηση του βαθμού ιοντισμού των μονάδων του μονομερούς. Επίσης εξετάστηκε η επίδραση του βαθμού διασταύρωσης στο βαθμό διόγκωσης των μικροπηκτωμάτων του PDEA. Πειράματα ηλεκτρονικής μικροσκοπίας σάρωσης και διέλευσης (SEM και TEM) επιβεβαίωσαν το σφαιρικό σχήμα και την ομοιογένεια στο μέγεθος των σωματιδίων.

Στη συνέχεια της εργασίας συντέθηκαν μικτά μικροπηκτώματα με τα δύο μονομερή (DEA και MAA) τυχαία κατανεμημένα μέσα στο σωματίδιο. Από την καμπύλη τιτλοδότησης προσδιορίστηκε το εύρος ιοντισμού των σωματιδίων. Με δυναμική σκέδαση φωτός μελετήθηκε το μέγεθος των μικροπηκτωμάτων ως συνάρτηση του βαθμού ιοντισμού των δομικών μονάδων. Βρέθηκε ότι τα μικτά αυτά μικροπηκτώματα διογκώνονται σε χαμηλά και υψηλά pH όταν τα σωματίδια είναι θετικά ή αρνητικά φορτισμένα ενώ στο ισοηλεκτρικό σημείο όπου το συνολικό φορτίο

των σωματιδίων είναι ίσο με μηδέν κυριαρχούν οι υδρόφοβες αλληλεπιδράσεις και τα σωματίδια συρρικνώνονται.

Τέλος, συνθέσαμε μικροπηκτώματα με τοπολογία πυρήνα-φλοιού (core-shell). Συντέθηκαν σωματίδια με πυρήνα PDEA και φλοιό PMAA και σωματίδια με πυρήνα PMAA και φλοιό PDEA. Από τις καμπύλες τιτλοδότησης βρέθηκε ότι ο πυρήνας και ο φλοιός των μικροπηκτωμάτων ιοντίζονται χωριστά σε διαφορετικές περιοχές pH, σε αντίθεση με τα μικτά μικροπηκτώματα που συζητήθηκαν παραπάνω. Η διόγκωση των σωματιδίων σαν συνάρτηση του pH του διαλύματος εξετάστηκε με δυναμική σκέδαση φωτός. Ο αντιστρεπτός ιοντισμός του πυρήνα και του φλοιού των σωματιδίων σε διαφορετικές τιμές pH οδηγεί σε σωματίδια στα οποία μπορούμε να μεταβάλουμε ξεχωριστά το μέγεθος, το φορτίο και την υδροφιλικότητα του πυρήνα και του φλοιού των μικροπηκτωμάτων. Το σφαιρικό σχήμα των σωματιδίων και η ομοιόμορφη κατανομή μεγέθους παρατηρήθηκε με SEM ενώ το TEM επιβεβαίωσε την τοπολογία πυρήνα-φλοιού μετά από επιλεκτική χρώση του πυρήνα ή του φλοιού των μικροπηκτωμάτων.

Τα παραπάνω μικροπηκτώματα είναι ενδιαφέροντα υλικά και μπορούν να βρουν πληθώρα εφαρμογών όπως στην ελεγχόμενη δέσμευση, μεταφορά και αποδέσμευση δραστικών ουσιών, στην γονιδιακή θεραπεία, κτλ.

Abstract

The aim of this study is the synthesis and characterization of pH-responsive microgel particles. We have synthesized pH-responsive homopolymer microgel particles based on 2-(diethylamino)ethyl methacrylate (DEA) or methacrylic acid (MAA) using emulsion polymerization. Ethylene glycol dimethacrylate (EGDMA) was used as the cross-linker. Steric stabilization of the microgel particles was achieved using poly(ethylene glycol methacrylate) (M_n=2000 gr/mole) as the stabilizer. PMAA-based microgel particles were prepared using *tert*-butyl methacrylate (*t*-BuMA) as the protected form of MAA. Next, the P(*t*-BuMA)-based microgels were hydrolyzed to convert the *t*-BuMA segments into MAA units via acid hydrolysis. The above microgels exhibit reversible swelling properties in water by adjusting the solution pH or the degree of ionization of the monomer units. Thus, the PDEA-based microgel particles, swell at low pH upon ionization of the DEA units due to the hydrophilicity of the protonated amine groups, while an increase of the solution pH leads to the deprotonation of the DEA moieties and the formation of hydrophobic latex particles. The PMAA-based microgel particles swell at high pH due to the ionization of the carboxylic acid units, while at low pH values the acidic moieties become neutral and the particles shrink. The effective equilibrium constants pK_α's of the PDEA and PMAA microgel particles were calculated from potentiometric titration curves of the microgel dispersions. The pH-responsive character of the microgel particles and its effect on the particle size of the microgels was examined by dynamic light scattering (DLS) as a function of the degree of ionization of the monomer units. The effect of the cross-link density on the degree of swelling of the PDEA microgels was also investigated. Scanning and Transmission Electron Microscopy studies verified the spherical shape and the uniform size distribution of the particles.

In the second part of our study mixed polyampholyte microgel particles comprising both DEA and MAA units randomly distributed within the particle have been prepared. Potentiometric titrations were used to determine the ionization range of the microgels. The size of the mixed microgels particles as a function of the degree of ionization of the monomer units was studied by DLS. The microgels swell at both high and low pH when the particle net charge is negative or positive, respectively, while collapsed microgel particles were found at the isoelectric point at zero net charge when the hydrophobic interactions dominate.

Finally, we have synthesized microgel particles with a core-shell topology comprising either a PDEA core and a PMAA shell or a PMAA core and a PDEA shell. Potentiometric titration curves revealed the independent ionization range of the core and the shell of the particles, in contrast to the mixed polyampholyte microgel particles discussed above which exhibit a common ionization region for the basic and acidic monomer units. The swelling properties of the microgel particles as a function of the solution pH were examined by DLS. The core and the shell of the particles were found to swell at a different pH range resulting in microgel particles in which the overall size, the net charge, the softness and the hydrophylicity of the core and the shell can be tuned independantly. SEM showed spherical particles of a narrow size distribution, while TEM verified their core-shell topology by selectively staining the core or the shell of the microgels.

These core-shell microgels carrying different responsive functionalities in the core and the shell of the particle are very attractive materials for use in numerous applications such as targeted drug-delivery, chemical separations, etc.

Contents

Chapter 1

1.1 Introduction

1.1.1 Microgel particles

A microgel is a chemically cross-linked polymer network in the form of a colloidal particle stabilized in a continuous medium. The size of the particle is below 1 μm and usually varies from 100 to 700 nm. Responsive microgels typically comprise lightly cross-linked latex particles of submicrometer dimensions that can become highly swollen in response to a certain external stimuli (**Figure 1.1**). These materials have attracted particular attention because of their potential applications in various fields such as drug delivery,[1,2] biotechnology,[3-13] bioseperation,[14] catalysis[15,16] and microelectronics.[17-19]

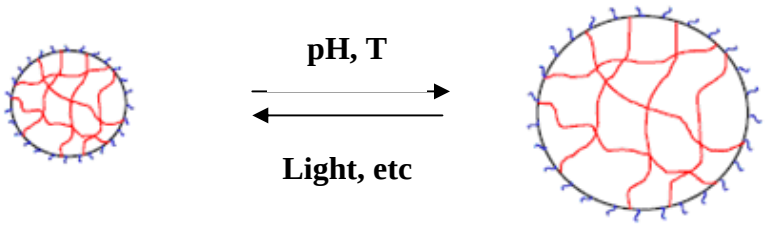

Figure 1.1: Shematic representation of the swelling-deswelling process of responsive microgels.

Photo, thermo and pH-responsive microgels have been reported in the literature.[20-27] Photo-responsive microgels were prepared[28] by precipitation polymerization of the thermo-responsive monomer N-isopropylacrylamide (NIPAM) followed by convalent conjugation of the temperature-jump dye malachite green. The photo-responsivity of the dye-lebeled microgels was characterized by a pump-probe optical setup. A HeNe laser was used to excite the dye molecules, while a near-IR-

diode laser was used to simultaneously measure the turbidity of the colloidal dispersion. Irradiation of malachite green increased the temperature of the sample through rapid nonradiative decay, thereby causing the polymer chains to aggregate. On deswelling, a decrease in the intensity of transmitted light was observed due to scattering. It was found that the photo-responsive behaviour of the microgels depended on the concentration of the dye, the intensity of the laser and the bath temperature.

One type of microgel particles that has attracted particular academic interest due to their thermosensitivity are those based on PNIPAM.[29,30] Above the lower critical solution temperature of PNIPAM, (LCST ~ 32^{o} C) these lightly cross-linked PNIPAM particles exist in their nonsolvated latex-like form, while for temperatures below the LCST the particles become hydrophilic and thus water-swollen microgels comprising chains held together by permanent cross-links are obtained.

Such PNIPAM microgels with spherical voids were prepared using a microfluidic device.[31] The swelling and shrinking response of these microgels when changing the solution temperature were compared to those of voidless microgels of the same size and chemical composition prepared using the same microfluidic device. It was shown that the PNIPAM microgels with the voids respond faster to changes of the temperature as compared to their voidless counterparts. However, the voids did not have a detrimental effect on the equilibrium volume change of the microgels. Thus the kinetics of the volume phase transition of the microgels could be finely tuned by controlling the number and size of the voids.

A series of PNIPAM microgels were also prepared, by a surfactant-free emulsion polymerization method, in which the concentration of the cross-linker was varied between 0.25 – 30 wt % with respect to the monomer.[32] Turbidimetry, light scattering and differential scanning calorimetry (DSC) analyses of aqueous dispersions of these microgels showed that the temperature and the half-width of the overall volume phase transition (VPT) of the colloidal dispersions increased with increasing the concentration of the cross-linker. DSC analysis also revealed a decrease in the overall calorimetric enthalpy of the VPTs with increasing cross-linker concentration. The DSC thermograms were deconvoluted into two component transitions: one was asymmetric and was attributed to the aggregation of the "free" NIPAM monomers/oligomers and the second, a two-state conformational transition, was associated with the cross-linked microgels. Pulsed-gradient spin-echo NMR diffusion

measurements showed that the diffusion rate of water within the particles decreased with increasing cross-link density. Complementary fluorescence studies showed an increase in the hydrophobicity of the particles as the cross-link density increased.

1.1.2 pH-responsive microgel particles

pH-responsive microgels usually consist of either acidic or basic monomer units and in some cases hydrophobic comonomers are also incorporated. Until now, the fraction of pH-responsive moieties within the gel phase was limited to a few percent and thus the microgel particles exhibited a weak pH-responsive behavior. There are only few examples in the literature on the preparation of pH-responsive microgels based solely on pH-sensitive monomers.

The synthesis of acid-swellable microgel particles based on poly((2-diethylamino)ethyl methacrylate) (PDEA) has been reported.[33,34] Reversible swelling occurred, with the swollen microgel particles obtained at low pH due to the protonation of the tertiary amine groups. The critical pH for this latex-to-microgel transition was found between pH 6 and 7, which is in good agreement with the known pK_a ~ 7 for linear PDEA homopolymers.

Lightly cross-linked microgel particles based on 2-vinylpyridine (2VP) have been also synthesized by emulsion polymerization.[35] Steric stabilization was achieved using a monomethoxy-capped poly((ethylene glycol) methacrylate) (PEGMA) stabilizer. Scanning electron microscopy studies confirmed near-monodispersed spherical morphologies, with mean weight-average particle diameters ranging from 370 to 970 nm depending on the initiator, polymeric stabilizer and surfactant concentration. These lightly cross-linked latexes acquired cationic microgel character at low pH. The critical pH for this latex-to-microgel transition was around pH 4 at 1 wt % cross-linker, which is significantly lower than the pK_a of 4.9 estimated for linear P2VP homopolymer. ^{1}H NMR and aqueous electrophoresis studies indicated that substantial swelling occurred at low pH due to the protonation of the 2VP groups, while dynamic light scattering (DLS) measurements showed volumetric swelling ratios of up to 3 orders of magnitude, depending on the initial latex diameter. Systematic variation of the degree of cross-linking led to a monotonic decrease in the pK_α values and the critical swelling pH of the P2VP latexes.

In another study Dupin et. al. studied the kinetics of swelling of lightly cross-linked P2VP latexes with mean diameters ranging from 380 to 1010 nm as a function of solution pH.[36] These pH-responsive particles became substantially protonated at around pH 4, which led to a rapid latex-to-microgel transition within a time scale of tens of milliseconds. The characteristic swelling time correlated linearly with the mean particle diameter, as predicted by the Tanaka equation.

Recently, Dupin et. al. reported the synthesis of P2VP-based microgels via emulsion polymerization using a styrene-functionalized poly((2-dimethylamino) methacrylate) (PDMA) macromonomer as a reactive steric stabilizer.[37] The solution pH was shown to be a critical parameter for the successful syntheses of stable latexes with minimal coagulum taking place only at neutral pH. The size of the particles was 280 nm in diameter. DLS and electrophoretic studies indicated that these PDMA-P2VP particles exist in three states depending on the solution pH: swollen cationic microgels were obtained below pH 4.1, nonsolvated latex particles with cationic stabilizer layer were obtained at intermediate pH and flocculated latex particles with neutral PDMA stabilizer chains were obtained at around pH 8.5. Finally, these PDMA-P2VP latexes were shown to be superior Pickering emulsifiers for stabilizing water-in-1-undecanol emulsions compared to either poly(ethylene glycol)-stabilized P2VP latexes or charge-stabilized P2VP latexes. This study illustrated the important role of the steric stabilizer in determining particle wettability.

1.1.3 Multi-responsive and polyampholyte microgel particles

The systems described above consist of one type of monomer units and thus respond to a single stimulus (e.g. light, temperature or pH). However, even more complex microgel particles comprising two different monomers each responding to a different stimulus have been also prepared. Pelton et. al. reported the synthesis of microgels carrying temperature-responsive NIPAM groups and pH-responsive vinylacetic acid (VAA) moieties.[38] These microgel particles were shown to exhibit novel swelling properties compared to their analogues comprising acrylic acid (AA) or methacrylic acid (MAA) groups. They were ionized over a narrow pH range and ionization induced a much larger swelling response in these microgels which swelled three times more than either the AA-NIPAM or MAA-NIPAM microgel particles. The VAA-NIPAM microgels also displayed a sharp, PNIPAM-like thermal deswelling profile when protonated while, upon ionization, they did not undergo a thermal volume

phase transition up to at least 70 °C. The highly responsive character and the tunable ionization and swelling profiles observed for the VAA-NIPAM microgels were attributed to the tendency of VAA to act as a chain transfer agent, resulting in the incorporation of a large number of VAA units randomly distributed on the highly mobile chain ends or near the microgel surface.

In another study, the preparation of spherical phosphor europium-doped yttrium oxide (Y_2O_3:Eu) particles from a PNIPAM-*co*-PAA copolymer was described.[39] The resulting phosphor particles had smaller particle diameters (< 0.1 μm) compared to both the commercial Y_2O_3:Eu phosphors and the spherical particles synthesized by the urea precipitation method. Cathodoluminescent (CL) measurements demonstrated that an exceptional light output can be achieved from the particles with diameters smaller than 0.1 μm. The luminescent properties of the phosphors synthesized using the copolymer microgel were shown to be at least comparable to those of commercial products at lower voltages; however, they offer the distinct advantage of a higher packing density and therefore have higher resolution for field emission display (FED) and cathode ray tube (CRT) applications.

Recently, dual responsive polyampholytic microgels which consist of both negative and positive charged monomer units have been reported.[40-45] These polyampholyte microgel particles are very interesting materials because they possess dual pH-responsive functionalities of opposite charge and thus can mimic the behavior of proteins. Emulsion copolymerization of methacrylic acid (MAA) and 2-(diethylamino)ethyl methacrylate DEA yielded such pH-responsive polyampholyte microgels with a diameter between 200-300 nm.[40] Poly((ethylene glycol) methacrylate) (PEGMA) was grafted onto the surface of the particles to provide steric stabilization. These microgels showed enhanced hydrophilic behavior in aqueous media at low and high pH, while between pH 4 and 6, they possesed a mobility close to zero, a minimum in their size and a negative second virial coefficient, A_2, due to overall charge neutralization near their isoelectric point. By varying the composition of MAA and DEA in the microgels, it was possible to vary the isoelectric point of the colloidal particles and thus tune their swelling properties.

Recently, Bradley et. al. reported the synthesis of biocompatible, polyampholyte microgel particles.[41] These microgel particles have been prepared by the emulsion copolymerization of DEA and *t*-butyl methacrylate followed by the acid hydrolysis of the *t*-butyl groups to obtain DEA-*co*-MAA microgels. The hydrodynamic

diameter and the electrophoretic mobility of both the initial and the hydrolyzed microgel particles have been investigated as a function of pH for three microgel samples of different comonomer compositions (DEA/MAA = 2, 1 and 0.5 molar ratio). The swelling properties and the isoelectric point of the particles were shown to be depended on their composition. Thus, as the DEA/MAA molar ratio decreased the isoelectric point of the microgels also decreased and the degree of swelling of the microgels at high pH values increased slightly.

Finally, Hampton et. al. prepared monodisperse polyampholyte latexes containing 25/23 and 29/18 mole % styrylmethyl-(trimethyl)ammonium chloride/MAA,[46] and their precursor cationic quaternary ammonium chloride analogues, by emulsion polymerization of vinylbenzyl chloride (VBC), *tert*-butyl methacrylate (*t*-BuMA), styrene and divinylbenzene followed by the stepwise conversion of the VBC and *t*-BuMA groups to the ammonium salt and the acidic moieties, respectively. Upon the addition of NaCl to the aqueous microgel dispersion, the polyampholyte latexes shrunk for up to 0.5 M NaCl and then swelled again for up to 5 M NaCl, and became colloidally stable. These polyampholyte latexes were also shown to be colloidally stable in 1.2 M $BaCl_2$ solution, in contrast to their cationic quaternary ammonium chloride analogues which coagulated rapidly in both NaCl and $BaCl_2$. This is attributed to the different charge ratio (COO^- / N^+) in the two systems. The polyampholyte latexes always possessed an excess of positive charge and were stable in aqueous solutions up to pH 11.3 with no added electrolyte whereas their cationic quaternary ammonium chloride analogues possessed an excess of positive charge only at neutral pH due to incomplete ionization of the carboxylic acid groups and they coagulated slowly at pH 9.4 and rapidly at pH 9.9, when the particles had little or no net charge.

1.1.4 Core-shell microgel particles

Apart from the polyampholyte and multi-responsive microgel particles described above in which the responsive moieties were randomly distributed within the particle (e.g. PDEA-*co*-PMAA microgel particles) microgel particles with a core-shell topology have been also prepared.[20,29] In these systems the core of the particle consists of one type of monomer units that responds either to the temperature or the pH, while the shell carries moieties that respond to a different external stimulus. These are thus multi-responsive systems with a different responsive character in the core and the shell

of the particle. In order to prepare such core-shell microgel particles a two step polymerization technique is required.[47-51] In the first step the core of the particle is formed and in the second step these core particles are used as the seeds for the synthesis of the shell, thus resulting in a particle with a core-shell topology. This method allows to control both the size and the functionality of the core and the shell of the particles. Until now temperature-responsive core-shell microgel particles have been only reported and there are very few reports on pH-responsive core and temperature-responsive shell particles or vice versa.[52]

Dingenouts et. al. in their study investigated the volume transition in colloidal core-shell particles composed of a non-responsive polystyrene (PS) core and a shell of thermosensitive cross-linked PNIPAM chains by small-angle X-ray scattering (SAXS).[53] The core of the particles had a diameter of 80 nm whereas the shell thickness varied from 32 nm in the swollen state at 25 °C to 18 nm when shrunk following a continuous volume transition. The SAXS intensities measured at high scattering angles were described by a Lorentz-type function at both states. This indicates the presence of liquid-like local concentration fluctuations of the gel which are still present in the shrunk state. The correlation lengths ξ measured at both states were of the order of a few nanometers (25 °C, ξ=3.2 nm, 50 °C, ξ=2.1 nm). This analysis therefore showed that the core-shell microgels behave in a distinctively different manner than ordinary thermosensitive gels: the cross-linked chains in the shell were bound to a solid boundary which was independent of temperature. The spatial constraint by this boundary decreased the maximum degree of swelling at low temperatures but also prevented a full collapse of the network above the volume transition temperature.

In another study, thermoresponsive PNIPAM microgels possessing a hollow structure were synthesized from core-shell nanoparticles upon oxidation of the particle core, followed by the removal of the oxidized polymer segments by centrifugation.[54] N,N'-(1,2-dihydroxyethylene) bisacrylamide (DHEA) was used as the cross-linker for the synthesis of the degradable core, whereas the non degradable N,N'-methylenebis(acrylamide) (BIS) was used as the cross-linker for the formation of the PNIPAM shell. Addition of $NaIO_4$ to a suspension of these particles in water led to the controlled degradation of the particle core by cleavage of the 1,2-glycol DHEA bonds. Fluorescence spectroscopy, UV/Vis spectroscopy and photon correlation spectroscopy were used to characterize the hollow particles produced. Thus, in comparison to the

non-degradable core-shell particles, hollow particles exhibited higher equilibrium swelling volumes below the LCST and greater deswelling ratios at temperatures above the LCST.

Moreover, Li et. al. prepared narrowly distributed spherical core-shell nanogels by a two step aqueous dispersion polymerization.[55] The cores of the particles comprized of temperature-responsive cross-linked PNIPAM chains and were used as nuclei for the subsequent addition of the pH-responsive poly(4-vinylpyridine) (P4VP) shells. The spherical morphology and the structure of the core-shell particles were confirmed by scanning electron microscopy (SEM) and transmission electron microscopy (TEM) and the size distribution was determined by DLS. Temperature and pH-induced phase transitions of the latex particles were also investigated. It was shown that the P4VP shell does not significantly perturb the temperature induced volume phase transition of the parent core whether P4VP is ionized or not, while the deswelling behavior differs significantly from that of other polyelectrolyte gels in which the ionic groups are randomly distributed.

Recently Bradley et. al. reported the use of core-shell microgel particles for the controlled uptake and release of active species.[56] The compatibility of the microgel particles with their environment and the functionality of the particles was achieved by the modification of the core microgel via the addition of a shell. They prepared core-shell microgel particles with a pH-responsive P2VP core and a temperature-responsive PNIPAM shell. The uptake and release of an anionic surfactant from these microgels was investigated as a function of solution pH and temperature. The results indicated that electrostatic attraction between the anionic surfactant and the cationically charged core of the microgel particles dominated the absorption of the surfactant within the core-shell microgel particles.

In another study, Jones et. al. reported the synthesis and characterization of temperature and pH-responsive microgel particles with a core shell morphology.[29] Core particles composing of cross-linked PNIPAM or P(NIPAM-*co*-AA) were synthesized via precipitation polymerization and were used as nuclei for the subsequent polymerization of P(NIPAM-*co*-AA) or PNIPAM, respectively. The core-shell morphology was confirmed by TEM. Thermally induced volume phase transitions were studied as a function of solution pH. The P(NIPAM-*co*-AA) core microgels displayed both a strong temperature and pH dependent swelling. However, the core-shell particles displayed a more complex pH dependence compared to the

homogeneous particles. Thus, a multistep volume phase transition appeared when the AA units became highly charged at high pH. It was also apparent from the measured deswelling curves that to some extend the swelling behavior of the particles was dominated by PNIPAM regardless of its location within the particle. However, a deswelling behavior that was due to the mixture of P(NIPAM-*co*-AA) and PNIPAM was also evident, as well as a regime that was largely attributed to the P(NIPAM-*co*-AA) alone.

Finally, Plunkett et. al. in their study prepared dual pH-responsive core-shell microgels containing both vinyl pyridine and 2-(dimethylamino)ethyl methacrylate (DMA) using an in situ photopolymerization process.[20] Complementary photomasks were utilized to prepare microgel particles with core-shell volume ratios of 2:1, 1:1 and 1:2. Depending on the spatial location of each polymer component, dramatically different swelling profiles were obtained. Selective swelling of the shell followed by the swelling of the core allowed the microgel to expand with the usual kinetics: however, by switching the location of each polymer component and swelling the core first, caused the swelling rates to decrease by over one order of magnitude and were dependent on the volume of the shell.

1.1.5 Emulsion polymerization

An emulsion is a colloidal suspension of one liquid phase in another incompatible liquid.[57] The emulsions can be classified according to their droplet size. Thus for droplet diameters below 100 nm the emulsions known as microemulsions, for droplet diameters between 100 and 500 nm the emulsions are classified as miniemulsions and finally for droplet diameters above 500 nm the emulsions are called macroemulsions.

Emulsions are thermodynamically unstable systems, so an input of energy is required for their formation. This energy may be derived from chemical or mechanical processes. The droplet size dristribution of the resulting emulsion is usually quite broad: such emulsions are said to be polydisperse. Liquid-in-liquid emulsions are unstable with respect to the bulk phases and they separate into these two phases unless this is prevented by some mechanism such as surfactant stabilization. Emulsions that appear stable are in fact metastable.

Monodisperse, spherical polymer latex particles may be formed when water-insoluble monomers are dispersed in water (emulsion) in the presence of an initiator.

When a surfactant such as sodium dodecyl sulfate (SDS) is used, particle nucleation takes place in the monomer-swollen micelles. For surfactant-free emulsion polymerization where no added surfactant is present, other mechanisms have been proposed, including homogenous nucleation,[58,59] nucleation in oligomer micelles,[60] and coagulative nucleation.[61-63]

Emulsion polymerization refers to a unique process employed for some radical chain polymerizations and involves the polymerization of monomers that are in the form of emulsions. Polymerization does not occur to any significant extent within the dispersed monomer droplets since the total droplet area is much smaller than that of the growing micelles/latex particles. The locus of polymerization is almost exclusively to the monomer-swollen micelles, where it has been estimated that 99.9 % of chain growth occurs.

Emulsion polymerization has various advantages compared to bulk or solution polymerization. The aqueous continuous phase has a high heat capacity, which allows efficient removal of the heat generated during the polymerization. High molecular weight polymers are produced at very high monomer conversion and the final latex has low viscosity. In view of these advantages, emulsion polymerization is applied in an industrial scale for the production of emulsion paints, adhesives and sealants.

Most of the monomer in emulsion polymerization is dispersed in the form of monomer droplets. The mean diameter of the monomer droplets is usually not less than 1 μm. Thus in a typical emulsion polymerization the monomer droplets are much larger than the monomer-swollen micelles. Another difference between micelles and monomer droplets is that the micelles have a much greater total surface area. Thus, polymerization takes place almost exclusively in the interior of the monomer-swollen micelles. The micelles act as a meeting place for the monomer and the water-soluble initiator. As the polymerization proceeds, the micelles grow by the transport of the monomer from the aqueous solution whose concentration is replenished by dissolution of monomer from the monomer droplets. An emulsion polymerization usually consists of three types of particles: monomer droplets, inactive micelles in which polymerization is not occurring and active micelles in which polymerization occurs. The latter are no longer considered as micelles but are referred to as growing polymer particles.

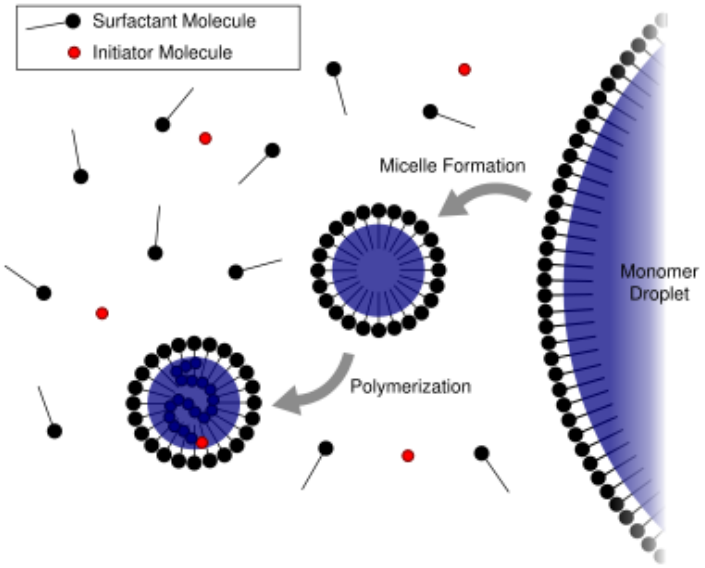

Figure 1.2: Simplified representation of an emulsion polymerization.

The mechanism for the formation of polymer particles proceeds by two simultaneous processes. One is the entry of radicals from the aqueous phase into the micelles (micellar nucleation) and the other (homogeneous nucleation) involves solution-polymerized oligomeric radicals becoming insoluble and co-precipitating to form polymer nuclei. Higher water solubility and low surfactant concentration favor homogeneous nucleation, which is likely to be the primary mechanism of particle formation for a relatively water-soluble monomer.

Emulsion polymerization can be conducted in the presence of a surfactant or under surfactant-free conditions. Anionic surfactants are the most common surfactants. An increase in particle number and a decrease in particle size occurs as the surfactant concentration is increased. Delayed addition of more surfactant after nucleation is complete, can improve the stability of the particles without affecting the particle number, size or size distribution. The presence of a surfactant is a disadvantage for certain applications of emulsion polymers such as those involving instrument calibration and pore size determination. The presence of the absorbed surfactant gives rise to somewhat variable properties since the amount of absorbed surfactant can vary with the polymerization and application conditions. Removal of the surfactant, on the other hand, can lead to coagulation or flocculation of the destabilized latex. Latexes prepared by the surfactant-free technique are stabilized by ionic surface groups such as anionic sulfate groups derived from a persulfate initiator. DEA has higher water-

solubility than most other hydrophobic vinyl monomers, e.g. styrene. Thus, in the case of the emulsion polymerization of DEA, it seems reasonable that, under surfactant-free conditions, homogeneous polymerization occurs initially in the aqueous phase to form DEA oligomers, which then form micelles. These oligomer micelles then act as the locus of polymerization for the vast majority of the DEA monomer.

1.1.5.1 Initiators and particle size in emulsion polymerization

The initiators used in emulsion polymerization have either very high water solubilities or are completely miscible with water. If ionic initiators are used, the appearance of initiator residues at the particle surface gives rise to a surface charge. In the case of the persulfate initiator, anionic latex surfaces are obtained.

The final latex particle size is determined by various factors[64] such as the reaction temperature, monomer type and concentration, initiator type and concentration and the overall ionic strength.

In surfactant-free emulsion polymerization, the number of nuclei initially formed dictates the number of latex particles eventually formed, which hence affects the final particle diameter. The more hydrophobic the monomer, the more nuclei will be formed, since the precipitation of the polymer chains will occur earlier (at lower molecular weight).

1.1.5.2 Colloidal stability

Emulsion polymer particles are often produced in the presence of stabilizer. A stabilizer is usually either a small molecule or a polymer. There are two stabilization mechanisms for latex particles: charge stabilization and steric stabilization.

The so-called steric stabilization mechanism involves absorbed or grafted polymer chains, which are located at the surface of the latex particles. These chains are hydrophilic and well-solvated: collisions between latex particles due to Brownian motion are elastic because inter-mixing of the polymeric stabilizer layers is unfavourable on both enthalpic and entropic grounds. Poly(ethylene glycol methacrylate) (PEGMA) is often used to prepare sterically-stabilized latexes. Here the terminal methacrylate group participates in the in situ polymerization, leading to chemical grafting of the PEGMA chains to the latex surface.

In the case of charge stabilization, each latex particle carries a surface charge and a corresponding diffuse layer of ions of opposite charge (the electrical double

layers or EDL).[65] This mechanism is only effective in aqueous or highly polar solvents of high dielectric constant, in which surface ionization can occur and EDL are created as a result (Figure 2).

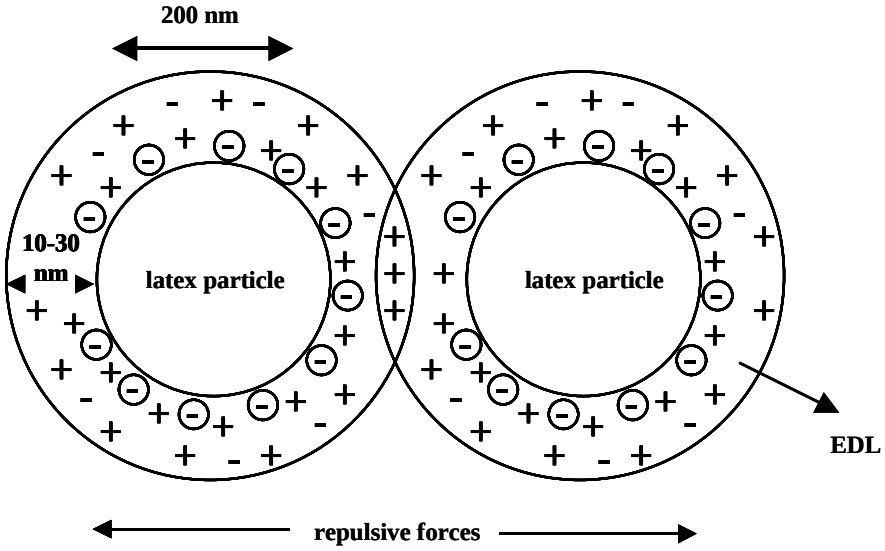

Figure 1.3: Electrical double layers (EDL) lead to repulsion between impinging latex particles.

The overlap of the electrical double layers is energetically unfavourable and leads to repulsive forces between the particles, which prevent aggregation.

1.1.6 Current work

In the present study we synthesized homopolymer microgel particles based on 2-(diethylamino)ethyl methacrylate (DEA) or methacrylic acid (MAA) using emulsion polymerization. Steric stabilization of the microgel particles was achieved using poly(ethylene glycol) methacrylate (M_n=2000) as a stabilizer. In order to synthesize the PMAA-based microgel particles *tert*-butyl methacrylate (*t*-BuMA) was used as the protected form of MAA. After the synthesis the P(*t*-BuMA)-based microgels were hydrolyzed to convert the *t*-BuMA segments into MAA via acid hydrolysis. These microgels exhibit reversible swelling properties in water by adjusting the solution pH or the degree of ionization of the monomer units. Thus the DEA based microgel particles, swell at low pH upon ionization of the DEA units due to the hydrophilicity of the protonated amine units, while an increase of the solution pH leads to the deprotonation of the DEA units and the formation of hydrophobic latex particles. The PMAA-based microgel particles swell at high pH due to the ionization of the carboxyl

units, while at low pH values the MAA moieties become neutral and the particles shrink. The pH responsive character of the microgel particles was examined by DLS as a function of the degree of ionization of the monomer units. The effect of the cross-link density on the degree of swelling of the PDEA microgels was also investigated. The effective equilibrium constants pK_α's of the PDEA microgel particles were calculated from the potentiometric titration curves of the microgel dispersions. SEM and TEM were used to investigate the shape and the size distribution of the particles.

In the second part of our study polyampholyte mixed microgel particles comprising both DEA and MAA units randomly distributed within the particle have been prepared. Potentiometric titrations were used to determine the ionization range of the microgels. The dependence of the size of the mixed microgels particles on the degree of ionization of the monomer units was examined by DLS. Finally, we synthesized microgel particles with a core-shell topology comprising either a PDEA core and a PMAA shell or a PMAA core and a PDEA shell. Potentionmetric titration curves were used to determine the ionization behavior of the particles. The swelling properties of the microgel particles as a function of the solution pH were also examined by DLS. SEM was used to determine the shape of the microgels and their size distribution while TEM was used to verify their core-shell topology by selectively staining the core or the shell of the microgels.

1.2 References

[1] Vinogradov, S. V. *Current Pharmaceutical Design* **2006**, *12*, 4703-4712.

[2] Lopez, V. C.; Hadgraft, J.; Snowden, M. J. *International Journal of Pharmaceutics* **2005**, *292*, 137-147.

[3] Elaissari, A.; Ganachaud, F.; Pichot, C. In *Colloid Chemistry Ii* 2003; Vol. 227, p 169-193.

[4] Murthy, N.; Xu, M. C.; Schuck, S.; Kunisawa, J.; Shastri, N.; Frechet, J. M. J. *Proceedings of the National Academy of Sciences of the United States of America* **2003**, *100*, 4995-5000.

[5] Ogawa, K.; Wang, B.; Kokufuta, E. *Langmuir* **2001**, *17*, 4704-4707.

[6] Ma, Y. H.; Tang, Y. Q.; Billingham, N. C.; Armes, S. P.; Lewis, A. L. *Biomacromolecules* **2003**, *4*, 864-868.

[7] Nayak, S.; Lee, H.; Chmielewski, J.; Lyon, L. A. *Journal of the American Chemical Society* **2004**, *126*, 10258-10259.

[8] Qiu, X. P.; Leporatti, S.; Donath, E.; Mohwald, H. *Langmuir* **2001**, *17*, 5375-5380.

[9] Eichenbaum, G. M.; Kiser, P. F.; Dobrynin, A. V.; Simon, S. A.; Needham, D. *Macromolecules* **1999**, *32*, 4867-4878.

[10] Lynn, D. M.; Amiji, M. M.; Langer, R. *Angewandte Chemie-International Edition* **2001**, *40*, 1707-1710.

[11] Grabstain, V.; Bianco-Peled, H. *Biotechnology Progress* **2003**, *19*, 1728-1733.

[12) Serpe, M. J.; Yarmey, K. A.; Nolan, C. M.; Lyon, L. A. *Biomacromolecules* **2005**, *6*, 408-413.

[13] Cao, R.; Gu, Z. Y.; Patterson, G. D.; Armitage, B. A. *Journal of the American Chemical Society* **2004**, *126*, 726-727.

[14] Ulbricht, M. *Journal of Chromatography B-Analytical Technologies in the Biomedical and Life Sciences* **2004**, *804*, 113-125.

[15] Zhang, M. C.; Zhang, W. Q. *Journal of Physical Chemistry C* **2008**, *112*, 6245-6252.

[16] Li, D. J.; Dunlap, J. R.; Zhao, B. *Langmuir* **2008**, *24*, 5911-5918.

[17] Pich, A.; Bhattacharya, S.; Lu, Y.; Boyko, V.; Adler, H. A. P. *Langmuir* **2004**, *20*, 10706-10711.

[18] Zhang, J. G.; Xu, S. Q.; Kumacheva, E. *Journal of the American Chemical Society* **2004**, *126*, 7908-7914.

[19] Gao, J.; Hu, Z. B. *Langmuir* **2002**, *18*, 1360-1367.

[20] Plunkett, K. N.; Moore, J. S. *Langmuir* **2004**, *20*, 6535-6537.

[21] Daly, E.; Saunders, B. R. *Langmuir* **2000**, *16*, 5546-5552.

[22] Gan, D. J.; Lyon, L. A. *Macromolecules* **2002**, *35*, 9634-9639.

[23] Gan, D. J.; Lyon, L. A. *Journal of the American Chemical Society* **2001**, *123*, 7511-7517.

[24] Peng, S. F.; Wu, C. *Journal of Physical Chemistry B* **2001**, *105*, 2331-2335.

[25] Peng, S. F.; Wu, C. *Macromolecules* **2001**, *34*, 568-571.

[26] Saunders, B. R.; Crowther, H. M.; Vincent, B. *Macromolecules* **1997**, *30*, 482-487.

[27] Dalmont, H.; Pinprayoon, O.; Saunders, B. R. *Langmuir* **2008**, *24*, 2834-2840.

[28] Nayak, S.; Lyon, L. A. *Chem. Mater.* **2004**, *16*, 2623-2627.

[29] Jones, C. D.; Lyon, L. A. *Macromolecules* **2000**, *33*, 8301-8306.

[30] Deng, Y. L.; Pelton, R. *Macromolecules* **1995**, *28*, 4617-4621.

[31] Chu, L. Y.; Kim, J. W.; Shah, R. K.; Weitz, D. A. *Advanced Functional Materials* **2007**, *17*, 3499-3504.

[32] Woodward, N. C.; Chowdhry, B. Z.; Snowden, M. J.; Leharne, S. A.; Griffiths, P. C.; Winnington, A. L. *Langmuir* **2003**, *19*, 3202-3211.

[33] Amalvy, J. I.; Wanless, E. J.; Li, Y.; Michailidou, V.; Armes, S. P.; Duccini, Y. *Langmuir* **2004**, *20*, 8992-8999.

[34] Palioura, D.; Armes, S. P.; Anastasiadis, S. H.; Vamvakaki, M. *Langmuir* **2007**, *23*, 5761-5768.

[35] Dupin, D.; Fujii, S.; Armes, S. P.; Reeve, P.; Baxter, S. M. *Langmuir* **2006**, *22*, 3381-3387.

[36] Dupin, D.; Rosselgong, J.; Armes, S. P.; Routh, A. F. *Langmuir* **2007**, *23*, 4035-4041.

[37] Dupin, D.; Armes, S. P.; Connan, C.; Reeve, P.; Baxter, S. M. *Langmuir* **2007**, *23*, 6903-6910.

[38] Hoare, T.; Pelton, R. *Macromolecules* **2004**, *37*, 2544-2550.

[39] M. I. Martinez-Rubio, T. G. I., G. R. Fern, J. Silver and M. J. Snowden *Langmuir* **2001**, *17*, 7145-7149.

[40] Tan, B. H.; Ravi, P.; Tan, L. N.; Tam, K. C. *Journal of Colloid and Interface Science* **2007**, *309*, 453-463.

[41] Bradley, M.; Vincent, B.; Burnett, G. *Australian Journal of Chemistry* **2007**, *60*, 646-650.

[42] Tan, B. H.; Ravi, P.; Tam, K. C. *Macromolecular Rapid Communications* **2006**, *27*, 522-528.

[43] Ho, B. S.; Tan, B. H.; Tan, J. P. K.; Tam, K. C. *Langmuir* **2008**, *24*, 7698-7703.

[44] Cloitre, M.; Borrega, R.; Monti, F.; Leibler, L. *Comptes Rendus Physique* **2003**, *4*, 221-230.

[45] Karg, M.; Pastoriza-Santos, I.; Rodriguez-Gonzalez, B.; von Klitzing, R.; Wellert, S.; Hellweg, T. *Langmuir* **2008**, *24*, 6300-6306.

[46] Hampton, K. W.; Ford, W. T. *Macromolecules* **2000**, *33*, 7292-7299.

[47] Blackburn, W. H.; Lyon, A. *Colloidal Polymer Science* **2008**, *286*, 563-569.

[48] Lu, Y.; Wittemann, A.; Ballauff, M.; Drechsler, M. *Macromolecular Rapid Communications* **2006**, *27*, 1137–1141.

[49] Cai, J.; Guo, J.; Ji, M.; Yang, W.; Wang, C.; Fu, S. *Colloidal Polymer Science* **2007**, *285*, 1607–1615.

[50] Berndt, I.; Pedersen, J. S.; Richtering, W. *Angewandte Chemie-International Edition* **2006**, *45*, 1737 –1741.

[51] Nayak, S.; Lyon, L. A. *Angewandte Chemie-International Edition* **2004**, *43*, 6706 –6709.

[52] Jones, C. D.; Lyon, L. A. *Macromolecules* **2003**, *36*, 1988-1993.

[53] N. Dingenouts, C. N., and M. Ballauff *Macromolecules* **1998**, *31*, 8912-8917.

[54] Satish Nayak, D. G., Michael J. Serpe, and L. Andrew Lyon *Small* **2005**, *1*, 416-421.

[55] Li, X.; Zuo, J.; Guo, Y. L.; Yuan, X. H. *Macromolecules* **2004**, *37*, 10042-10046.

[56] Bradley, M.; Vincent, B. *Langmuir* **2008**, *24*, 2421-2425.

[57] Becher, P. *Emulsion: Theory and Practice*; 2nd ed.; Reinhold: New York, 1965.

[58] Arai, M.; Arai, K.; Saito, S. *Journal of Polymer Science Part a-Polymer Chemistry* **1979**, *17*, 3655-3665.

[59] Robert M. Fitch, M. B. P.; and Karen J. Sprick *Journal of Polymer Science Part C* **1969**, *27*, 95-118.

[60] Goodall, A. R.; Wilkinson, M. C.; Hearn, J. *Journal of Polymer Science Part a-Polymer Chemistry* **1977**, *15*, 2193-2218.

[61] Lichti, G.; Gilbert, R. G.; Napper, D. H. *Journal of Polymer Science Part a-Polymer Chemistry* **1983**, *21*, 269-291.

[62] Feeney, P. J.; Napper, D. H.; Gilbert, R. G. *Macromolecules* **1984**, *17*, 2520-2529.

[63] Feeney, P. J.; Napper, D. H.; Gilbert, R. G. *Macromolecules* **1987**, *20*, 2922-2930.

[64] Xiao, X. C.; Chu, L. Y.; Chen, W. M.; Wang, S.; Xie, R. *Langmuir* **2004**, *20*, 5247-5253.

[65] Goodwin, J. W.; Hearn, J.; Ho, C. C.; Ottewill, R. H. *British Polymer Journal* **1973**, *5*, 341-362.

Chapter 2

2.1 Experimental section

2.1.1 Materials

2-(diethylamino)ethyl methacrylate (DEA) (Aldrich), *t*-butyl methacrylate (*t*-BuMA) (Aldrich) and ethylene glycol dimethacrylate (EGDMA) (Aldrich) were all passed through a basic alumina column to remove the inhibitor before use. Potassium persulfate ($K_2S_2O_8$) (Aldrich), methoxy, poly(ethylene glycol) methacrylate (PEGMA) (M_n 2000 gr/mole, Aldrich), trifluoroacetic acid (TFA) (Aldrich), tetrahydrofuran (THF) (Aldrich), dichloromethane (DCM) (Aldrich) and dioctyl sulfosuccinate salt (AOT) (Aldrich) were used as received. Milli-Q (18.2 MΩ) water and aqueous solutions of HCl (0.1 and 0.5 M) and NaOH (0.1, 0.5 and 10 M) were used for all preparations. The Tables below show the chemical formulas of the monomers, the cross-linker, the stabilizers and the initiator used for the synthesis of the microgel particles.

Table 3.1: Chemical structures of the monomers and cross-linker used in the microgel synthesis.

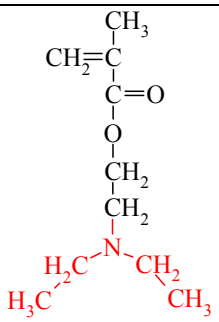 DEA (2-(diethylamino)ethyl methacrylate)	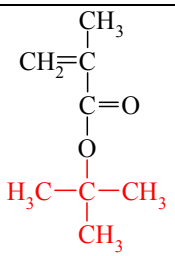 *t*-BuMA (*tert*-butyl methacrylate)	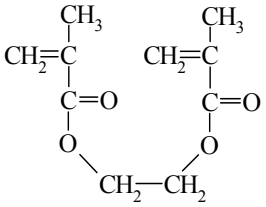 EGDMA (ethylene glycol dimethacrylate)

Table 3.2: Chemical structures of the stabilizers and initiator used in the microgel synthesis.

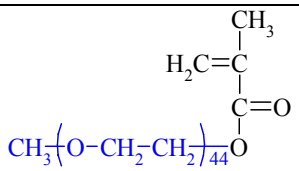 PEGMA (poly(ethylene glycol) methacrylate)	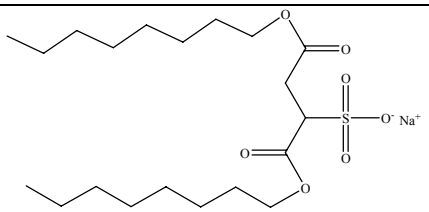 AOT (dioctyl sulfosuccinate salt)	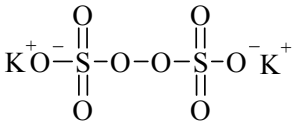 $K_2S_2O_8$ potassium persulfate

2.1.2 Homopolymer and mix microgel synthesis

The synthesis of the microgel particles was carried out by emulsion copolymerization of a functional monomer with a cross-linker in the presence of a polymerizable stabilizer. The functional monomers used were DEA (hydrophobic, pH-sensitive, ionizable) and *t*-BuMA (hydrophobic) which is a protected ester of MAA. Ethylene glycol dimethacrylate was used as the cross-linker, while PEGMA, M_n = 2000 gr/mole was used as the stabilizer. A typical synthetic procedure followed for the preparation of the homopolymer microgel particles is summarized below. [1]

In a 100 ml round-bottom flask, fitted with a nitrogen gas inlet and a magnetic stirrer bar, water (45 gr) was added, followed by the addition of the macromonomer stabilizer (typically 10 wt % based on the monomer). Next, a mixture of DEA (or *t*-BuMA) (2.5 gr) and EGDMA cross-linker (0.025 gr, 1 wt % based on the monomer) was added under stirring. The solution was degassed for ~ 30 minutes and then stirred for 30 minutes under nitrogen at 65^{o} C. The polymerization commenced upon addition of a previously degassed aqueous solution of the potassium persulfate ($K_2S_2O_8$) initiator (1 wt % based on the monomer). The reaction was allowed to proceed for ~ 8 hours and was then stopped by cooling under a water flow. Ultrafiltration was used to eliminate the excess stabilizer, as well as traces of unreacted monomer and initiator, in order to purify the PDEA or P(*t*-BuMA) latex particles. **Figure 2.1** illustrates the synthetic route followed for the preparation of the sterically stabilized microgel particles.

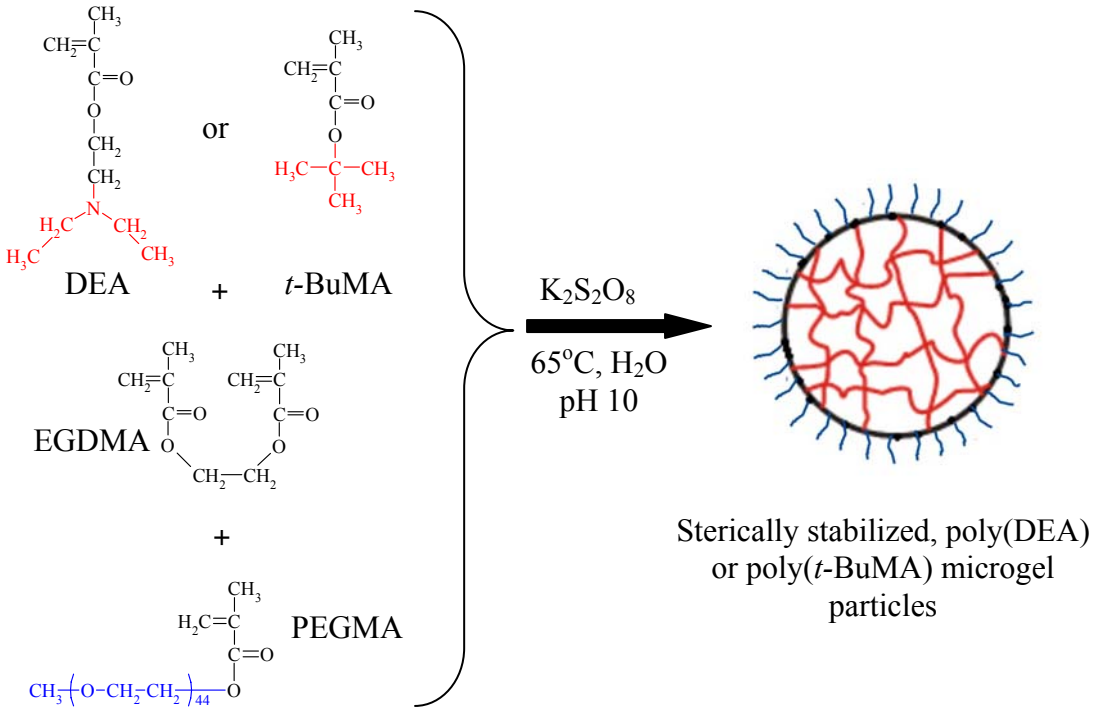

Figure 2.1: Synthetic route followed for the synthesis of the sterically stabilized microgel particles.

Dispersed microgel particles at higher volume fractions were prepared by increasing the monomer, cross-linker and stabilizer concentration while keeping the amount of water constant. Microgel particles of higher cross-link density were prepared by increasing the amount of cross-linker (0.5-3 wt % based on the monomer) at a constant monomer/water ratio. Finally, microgels with mix DEA and *t*-BuMA moieties were prepared by the addition of a premixed solution of DEA and *t*-BuMA with EGDMA followed by their copolymerization upon the addition of the initiator.

2.1.3 Synthesis of core-shell microgel particles

In this work we have also synthesized microgel particles with a core-shell topology with the core consisting of either PDEA or P(*t*-BuMA) and the shell comprising P(*t*-BuMA) or PDEA, respectively. The synthetic procedure followed for the preparation of the core-shell particles involved a two step polymerization.[2]

In the first step, the core is formed by a procedure similar to that described above for the homopolymer microgels. The required amount of water (37.6 gr) and an anionic stabilizer sodium dodecyl sulfate (SDS) (typically 20 wt % based on the monomer) were added in the flask. A mixture of DEA (or *t*-BuMA) (1.2 gr) with

EGDMA (1 wt % based on the monomer) were added next in the 100 ml round-bottom flask. The solution was degassed and then stirred for 30 minutes under nitrogen at 65° C. The polymerization commenced on addition of a previously degassed aqueous solution of the $K_2S_2O_8$ initiator (1 wt % based on the monomer). The reaction was allowed to proceed for 5 hours before being stopped by cooling the reaction flask with water. This process resulted in the formation of latex particles that were electrostatically stabilized by the anionic surfactant.

A sample was extracted for analysis before proceeding in the second step of the polymerization. The core particles prepared in the first step were used as the seeds for the synthesis of the shell, by seed polymerization. The dispersion of the core particles was heated again at 65° C and next a degassed mixture of water (10 gr), monomer (1.2 gr), cross-linker (0.012 gr) (1 wt % based on the monomer), initiator (0.012 gr) (1 wt % based on the monomer) and PEGMA stabilizer (0.24 gr) (20 wt % based on the monomer) was added under a nitrogen atmosphere via a double tipped needle. The reaction was allowed to proceed at 65° C for 6 hours, before being stopped by cooling the reaction flask with water. Ultrafiltration was used to eliminate the excess stabilizers and traces of unreacted monomers and initiator, in order to purify the core-shell latex particles. **Figure 2.2** illustrates the synthetic route followed for the preparation of the sterically stabilized core-shell microgel particles.

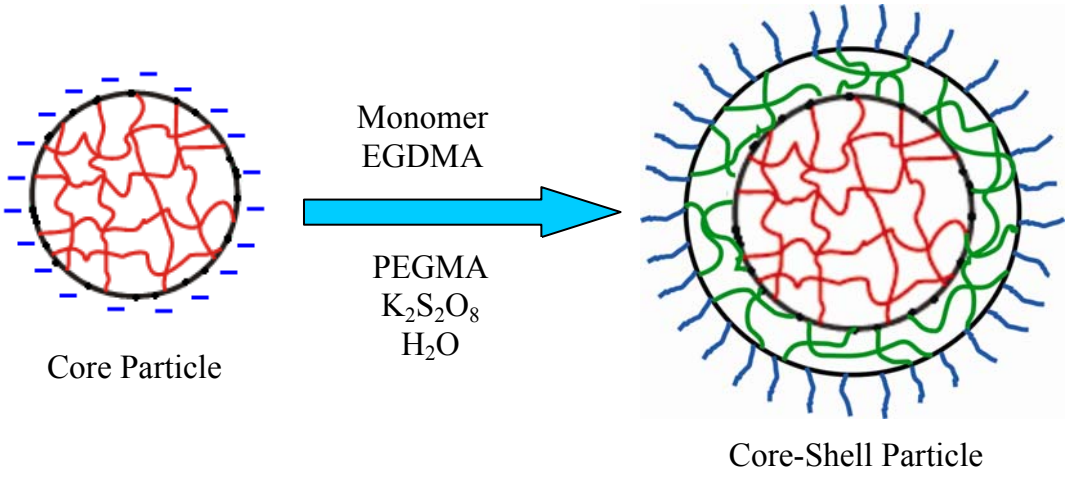

Figure 2.2: Synthetic route followed for the preparation of the sterically stabilized core-shell microgel particles.

2.1.4 Deprotection of the P(*t*-BuMA) homopolymer, P(DEA-*co*-*t*-BuMA) mix and P(*t*-BuMA)-PDEA and PDEA-P(*t*-BuMA) core-shell particles

t-BuMA is a protected ester which upon hydrolysis gives MAA. Thus, after synthesis, all the *t*-BuMA containing microgel particles were deprotected by acid hydrolysis to obtain the acidic groups. The hydrolysis was carried out by trifluoroacetic acid (TFA) in dichloromethane (DCM).[3] 5 ml of the as synthesized microgel dispersion after ultrafiltration were first dried in a vacuum oven to remove all traces of water and were then redispersed in 5 ml DCM. In the DCM solution TFA was added (10 fold excess TFA with respect to the moles of *t*-BuMA). The solution was allowed to stir for 3 days before the addition of 5 ml tetrahydrofuran (THF) and 5 ml of deionized water. THF was used as a co-solvent to compatibilize the organic (DCM) and aqueous phases. Next, equal moles of base (NaOH 10 M) to those of the added TFA were used to neutralize the acid. The solution was stirred in air to remove the DCM and THF solvents and the deprotected microgel particles were obtained in water. Finally, ultrafiltration was used to eliminate the excess salt formed by the addition of TFA and NaOH and to isolate the pure microgel particles.

2.2 Sample preparation

2.2.1 Potentiometric titrations

Nanopure (18.2 MΩ) water was used for the preparation for all samples. A 20 ml microgel dispersion (c=0.2 wt %) was prepared in each case. A known amount of acid (HCl 0.5 M) or base (NaOH 0.5 M) was first added in pure water in order to decrease or increase the pH of the solution to ~ 2 or ~ 11, respectively. Next, a concentrated microgel disoersion (c=5 wt %) was added to obtain a final microgel concentration of 0.2 wt % and the sample was stirred for 15 min.

The titration was performed by the addition of small amounts (20-100 μl) of acid (HCl 0.1 M) or base (NaOH 0.1 M), while monitoring the solution pH using a Crison GLP 21 pH-meter. This procedure resulted in the gradual decrease of the solution pH from 11 to 2 for the addition of HCl or in the increase of the solution pH from 2 to 11 for the addition of base.

2.2.2 Dynamic light scattering (DLS)

Samples for dynamic light scattering were prepared following a procedure similar to that described above. The microgel particles were first diluted with nanopure water to the required concentration (typically 0.005 wt %) from an initial concentrated (c=5 wt %) latex dispersion. The pH or degree of ionization (α) of the microgel sample was adjusted to the required value by the addition of 0.1 M NaOH or 0.1 M HCl. In order to obtain the desirable α value, the amount of added acid or base was calculated from the ratio:

$$\frac{\text{moles acid / base}}{\text{moles ionizable polymer repeat units}} = \frac{\alpha}{1}$$

assuming that all the H^+ or OH^- from the added acid or base react with the polymer groups. All samples were allowed to equilibrate overnight before measurement. One hour before the measurement, the samples were filtered using syringe filters with pore size 1.2 μm for the hydrophobic latex particles and 5 μm for the ionized samples. An ALV spectrophotometer with a Nd-YAG laser at λ=532 nm was used, and all measurements were performed at 20^o C.

2.2.3 Transmission electron microscopy (TEM)

Samples for TEM were prepared following a procedure similar to that described above for the DLS experiments. All samples were previously diluted with water to c=0.05 wt % and adjusted to the appropriate degree of ionization by the addition of HCl or NaOH. The samples were selectively stained using potassium hexachloroplatinate (K_2PtCl_6) for the PDEA containing microgels and with cadmium nitrate ($Cd(NO_3)_2$) for the PMAA containing microgels at a monomer / metal = 2 / 1 mole ratio. A drop of the diluted sample was then placed on a carbon-coated cooper grid and left to dry in air overnight. A JOEL JEM-100C instrument at an electron accelerating voltage of 80 kV was employed for the measurements.

2.2.4 Scanning electron microscopy (SEM)

Samples for SEM were prepared following a procedure similar to that described above. All samples were previously diluted with nanopure water to c=0.05 wt %. The samples were then spin coated onto glass slides at 1000 rpm for 45 sec. A

JEOL JSM-6390LV instrument at an electron acceleration voltage of 10 kV was employed for the measurements.

2.3 Potentiometric Titrations

2.3.1 Acids and Bases

Acids and bases exist as conjugate acid-base pairs. The term conjugate comes from the Latin stem meaning "joined together" and refers to things that are joined, particularly in pairs, such as Brønsted acids and bases.[4, 5]

When a Brønsted acid acts as a H^+-ion donor, it forms a conjugate base. Imagine, for example, a generic acid, HA. When this acid donates an H^+ ion to water, one product of the reaction is the A^- ion, which is a hydrogen-ion acceptor, or Brønsted base.

$$\underset{\text{Acid}}{HA} + H_2O \rightleftharpoons H_3O^+ + \underset{\text{base}}{A^-}$$

For a base B in water, the characteristic equilibrium is

$$\underset{\text{base}}{B} + H_2O \rightleftharpoons OH^- + \underset{\text{acid}}{BH^+}$$

Acids and bases in the Brønsted model therefore exist as conjugate pairs whose formulas are related by the loss or gain of a hydrogen ion.

Our use of the symbols HA and A^- for a conjugate acid-base pair does not mean that all acids are neutral molecules or that all bases are negative ions. It signifies only that the acid contains an H^+ ion that isn't present in the conjugate base. Brønsted acids or bases can be neutral molecules, positive ions, or negative ions.

The relative strengths of acids is often described in terms of an acidity constant, K_a. To understand the nature of this equilibrium constant, let's assume that the reaction between an acid and water can be represented by the following generic equation.

$$HA(aq) + H_2O(l) \rightleftharpoons H_3O^+(aq) + A^-(aq)$$

In other words, some of the HA molecules react to form H_3O^+ and A^- ions.

By convention, the concentrations of these ions in units of moles per liter are represented by the symbols $[H_3O^+]$ and $[A^-]$. The concentration of the HA molecules that remain in solution is represented by the symbol [HA].

The value of K_a for an acid is calculated from the following equation:

$$K_a = \frac{[H_3O^+][A^-]}{[HA]} \tag{2.1}$$

When a strong acid dissolves in water, the acid reacts extensively with water to form H_3O^+ and A^- ions. (Only a small residual concentration of the HA molecules remains in solution.) The product of the concentrations of the H_3O^+ and A^- ions is therefore much larger than the concentration of the HA molecules, so K_a for a strong acid is greater than 1. Weak acids, on the other hand, react only slightly with water. The product of the concentrations of the H_3O^+ and A^- ions is therefore smaller than the concentration of the residual HA molecules. As a result, K_a for a weak acid is less than 1. K_a can therefore be used to distinguish between strong acids and weak acids.

Strong acids: $K_a > 1$

Weak acids: $K_a < 1$

Likewise we define the constant K_b according to the following equation:

$$K_b = \frac{[BH^+][OH^-]}{[B]} \tag{2.2}$$

An acid is strong if pK_α is small and a base is weak if pK_b is big.

2.3.2 Water

Water molecules consist of one part of oxygen and two parts of hydrogen and exist in equilibrium with their components: hydronium ions (H_3O^+) and hydroxyl ions (OH^-), in accordance with the following equation

$$H_2O + H_2O \rightleftharpoons H_3O^+ + OH^-$$

This reaction at equilibrium establishes the following quantitative relationship between H_3O^+ and OH^- in solution

$$K_w = [H_3O^+] \times [OH^-] \tag{2.3}$$

K_w is the symbol for the dissociation constant of water and is a function of temperature only. For instance, its value is 10^{-14} in 25° C while it increases to $10^{-12.32}$ at 100° C.

We notice that $K_w = K_a K_b$. If we take the negative of the log to the base 10 of K_w we have the relation:

$$pK_w = pK_a + pK_b \tag{2.4}$$

Based on the law of equilibrium the product $[H_3O^+] \times [OH^-]$ must always be equal to 10^{-14}. Thus a solution with $[H_3O^+]=10^{-7}$ must have a $[OH^-]=10^{-7}$ and a solution with $[H_3O^+]=10^{-2}$ must have a $[OH^-]=10^{-12}$ and so on.

pH is a measure of the hydrogen ion activity in an aqueous solution. We define pH as the negative of the log to the base 10 of the quantity it proceeds. Therefore, the H^+ concentration of an aqueous solution maybe represented as:

$$pH = -\log_{10}[H_3O^+] \tag{2.5}$$

This notation allows for a convenient pH scale of 0 through 14 corresponding to H_3O^+ concentration of 1 M to 10^{-14} M.

2.3.3 Titration curves

Titration is a laboratory technique by which we can determine the concentration of an unknown reagent using a standard concentration of another reagent that chemically reacts with the unknown. This standard solution is referred to as the "titrant". In any titration there must be a rapid, quantitative reaction taking place as the titrant is added, and in acid-base titrations this is a stoichiometric neutralization. In

other words an acid-base titration involves the reaction between a conjugate acid/base pair. The titration curve for an acid-base titration is a plot of the solution pH against the volume of titrant added. Titration curves can be used to define the value of pH that signals the equivalent point, this is the point when the reaction is complete and all the analyte (acid or base) has reacted with the titrant (base or acid respectively). The determination of the equivalence point is achieved by monitoring the pH changes during the titration. **Figure 2.3** shows the titration curve for a strong acid-strong base pair. The initial pH of the solution is 2 prepared by the addition of HCl 12 M in pure water. Upon addition of base (NaOH 0.1M) the OH^- react with the H^+ of the acid to produce water molecules. The pH increases slowly because the $[H^+]$ decreases. As the equivalence point is reached, a small quantity of base in the solution results in a sharp increase of the pH while beyond the equivalence point, the pH is determined by the concentration of excess base present in the solution.

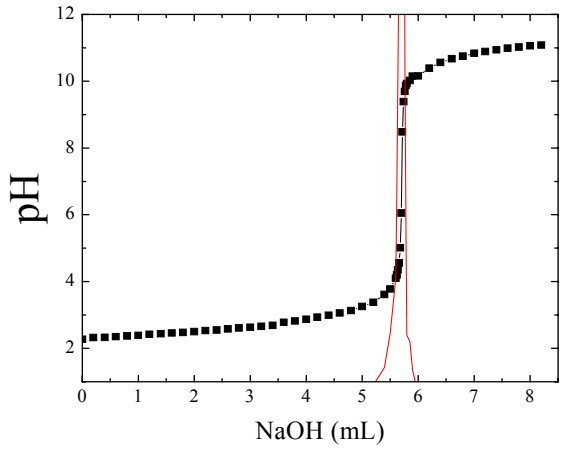

Figure 2.3: Titration curve for 0.01M HCl and the first derivative (red line).

The equivalent point occurs when the slope of the titration curve changes as shown in **Figure 2.3** and can be calculated from the maximum of the first derivative of the data. In the above plot an equivalent point at pH 7 is obtained as expected from a strong acid-strong base pair.

The titration of a weak acid with a strong base is different from that of a strong acid/base titration, primarily in the beginning of the titration, i.e., before the equivalent point. Moreover, the equivalent point itself is shifted upwards in pH. The reaction that occurs in the solution is

$$HA(aq) + OH^-(aq) \rightarrow A^-(aq) + H_2O(l)$$

As base is added, a buffer solution forms and the pH does not change rapidly until all of the weak acid reacts with the base. Analysis of the titration curve provides a means of determining the dissociation constant of the acid. The pK_α of the acid is equal to the pH at the midpoint of the titration curve. This can be seen from the following form of the equation, which describes the weak acid equilibrium

$$pH = pK_\alpha + \log([A^-]/[HA]) \quad (2.6)$$

where $[A^-]$ is the concentration of the basic form of the acid and [HA] is the concentration of the acid.

At the midpoint $[A^-]$ = [HA] and the second term on the right side of the equation becomes zero.

2.3.4 Degree of ionization

The degree of ionization, α, of a weak acid is defined as the ratio of the concentration of the ionized units divided by the total concentration of acid units in the solution.

In accordance, the fraction of charged monomer units of the microgel particles prepared in this study is defined as the degree of ionization. Assuming that all of the protons or OH^- groups from the added HCl or NaOH ionize the monomer groups the degree of ionization is defined as the net moles of the HCl or NaOH divided by the moles of the monomer units in the solution. This is expressed as:

$$\alpha = \frac{[\text{net acid / base}]}{[\text{monomer units}]} \quad (2.7)$$

The effective pK_α values of the ionized monomer units is defined as the pH at a degree of ionization α=0.5. This value can be calculated from the pH versus α curve an example of which is shown in **Figure 2.4**. Based on weak acid equilibria the degree of ionization α can be calculated from the solution pH and the effective pK_α as follows:

$$\text{acid - H} \Leftrightarrow \text{base} + H^+$$

where K_α is:

$$K_{\alpha} = \frac{[base]\cdot[H^{+}]}{[acid]} \tag{2.8}$$

or

$$pH = pK_{\alpha} + \log\frac{1-\alpha}{\alpha} \tag{2.9}$$

which gives the calculated degree of ionization:

$$\alpha = \frac{1}{10^{pH-pK_{\alpha}}+1} \tag{2.10}$$

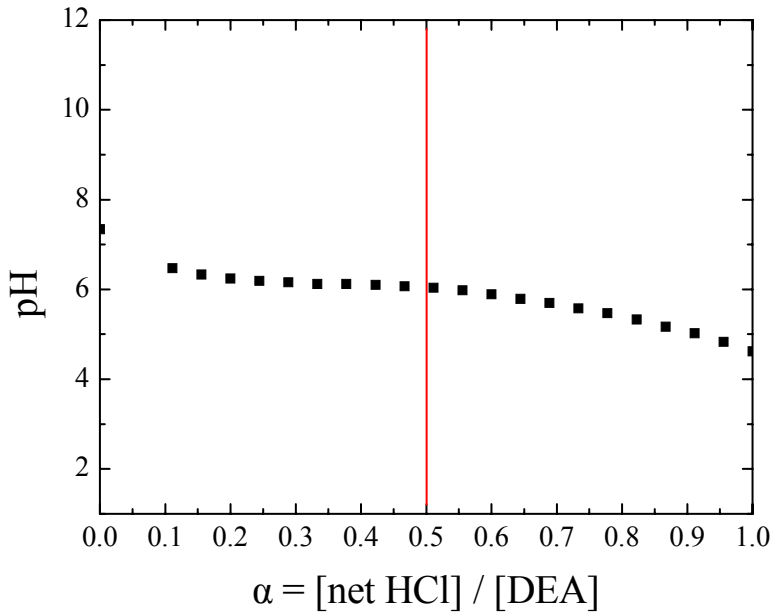

Figure 2.4: Solution pH versus degree of ionization for a 0.1 wt % PDEA-based microgel sample.

2.4 Dynamic Light Scattering

The interaction of light with matter can be used to obtain important information about the structure and dynamics of matter. Light scattering experiments are based on such light-matter interactions.

When light impinges on matter it is either scattered or absorbed, thus providing information about the electronic, vibrational and rotational degrees of freedom of the molecules. From this interaction, photons can either impact or gain energy and they

thereby suffer frequency shifts. Thus the frequency spectrum of the light will exhibit resonances at the frequencies corresponding to these transitions.

When light impinges on matter, the electric field of the light induces an oscillating polarization of the electrons in the molecules. The molecules then serve as a secondary source and scatter light. The frequency shifts, the angular distribution, the polarization and the intensity of the scattered light are determined by the size, shape and the molecular interaction in the scattering material. Thus from the light scattering characteristics of a given system it is possible, with the aid of the theory of time dependant statistical mechanics and electromagnetism, to obtain information about the structure and molecular dynamics of the scattering medium.[6-8]

Light scattering can occur with a shift in the frequency of the incoming light (inelastic light scattering), or not (elastic light scattering). The elastic scattering is called Rayleigh scattering and deals with the characteristics of the light scattered from the translational and rotational degrees of freedom. On the other hand, vibrational degrees of freedom give Raman scattering. The development of laser techniques enabled the measurement of very small frequency shifts in the light scattered from matter, because of their high intensity that measures even weak scattering from molecules.

The basic theory of Rayleigh scattering was developed more than half a century ago by Rayleigh, Mie, Smoluchowski, Einstein and Debye. Light scattering was first studied experimentally by Tyndall[9] and then theoretically by Rayleigh.[10] These studies concerned scattering from assemblies of non-interacting particles sufficiently small compared to the wavelength of the light to be regarded as point dipole oscillations. Rayleigh derived the full formula of scattered light from spheres of arbitrary size.

Although Rayleigh developed a theory of light scattering from gases with some success, it was found that the intensity of scattering by condensed phases was more than on order of magnitude lower than that predicted by this formula. This effect was correctly attributed to the destructive interference between the wavelets scattered from different molecules. Smoluchowski[11] and Einstein[12] elegantly circumvented this difficulty by considering the light to be a continuous medium in which thermal fluctuations give rise to local inhomogeneities and thereby to intensity and concentration fluctuations. The authors developed the fluctuation theory of light scattering. According to this theory, the intensity of the scattered light can be calculated from the mean square fluctuations in density and concentration that in turn

can be determined from the macroscopic dependence of the osmotic pressure. The intensity of the light is thus obtained without considering the detailed molecular structure of the medium. This approach to light scattering has played a very important role in the theory of light scattering.

Dynamic light scattering examines the relaxation time of the fluctuations providing information in reciprocal space for the spatial Fourier length $2\pi/q$, where q is the scattering vector. This length is related to a characteristic time, which is the time that the particle needs to travel a distance equal to $2\pi/q$.

In a light-scattering experiment, light from a laser passes through a polarizer to define the polarization of the incident beam and then impinges on the scattering medium. The scattered light then passes through an analyzer which selects a given polarization and finally enters the detector. The position of the detector defines the scattering angle θ. In addition, the intersection of the incident beam and the beam intercepted by the detector defines a scattering region of volume V. This is illustrated in **Figure 2.5.** The quantity measured in a light-scattering experiment is the time-correlation function of the scattered intensity I(t). Based on the continuous movement of the molecules, their position changes and the scattered intensity fluctuates. The fluctuations of I(t) are characterized by the diffusion coefficient, D.

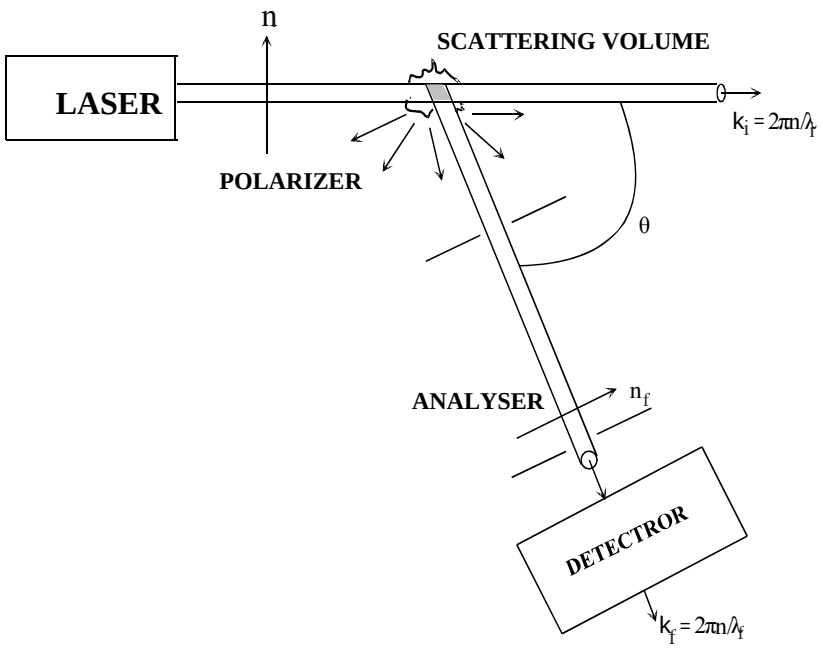

Figure 2.5: Typical experimental setup for a light scattering experiment.

2.4.1 Electromagnetic theory

The theory of light scattering can be developed on the basis of quantum field theory. The major results of this theory differ little from classical theory of light scattering. So we do not dwell on the electrodynamical theory.

Consider a non-magnetic, non-conducting, non-absorbing medium with average dielectric constant ε_o and refractive index n = $\sqrt{\varepsilon_o}$. Let the incident electric field be a plane wave of the form

$$\mathrm{E}_i(\vec{r},t) = \hat{n}_i E_o \exp i(\vec{k}_i\vec{r} - \omega_i t) \tag{2.11}$$

where n_i is a unit vector in the direction of incident electric field; E_o is the field amplitude; k_i is the propagation vector and the ω_i is the angular frequency.

This plane wave is incident upon a medium that has a local dielectric constant

$$\vec{\vec{\varepsilon}}(\vec{r},t) = \varepsilon_o \vec{\vec{I}} + \delta\vec{\vec{\varepsilon}}(\vec{r},t) \tag{2.12}$$

where $\delta\varepsilon(r,t)$ is the dielectric constant fluctuation tensor at position r and time t and I is the second-rank unit tensor.

It can be shown that the component of the scattered electric field at a large distance R from the scattering volume with polarization n_f, propagation vector k_f, and frequency ω_f is

$$E_s(R,t) = \frac{E_o}{4\pi R\varepsilon_o}\exp(ik_f R)\int_V d^3r \exp[i(\vec{q}\cdot\vec{r} - \omega_i t)][\vec{n}_f \cdot [\vec{k}_f \times (\vec{k}_f \times (\delta\vec{\vec{\varepsilon}}(\vec{r},t)\cdot\vec{n}_i))]] \tag{2.13}$$

where the subscript V indicates that the integral is over the scattering volume. The vector q is defined in terms of the scattering geometry as $\vec{q} = \vec{k}_i - \vec{k}_f$ where k_i and k_f point, in the directions of the propagation of the incident wave and of the wave that reaches the detector, respectively. This is illustrated in **Figure 2.6**. The angle between k_i and k_f is called the scattering angle.

The magnitude of k_i and k_f are respectively $2\pi n/\lambda_i$ and $2\pi n/\lambda_f$ where $\lambda_ι$ and λ_f are the wavelengths of the incident and scattered radiation and n is the refractive index of the scattering medium.

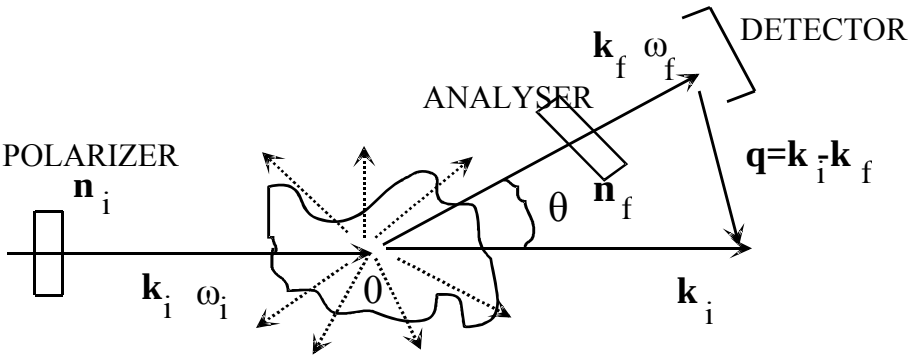

Figure 2.6: Light of polarization n_i and wave vector k_i is scattered in all directions. Only scattered light of wave vector k_f and polarization n_f arrives at the detector. The scattering vector $\vec{q} = \vec{k}_i - \vec{k}_f$ is defined by the geometry.

It is usually the case that the wavelength of the incident light changes very little in the scattering process so that $|k_i| \cong |k_f|$ and the scattering vector is

$$q^2 = |k_i - k_f|^2 = k_i^2 + k_f^2 - 2k_i \cdot k_f = 2k_i^2 - 2k_i^2 \cos\theta = 4k_i^2 \sin^2\left(\frac{\theta}{2}\right) \Rightarrow$$
$$q = 2k_i \sin\left(\frac{\theta}{2}\right) = \left(\frac{4\pi n}{\lambda_i}\right)\sin\left(\frac{\theta}{2}\right) \tag{2.14}$$

This condition specifies the wave vector component of the dielectric constant fluctuations that will give rise to scattering at an angle θ.

Spatial Fourier transform of the dielectric fluctuations $\delta\vec{\varepsilon}(\vec{q},t) = \int_V d^3r \exp[i(\vec{q}\cdot\vec{r})]\delta\vec{\varepsilon}(r,t)$ and **Equation 2.13** gives:

$$E_s(R,t) = \frac{-k_f^2 E_o}{4\pi R\varepsilon_o}\exp[i(k_f R - \omega_i t)]\delta\varepsilon_{if}(q,t) \tag{2.15}$$

where

$$\delta\varepsilon_{if}(\vec{q},t) \equiv \vec{n}_f \cdot \delta\vec{\varepsilon}(\vec{q},t)\cdot\vec{n}_i \tag{2.16}$$

is the component of the dielectric constant fluctuation tensor along the initial and final polarization directions. The time-correlation function of the electric field is:

$$< E_s^*(R,0)E_s(R,t) >= \frac{k_f^4 \mid E_o \mid^2}{16\pi^2 R^2 \varepsilon_o^2} \left\langle \delta\varepsilon_{if}(\vec{q},0)\delta\varepsilon_{if}(\vec{q},t) \right\rangle \exp(-i\omega_i t) \qquad (2.17)$$

and the spectral density of scattered light is

$$I(\vec{q},\omega_f,R) = \left[\frac{|E_o|^2 k_f^4}{16\pi^2 R^2 \varepsilon_o^2} \right] \frac{1}{2\pi} \int_{-\infty}^{\infty} dt < \delta\varepsilon_{if}(\vec{q},0)\delta\varepsilon_{if}(\vec{q},t) > \exp[\, i(\omega_f - \omega_i)t] \qquad (2.18)$$

Equation 2.18 indicates the inverse λ^4 and R^2 dependence of the characteristics of any spherical wave. The λ^4 dependence is related to the observation that the blue light is scattered more than the red light. It also indicates that radiowaves would not be scattered as much as visible light. As a consequence of the larger scattering intensities, it is much easier to perform scattering experiments with visible light than with longer wavelength infrared or radiowaves. It should be also noted that **Equation 2.18** is an expression for the light spectral density in terms of dielectric constant fluctuations. In a medium in which the dielectric constant does not fluctuate the light is scattered only in the q=0 direction.

The above theoretical expression is purely phenomenological. Any attempt to write this formula in molecular terms will necessarily involve some degree of approximation, nevertheless, it will contribute significantly in our intuitive understanding of light scattering and will be useful for practical applications.

2.4.2 Photon correlation spectroscopy (PCS)

In a photon correlation spectroscopy experiment the measured quantity is the normalized autocorrelation function of the scattered intensity *G(q,t)*, in polarized ($G_{VV}(q,t)$) or depolarized ($G_{VH}(q,t)$), geometry:

$$G(q,t) = \frac{< I(q,t)I(q,0) >}{< I(q,0) >^2} \qquad (2.19)$$

Polarized geometry gives us information about the fluctuations of the concentration or the density of the material, while the depolarized one gives us information regarding the fluctuations of the orientation of the molecules. Only the

polarized geometry has been used in this thesis. The quantity related with the dynamic response of the system is the autocorrelation function of the scattered field, g(q,t). The two autocorrelation functions are related via Siegert's relation:

$$G(q,t) = 1 + f^{*}(\alpha g(q,t))^{2} = 1 + f^{*} \mid C(q,t) \mid^{2} \qquad (2.20)$$

Where f^{*} is a spatial coherence factor that depends on the experimental setup, the scattered volume and the number of coherence areas viewed. The factor α is the scattered intensity percent in dynamics that can be measured with PCS. The advantages of the photon correlation spectroscopy are the large range of intervals (10^{-6}-10^{3}s) and the different relaxation times that can be measured at the same time.

2.4.3 Experimental setup

The experimental setup is shown in **Figure 2.7**. Scattering angles between 150^{o}-11^{o} ($q=2.28x10^{-2}$-$2.26x10^{-3}$ nm^{-1}) can be measured. The laser is Nd-YAG with a monochromatic beam at 532 nm (Adlas DPY 315II). The maximum power is ~100 mW, but 80 mW were used to ensure stability the laser source, and the diameter of the beam was 0.32 mm (TEM_{00}). The incident beam passes through optics (two mirrors M1, M2 and a polarizer P1) and a lens (F1) before it impinges the sample. The intensity and position of the beam are continuously recorded on a four Photo Diode (PD) system. The sample is contained in an optical glass cell of a diameter of 10 mm, and is placed in a bath that contains toluene in order to equate the refractive indexes (glass and toluene) and avoid refraction from the glass surface. The scattered beam passes through an optical system of a lens and two holes H1, H2 before it impinges the amplifier. The lens is 2f/2f and is placed in a distance equal to 2f from the scattering volume and the second hole H2 respectively. The amplifier is a photomultiplier (THORN EMI). The two holes H1 and H2 (0.3mm diameter) define the scattering volume. The polarization of the beam is defined by the two polarizers P1 and P2. The incoming beam is always polarized perpendicular to the scattering plane while P2 can be rotated so that both polarized (V) and depolarized (H) components are accessible. The bath temperature which is also the sample temperature, is controlled by the circulation of a thermostatic liquid (mixture of water and glycol) by means of a thermostat. Temperatures between 10^{o} C – 50^{o} C can be measured. A Bus Controller

RS-232C device controls the goniometer. A computer, embedded with an electronic correlation card, controls the whole setup. The software used is ALV-5000/E photon correlator. Details regarding the photon correlator are given in the next paragraph.

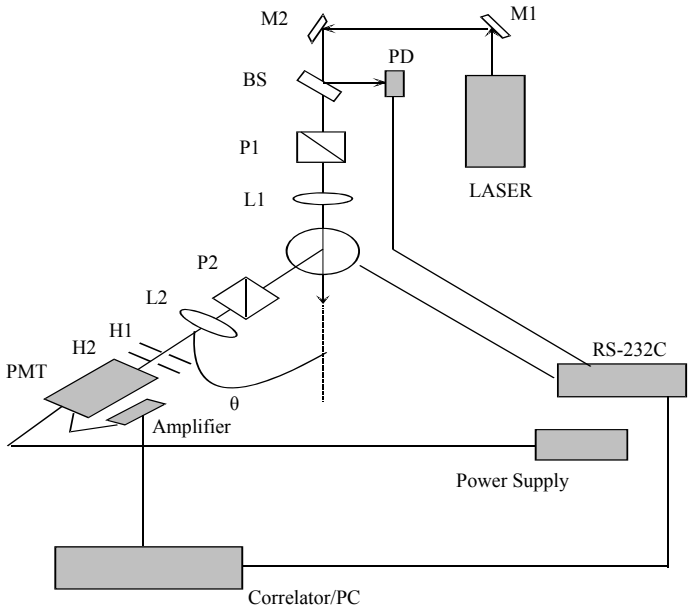

Figure 2.7: Experimental setup used in photon correlation spectroscopy.

2.4.4 Correlator

The correlator is the most important device of the photon correlation spectroscopy setup. It comprises an electronic card that calculates the correlation function[13, 14] of an electronic signal as following:

a) First, it counts the photoelectronic pulses n(t), during a storage time t_s (sample time), during the real time t of the experiment
b) Second, it lags the samples for integer multiplies of the sample time $\tau=kt_s$ (lag time)
c) Next, it multiplies the real time results with the lag time
d) Finally, it sums the products

From the above $n(q,t+\tau)n(q,t)$ is calculated over the duration of the whole measurement, for different values of τ while the photon correlation function is also calculated:

$$G(\tau) =< n(t+\tau)n(t) >= \lim_{T\to\infty} \frac{1}{T} \int_{-T}^{T} n(t+\tau)n(t)dt \qquad (2.21)$$

Which can be approximated by:

$$G(\tau) = \sum_{i=0}^{N-1} n_i n_{i+k} \qquad (2.22)$$

Normalization of the above equation gives:

$$G_{norm}(q,t) = \frac{< n(q,t)n(q,0) >}{< n(q,0) >^2} \qquad (2.23)$$

The photon correlator, used in this study, is an ALV-5000 Multi Tau Digital Correlator with 280 channels which can make $2x10^9$ multiplies/sums per second.

2.4.5 Autocorrelation function analysis

The autocorrelation function of a DEA based microgel particle at pH 10 and polymer concentration 0.005 wt% is shown in **Figure 2.8**. The above mentioned experimental setup was used for this measurment. The autocorrelation function in **Figure 2.8** is described with a simple exponential decay and can be fitted with a function of the form $C(q,t) = \alpha \exp(-t/\tau)$ which gives the intensity ($\sim\alpha$) and the relaxation time (τ).

The CONTIN analysis was used in order to analyze the correlation function. CONTIN[15, 16] takes $C(q,t)$ as an overlap of exponential decays:

$$C(q,t) = \int_{-\infty}^{\infty} L(\ln\tau)\exp(-t/\tau)d(\ln\tau) \qquad (2.24)$$

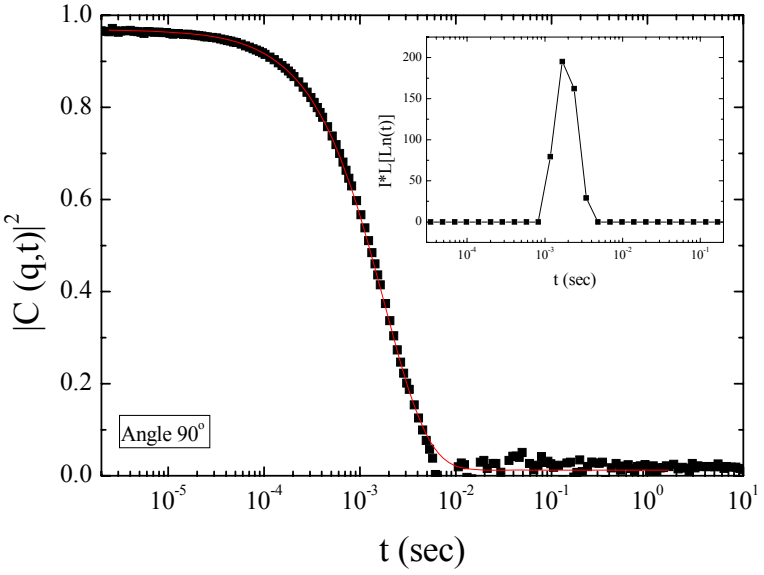

Figure 2.8: Autocorrelation function of a 0.005 wt% PDEA based microgel sample at 90° scattering angle and pH 10. The inset shows distribution of the relaxation times multiplied by the normalized intensity. The red line at the autocorrelation function is the fit by CONTIN analysis.

The chosen solution (see inset **Figure 2.8**) is that giving the minimum number of peaks and that with the best fit for C*(q,t)*. After choosing the best solution of the CONTIN, the Gaussian fit to each process, with the aid of Origin 7.0 graph and analysis software, is performed as shown in **Figure 2.9**. The parameters of the fit are shown in the inset of **Figure 2.9** where xc is the relaxation time and A is the area of each process at the specific angle. The area of each peak multiplied by the normalized scattered intensity calculates the intensity of each process from the equation:

$$I(\theta) = \frac{\bar{I}(\theta)}{I_{tol}(\theta)} \cdot \frac{A}{f^*} \tag{2.25}$$

where f^* is the spatial coherence factor mentioned above, $\bar{I}(\theta)$ is the mean intensity at θ angle, $I_{tol}(\theta)$ is the intensity of toluene at θ angle and A is the area of the process.

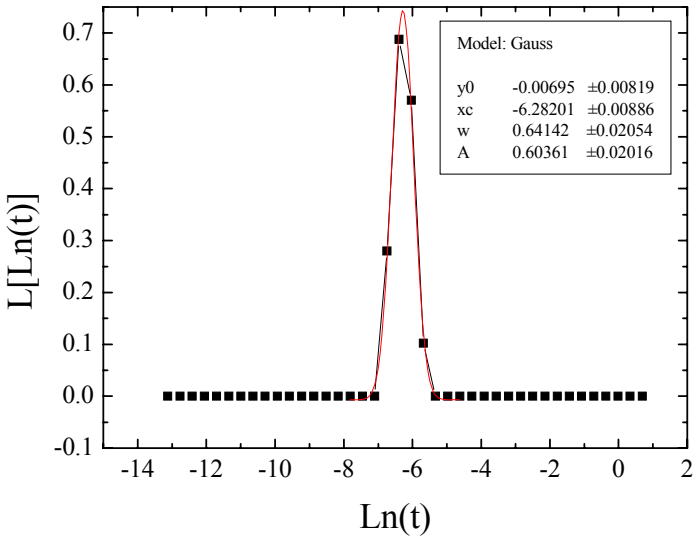

Figure 2.9: A characteristic inverse Laplace transformation and its Gaussian fit (red line) for a 0.005 wt% PDEA based microgel sample at 90^o scattering angle. The inset shows the Gaussian fit results.

Calculated results for a characteristic sample, are shown in **Figures 2.10** and **2.11**. The intensity of the process depends on the square of the wavelength (q^2). Such q-dependent processes can be fitted by Guinier's equation:

$$I(q) = I_o \cdot e^{-\frac{R_g^2 q^2}{3}} \tag{2.26}$$

where, R_g is the radius of gyration.

The output of the Guinier fit is I_o (scattered intensity at q=0) and the radius of gyration R_g of the scatterer.

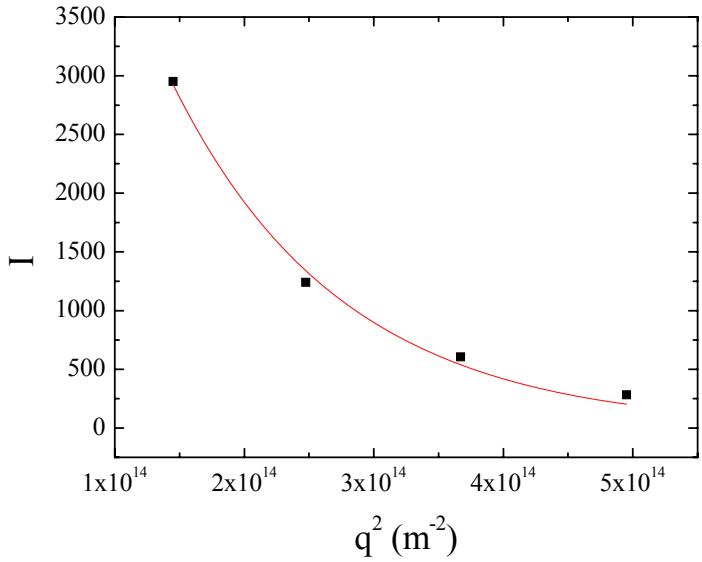

Figure 2.10: Scattered intensity as a function of q^2 for a 0.005 wt % PDEA based microgel sample at pH 10. The red line is the Guinier fit to the data.

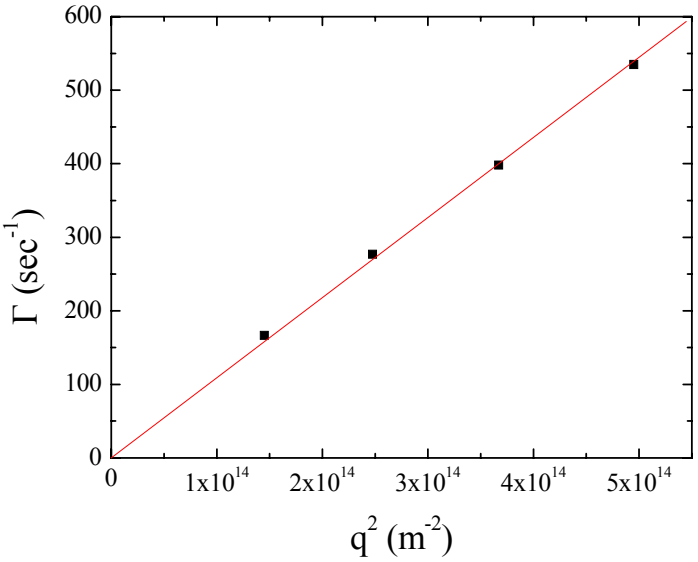

Figure 2.11: Rate as a function of q^2 for a 0.005 wt % PDEA based microgel sample at pH 10. The red line is the linear fit to the data.

The rate for each angle is calculated from equation:

$$\Gamma = \frac{1}{\tau} \tag{2.27}$$

where τ is calculated from the Gaussian fit of the inverse Laplace as mentioned above. A characteristic graph of Γ versus q^2 is shown in **Figure 2.11**. The red lines are the fits of the rate from equation:

$$\Gamma = D \cdot q^2 \tag{2.28}$$

where D is the diffusion coefficient and is calculated from the slope of the fit. The diffusion coefficient and the hydrodynamic radius R_H are related by the Stokes Einstein equation:

$$R_h = \frac{k_B T}{6\pi\eta D} \tag{2.29}$$

where η is the viscosity of the solvent, k_B is the Boltzmann constant and T is the temperature of the sample.

2.5 Transmission Electron Microscopy

Transmission electron microscopy (TEM) allows the visualization of the internal structure of specimens using transmitted electrons. A beam of highly focused electrons are directed toward a thinned sample. These highly energetic incident electrons interact with the atoms in the sample and produce characteristic radiation that is used in material characterization.[17]

Like all matter, electrons have both wave and particle properties. The expression that relates the motion of the electrons and their wavelength is:

$$\lambda = \frac{h}{mv} \tag{2.30}$$

where:

(h) Plank's constant

(m) electron mass

(v) electron velocity

Electrons are charged particles that can be accelerated by the application of an electrostatic field. Their velocity depends on the field and can be calculated by the expression:

$$\frac{mv^2}{2} = eV \qquad (2.31)$$

where:

(e) electron charge

(V) the accelerating voltage

Combining the above expressions and substituting with the relative constants the following expression is obtained:

$$\lambda(A) = \frac{12{,}3}{\sqrt{V(Volt)}} \qquad (2.32)$$

From this last expression, it is obvious that the wavelength can be tuned by adjusting the acceleration field and can become much smaller than that of light. Thus, microscopy using electrons offers a much greater resolving power than optical microscopy.

Transmission electron microscopy gives information about the size, shape and distribution of the phases that are present in a material. It also gives the distribution of the material elements, including segregation if present. It shows the crystal structure of the phases and the character of the crystal defects. However, it does have some limitations. Images of living systems cannot be obtained and the preparation of a specimen can be complicated and expensive.

2.5.1 The microscope

The incident electrons are usually generated by passing an electric current through a tungsten filament at the top of a column. A voltage, usually in the range 80-200 kV, is applied between the electron source (the cathode) and the rest of the column (the anode). This voltage accelerates the electrons down the column, towards the speciment (**Figure 2.12**). High potentials are necessary in order to give the electrons sufficient energy to penetrate the specimen.

Electromagnetic condenser coils collimate the beam, which then strikes the specimen. The specimen must be dry, solid, stable and capable of withstanding the heating effect of the electron beam. It must also be extremely thin and transparent to the beam.

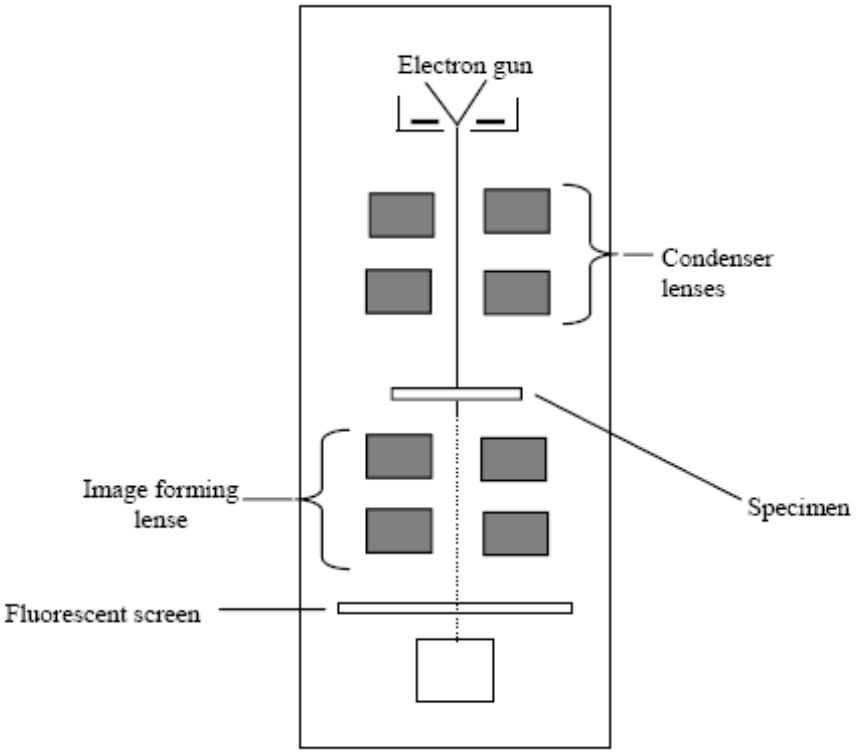

Figure 2.12: The transmission electron microscope (TEM).

Once the electron beam passes through the specimen it is magnified and focused by an image forming electromagnetic lens. It then strikes a fluorescent screen where the energy of the electrons is converted to visible light and the image is formed. Alternatively, the screen can be replaced by a camera so that a photographic image is recorded.

2.6 Scanning Electron Microscopy

The scanning electron microscope (SEM) is a type of electron microscope that images the sample surface by scanning it with a high-energy beam of electrons in a raster scan pattern.[17] The electrons interact with the atoms that make up the sample producing signals that contain information about the sample's surface topography, composition and other properties such as electrical conductivity.

The types of signals produced by a SEM include secondary electrons, back scattered electrons (BSE), characteristic x-rays, light (cathodoluminescence), specimen current and transmitted electrons. These types of signal require specialized detectors for their detection that are not usually all present on a single machine. The signals result from interactions of the electron beam with atoms at or near the surface of the sample. In the most common or standard detection mode, secondary electron imaging or SEI, the SEM can produce very high-resolution images of a sample surface, revealing details about 1 to 5 nm in size. Due to the way these images are created, SEM micrographs have a very large depth of field yielding a characteristic three-dimensional appearance useful for understanding the surface structure of a sample. A wide range of magnifications is possible, ranging from about x 25 (about equivalent to that of a powerful hand-lens) to about x 250,000, about 250 times the magnification limit of the best light microscopes. Back-scattered electrons (BSE) are beam electrons that are reflected from the sample by elastic scattering. BSE are often used in analytical SEM along with the spectra made from the characteristic x-rays. Because the intensity of the BSE signal is strongly related to the atomic number (Z) of the specimen, BSE images can provide information about the distribution of different elements in the sample. For the same reason BSE imaging can image colloidal gold immuno-labels of 5 or 10 nm diameter, that would otherwise be difficult or impossible to detect in secondary electron images in biological specimens. Characteristic X-rays are emitted when the electron beam removes an inner shell electron from the sample, causing a higher energy electron to fill the shell and release energy. These characteristic x-rays are used to identify the composition and measure the abundance of elements in the sample.

In a typical SEM, an electron beam is thermionically emitted from an electron gun fitted with a tungsten filament cathode. Tungsten is normally used in thermionic electron guns because it has the highest melting point and lowest vapour pressure of all metals, thereby allowing it to be heated for electron emission. The electron beam, which typically has an energy ranging from a few hundred eV to 40 keV, is focused by one or two condenser lenses to a spot about 0.4 nm to 5 nm in diameter. The beam passes through pairs of scanning coils or pairs of deflector plates in the electron column which deflect the beam in the x and y axes so that it scans in a raster fashion over a rectangular area of the sample surface (**Figure 2.13**).

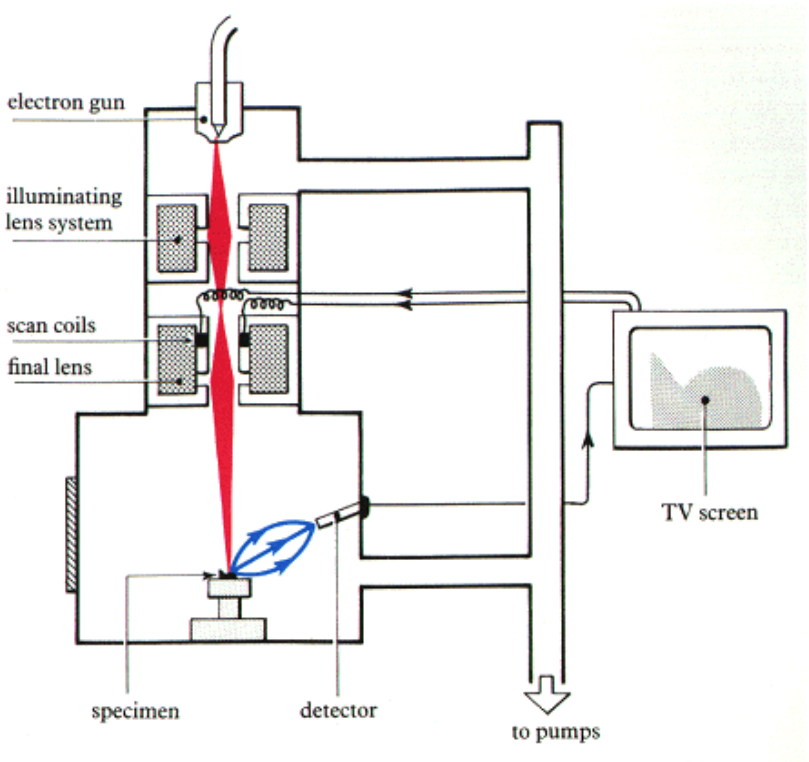

Figure 2.13: The scanning electron microscope (SEM).

When the primary electron beam interacts with the sample, the electrons lose energy by repeated random scattering and absorption within a teardrop-shaped volume of the specimen known as the interaction volume, which extends from less than 100 nm to around 5 µm into the surface. The size of the interaction volume depends on the electron's landing energy, the atomic number of the specimen and the specimen's density. The energy exchange between the electron beam and the sample results in the reflection of high-energy electrons by elastic scattering, emission of secondary electrons by inelastic scattering and the emission of electromagnetic radiation, each of which can be detected by specialized detectors. The beam current absorbed by the specimen can also be detected and used to create images of the distribution of specimen current. Electronic amplifiers of various types are used to amplify the signals which are displayed as variations in brightness on a cathode ray tube. The raster scanning of the CRT display is synchronised with that of the beam on the specimen in the microscope and the resulting image is therefore a distribution map of the intensity of the signal being emitted from the scanned area of the specimen. The image may be captured by photography from a high resolution cathode ray tube, but in modern

machines is digitally captured and displayed on a computer monitor and saved to a computer's hard disk.

For conventional imaging in the SEM, specimens must be electrically conductive, at least at the surface, and electrically grounded to prevent the accumulation of electrostatic charge at the surface. They are therefore usually coated with an ultrathin coating of electrically-conducting material, commonly gold, deposited on the sample either by low vacuum sputter coating or by high vacuum evaporation. Conductive materials in current use for specimen coating include gold, gold/palladium alloy, platinum, osmium, iridium, tungsten, chromium and graphite. Coating prevents the accumulation of static electric charge on the specimen during electron irradiation.

The spatial resolution of the SEM depends on the size of the electron spot, which in turn depends on both the wavelength of the electrons and the electron-optical system which produces the scanning beam. The resolution is also limited by the size of the interaction volume, or the extent to which the material interacts with the electron beam. The spot size and the interaction volume are both large compared to the distances between atoms, so the resolution of the SEM is not high enough to image individual atoms, as is possible in the shorter wavelength (i.e. higher energy) TEM. The SEM has compensating advantages, though, including the ability to image a comparatively large area of the specimen: the ability to image bulk materials (not just thin films or foils) and the variety of analytical modes available for measuring the composition and properties of the specimen. Depending on the instrument, the resolution can fall somewhere between less than 1 nm and 20 nm. In general, SEM images are easier to interpret than TEM images.

2.7 References

[1] Amalvy, J. I.; Wanless, E. J.; Li, Y.; Michailidou, V.; Armes, S. P.; Duccini, Y. *Langmuir* **2004**, *20*, 8992-8999.

[2] Jones, C. D.; Lyon, L. A. *Macromolecules* **2000,** *33*, 8301-8306.

[3] Li, Z.; Day, M.; Ding, J.; Faid, K. *Macromolecules* **2005**, *38,* 2620-2625.

[4] Skoog, D. A. *Analytical Chemistry: An Introduction* Brooks Cole 7th edition, August 23, 1999.

[5] Harris, D. C.; Harris, H. *Quantitative Chemical Analysis* W H Freeman & Co. 6th Edition, September 2003.

[6] Berne, B.; Pecora, R. *Dynamic Light Scattering,* Willey Interscience Pupblications, New York, 1976.

[7] Schmitz, K. S. *Dynamic Light Scattering by Macromolecules*, Academic Press, London, 1990.

[8] Doi, M.; Edwards, S. F. *The theory of polymer dynamics*, Science Publications, Oxford.

[9] Tyndall, J. *Phil. Mag.* **1869**, *37*, 364; **1869**, *38*, 156.

[10] Rayleigh, Lord, *Phil. Mag.* **1899**, *47*, 375; **1910**, *A84*, 25; **1914***, A90*, 219; **1919**, *A94*, 296.

[11] Smoluchowski, M. *Ann. Phys.* **1908**, *25*, 205.

[12] Einstein, A. *Ann. Phys.* **1910**, *33*, 1275.

[13] ALV-5000, Multiple Tau, Digital Correlator. User`s Rerference Manual.

[14] Schatzel, K. *Single-photon correlation techniques in Dynamic Light Scattering. The Method and some Applications* Ed. W. Brown, Oxford University Press, 1993.

[15] Provencher, S. W. *Computer Physics Communications* **1982**, *27*, 213; **1982**, *27*, 229.

[16] Provencher, S. W. *Macromol. Chem.* **1979**, *180,* 201.

[17] Faust, B. *Modern Chemical Techniques* Education Division, The Royal Society of Chemistry, London

Chapter 3

3.1 Responsive microgel particles

3.1.1 Microgel synthesis

In the present study we have synthesized by emulsion polymerization, homopolymer, mix and core-shell microgel particles based on a basic monomer, DEA and an acidic monomer, MAA. DEA is a hydrophobic, pH-sensitive monomer which behaves as a weak base in water due to its tertiary amine group. Thus, DEA is hydrophobic at high pH when it is in its neutral form while it becomes hydrophilic and positively charged at low pH upon protonation of the tertiary amine group. An effective equilibrium constant, $pK_\alpha = 7$, has been reported for the protonation of PDEA[1] which means that for pH values above 7 the polymer is neutral and hydrophobic while for pH below 7 it becomes positively charged and hydrophilic.(**Figure 3.1**)

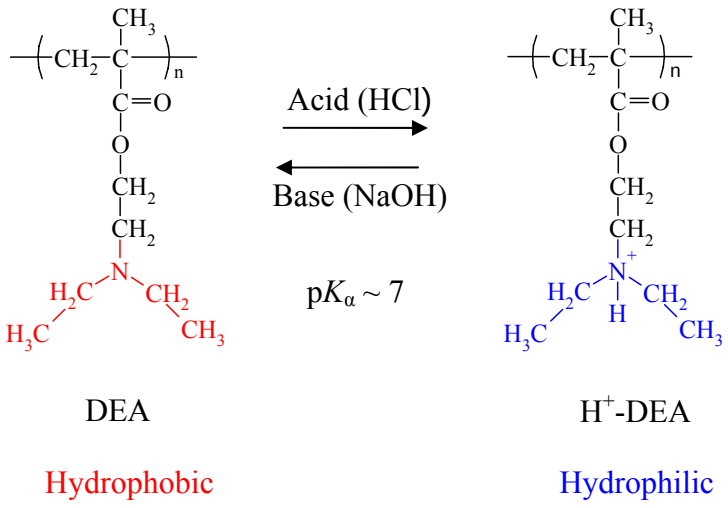

Figure 3.1: Protonation / deprotonation process of PDEA homopolymer.

The second monomer used was *t*-BuMA, which is also hydrophobic. *t*-BuMA is a protected ester and upon acid hydrolysis gives MAA which is hydrophilic and carries a carboxylic acid group. Thus MAA can be neutralized and becomes negatively charged at high pH values. An effective equilibrium constant pK_α = 5.5 has been reported for the neutralization process of PMAA[2] which means that for pH values below 5.5 the polymer is protonated and neutral while for pH above 5.5 it becomes neutralized and anionic. (**Figure 3.2**)

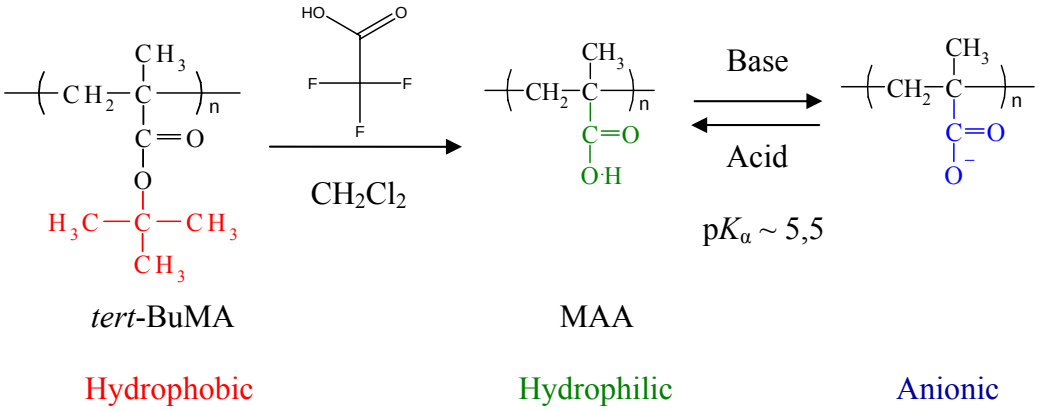

Figure 3.2: Deprotection reaction of P(*t*-BuMA) and reversible ionization process of PMAA homopolymer.

First we synthesized two homopolymer microgels based on DEA in which we have varied the monomer concentration in the feed at 5 and 10 wt % while keeping the concentration of the initiator, cross-linker and stabilizer constant. Next, we prepared four PDEA-based microgel samples at a constant monomer (5 wt %), and stabilizer concentration in which we have varied systematically the amount of the cross-linker (EGDMA) between 0.5 and 3 wt % based on the monomer. Moreover, we have synthesized a homopolymer microgel sample based on *t*-BuMA using 1 wt % cross-linker and after the deprotection of the *t*-BuMA segments and the cleavage of the *t*-butyl groups we obtained a PMAA-based microgel sample.

Furthermore, we have synthesized a more complex microgel structure with the DEA and the *t*-BuMA monomer units randomly distributed within the gel particle. We called this microgel, a mix microgel and following the deprotection of the *t*-BuMA segments to MAA units we obtained mix polyampholyte P(DEA-MAA) microgel particles. It should be noted that the hydrolysis of the *t*-BuMA segments to MAA does not affect the DEA segments of the microgels, as reported in earlier studies.[3,4] Finally, have also prepared even more complex

microgel particles with a core-shell topology which comprise a core consisting of one of the two monomers (DEA or MAA) and a shell consisting of the other monomer (MAA or DEA, respectively). Again, we used *t*-BuMA as the hydrophobic monomer for the microgel synthesis, which after the hydrolysis of the *tert*-butyl groups gave the carboxylic moieties and thus acid-containing microgels. The latter are polyampholyte microgel particles with a core-shell morphology in which the basic and acidic components of the microgels are spatially separate, located in the core or the shell of the particles. To the best of our knowledge, these are unique materials the synthesis of which has not been reported in the literature before. Thus their synthesis and characterization which is the aim of the present work is novel and results in new materials with interesting tunable properties as discussed later in this study. The microgel particles synthesized in this work and the mass fractions of the reagents used for their synthesis are summarized in the **Table 3.1**.

Table 3.1: Microgel samples synthesized and mass fraction of the reagents used in each case.

Sample	wt % DEA	wt % *t*-BuMA	Microgel Composition (mole %) DEA-*t*-BuMA	wt % EGDMA (based on monomers)	wt % $K_2S_2O_8$ (based on monomers)
5% DEA	5	0	100 - 0	1	1
10% DEA	10	0	100 - 0	1	1
5% DEA 0.5% EGDMA	5	0	100 - 0	0.5	1
5% DEA 1% EGDMA	5	0	100 - 0	1	1
5% DEA 2% EGDMA	5	0	100 - 0	2	1
5% DEA 3% EGDMA	5	0	100 - 0	3	1
8.33 % *t*-BuMA	0	8.33	0 - 100	1	1
mix DEA / *t*-BuMA	5	5	43 - 57	1	1
core DEA-shell *t*-BuMA	2	2	43 - 57	1	1
core *t*-BuMA-shell DEA	2	2	43 - 57	1	1

3.2 Ionization and swelling properties of the homopolymer microgel particles

3.2.1 PDEA-based microgel particles

3.2.1.1 Effect of monomer concentration

The effect of the monomer concentration in the feed on the latex particle size obtained was investigated first by DLS, for the two microgel samples prepared at 5 wt % and 10 wt % DEA. To ensure that potential strong interparticle interactions will not affect the light scattering results the concentration of the microgel was kept sufficiency low at c=0.005 wt % for both microgels. **Figure 3.3** illustrates the intensity autocorrelation functions, C(q,t), of the

two microgel solutions at 0.005 wt %. The corresponding inverse Laplace transformations are also shown in the inset.

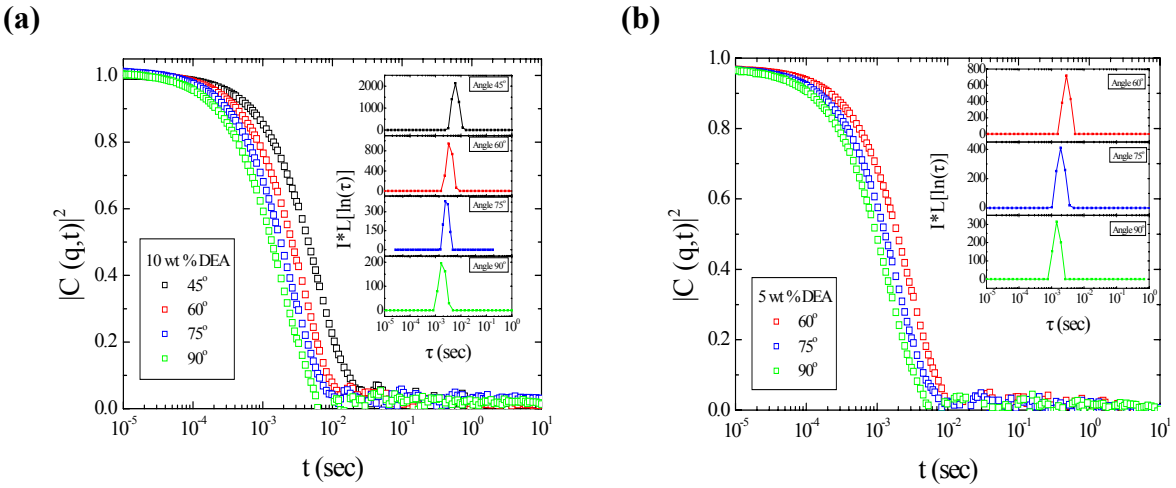

Figure 3.3: Intensity autocorrelation functions, C(q,t), of a 0.005 wt % microgel sample prepared using 10 wt % (a) and 5 wt % (b) DEA in the feed. Inset: distributions of relaxation times multiplied by total scattering intensities (normalized to that of toluene).

For both samples a single process with very strong intensity and dynamics dominates the autocorrelation functions. From the corresponding inverse Laplace transformations the diffusion coefficients and the hydrodynamic radii of the processes were calculated. For the 10 wt % DEA microgel a process with a diffusivity $D=1.09 \times 10^{-8}$ cm^2/sec which corresponds to a hydrodynamic radius R_h = 201 nm was calculated, while for the 5 wt % DEA microgel the diffusivity of the process $D=1.39 \times 10^{-8}$ cm^2/sec corresponding to a hydrodynamic radius R_h = 154 nm was found. The particle volume ratio for the two samples was thus calculated as ($200^3/154^3 = 2.2$) which is in good agreement with the volume ratio of the monomer used in the feed for the samples. This result suggests a good control of the latex particle nucleation and growth during synthesis and presents an efficient method to control the initial microgel particle size, by varying the amount of the monomer in the feed at a constant stabilizer concentration.

Next, we examined the effect of the degree of ionization of the DEA units on the swelling behaviour of the two microgels discussed above. The change in the hydrodynamic size of the microgel particles upon the addition of hydrochloric acid which causes the protonation of the tertiary amine groups was followed by DLS. **Figure 3.4** shows the

hydrodynamic radii of the two PDEA microgels as a function of the effective degree of ionization of the DEA units assuming that all added HCl protonates the tertiary amine groups.

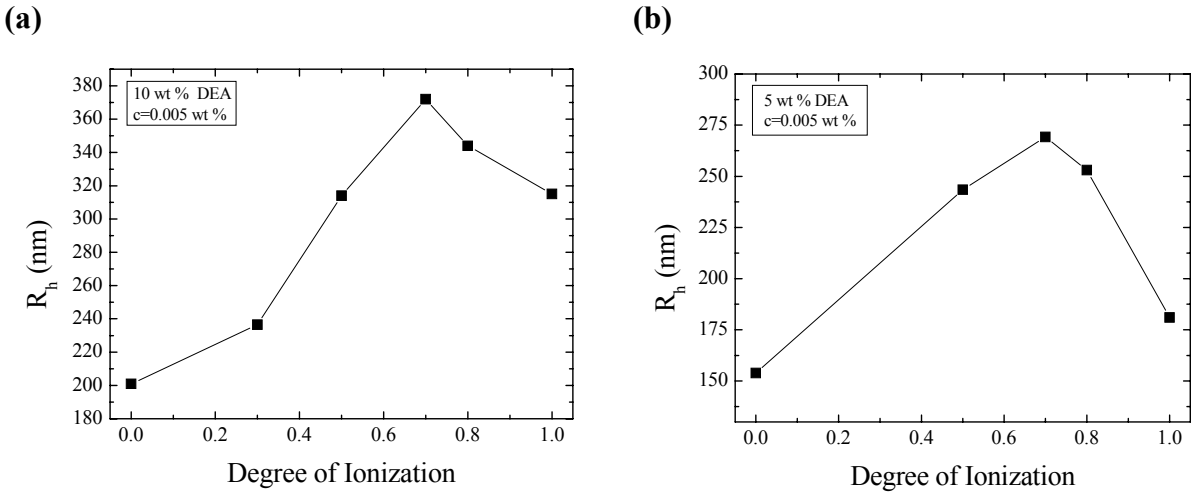

Figure 3.4: Hydrodynamic radii of the PDEA microgel particles as a function of the degree of ionization of the monomer units for 10 wt % DEA (a) and 5 wt % DEA (b) in the feed.

For both microgel samples the hydrodynamic radius of the particles was found to increase with the degree of ionization of the monomer units. This swelling of the microgels was attributed to the increase of the hydrophilicity of the polymer upon ionization of the DEA moieties and to the electrostatic repulsive forces developed between the positively charged monomer units which allow water to enter into the microgel particles. Besides, ionization creates an osmotic pressure within the microgels due to the counterions to the charged monomer units and causes the microgels to swell.[5] The decrease in the hydrodynamic size observed at high effective degrees of ionization for both microgels is attributed to the increase of the ionic strength of the solution upon the addition of excess acid. This causes screening of the electrostatic repulsive forces among the similarly charged DEA units and results in the shrinkage of the microgels. It is interesting to note that the maximum degree of swelling for both microgels is observed at degree of ionization 0.7 suggesting that at this ionization value the swelling due to ionization is counterbalanced by the ionic strength of the solution which causes the shrinkage of the microgels. From the swelling curves in **Figure 3.4** the maximum volumetric swelling factors for the two microgels were calculated as the cube of the ratio of the microgel radius at maximum swelling when ionized, to that of the collapsed hydrophobic latex particles at degree of ionization equal to zero. A volumetric swelling factor of 6.4 was found for the 10 wt % DEA microgel sample while for the 5 wt % DEA microgel the

volumetric swelling factor was 5.4. The similar values obtained for the volumetric swelling factor for the two samples suggest a similar swelling behaviour for the two microgels.

3.2.1.2 Influence of the cross-link density

The effect of the cross-link density of the microgel particles on their ionization and swelling behaviour was also examined for four PDEA-based microgels prepared at a 5 wt % monomer concentration and 0.5, 1, 2 and 3 wt % cross-linker based on the monomer. The ionization properties were investigated first by potentiometric titrations. **Figure 3.5** shows the potentiometric titration curve for the PDEA microgel prepared with 1 wt % EGDMA cross-linker at c=0.1 % wt.

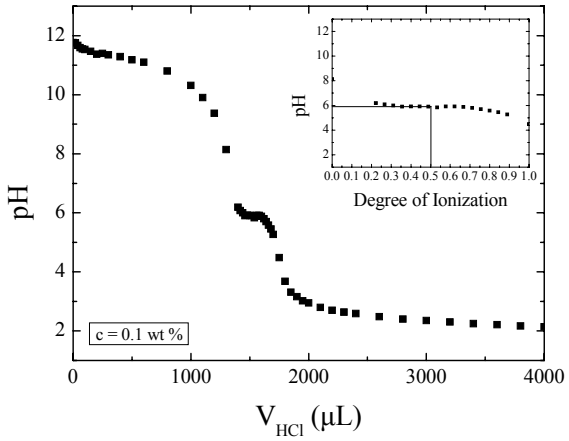

Figure 3.5: Potentiometric titration curve for the PDEA microgel with 1wt % cross-linker. Inset: The plateau region plotted as the pH versus the effective degree of ionization.

The appearance of a plateau region around pH ~ 6 signifies the protonation of the DEA units upon lowering the solution pH by the addition of HCl. The effective pK_α of the microgels was calculated from this plateau region plotted as the pH versus the effective degree of ionization, α_{eff} ($0 < \alpha_{eff} < 1$) of the DEA moieties, as the pH at 50% ionization (see inset). The effective pK_α for the PDEA particles prepared with 1wt % EGDMA was found 5.9. **Figure 3.6a** shows the plateau regions obtained from the titration curves for all four PDEA samples. From these plateau regions the effective pK_α values were calculated for the PDEA microgels and are plotted in **Figure 3.6b** as a function of the cross-link density of the microgels.

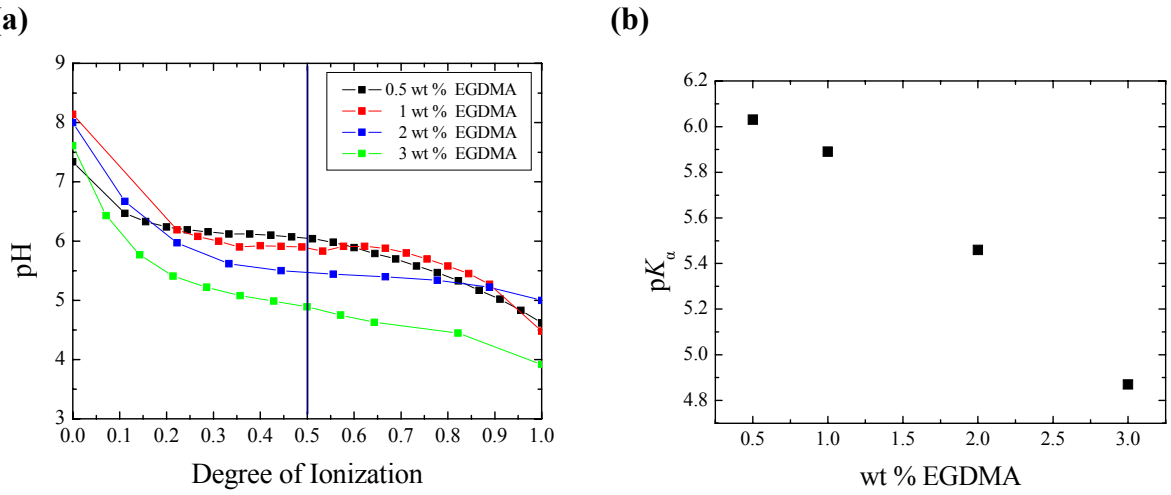

Figure 3.6: The plateau region of the titration curves plotted as the pH versus the effective degree of ionization for the four PDEA microgels (a) and the effective pK_α values calculated for the four PDEA microgels as a function of their cross-link density (b).

The effective pK_α values of the DEA units in all conetworks are significantly lower than the intrinsic dissociation constant of the PDEA homopolymer (pK_α ~ 7) due to the stronger polyelectrolyte effect in the gel phase. Moreover, the effective pK_α values were found to decrease from 6 to 4.9 as the cross-link density of the microgels increased from 0.5 to 3 wt % EGDMA suggesting that the protonation of the DEA units is progressively hindered by the increase of the cross-link density of the microgel. This is attributed to the polyelectrolyte effect and the Donnan equilibrium within the gel phase which became more important as the degree of cross-linking of the microgels increases.[6,7]

Next, we investigated the effect of the ionization of the DEA units on the swelling of the four by DLS. **Figure 3.7** shows the hydrodynamic radii of the PDEA microgels as a function of the effective degree of protonation of the tertiary amine groups.

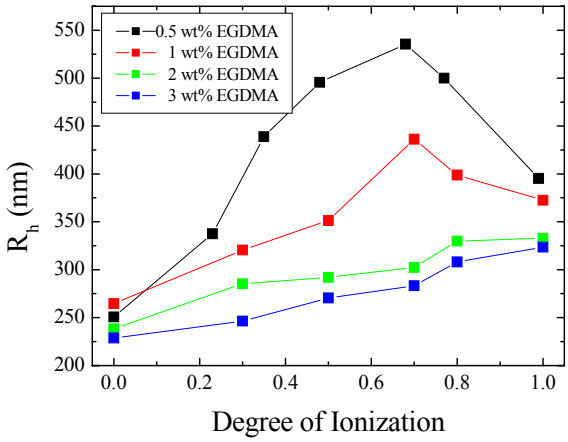

Figure 3.7: Hydrodynamic radii of the PDEA microgel particles as a function of the degree of ionization of the monomer units.

For all microgels the hydrodynamic radius was initially found to increase with the degree of ionization of the monomer units. This behaviour is similar to that discussed above for the PDEA microgels and was attributed to the electrostatic repulsive forces among the positively charged DEA moieties and the osmotic pressure within the microgels due to the counterions to the charged monomer units which cause the microgels to swell. Furthermore, the degree of swelling progressively decreases as the degree of cross-linking of the microgels increases, as expected. The decrease in the hydrodynamic size observed at high effective degrees of ionization for the microgels with 0.5 and 1 wt % EGDMA is attributed to the increase of the ionic strength of the solution upon the addition of the excess acid. This causes screening of the electrostatic repulsive forces among the similarly charged DEA units and results in the shrinkage of the microgels. Such a decrease in the degree of swelling is not observed for the microgels with 2 and 3 wt % EGDMA, possibly due to their lower degrees of swelling which result in a decrease in ion partitioning within the gel phase and thus in a less effective screening of the repulsion forces. From these swelling curves the maximum volumetric swelling factors of the microgels were calculated as the cube of the ratio of the microgel radius at maximum swelling when ionized to the radius of the collapsed hydrophobic latex particles at degree of ionization equal to zero. The volumetric swelling factor was found to decrease from 9.7 for the microgel with 0.5 wt % EGDMA to 5.8, 2.9 and 2.7 for the microgels with 1, 2 and 3 wt % EGDMA, respectively. This suggests that the microgels swell two and three times more when the cross-linker decreases by 2 and 4 times, respectively. Above 2 wt % of cross-linker the effect of the cross-linking on the degree of swelling is negligible.

The swelling process is accompanied by a change in the turbidity of the sample from milky-white in the collapsed state to clear-transparent for the swollen microgel. Furthermore, a change in the pH of the transparent solution to an effective degree of ionization equal to zero induces an increase in turbidity suggesting the reversibility of the swelling-deswelling process. **Table 3.2** summarizes the characteristics of the four PDEA microgels of different cross-link densities.

Table 3.2: Characteristics of the PDEA microgels of different cross-link densities.

wt % EGDMA	Effective pK_α	R_h (minimum)	R_h (maximum)	Volumetric swelling factor
0.5	6.03	250 nm	535 nm	9.7
1	5.89	264 nm	440 nm	5.8
2	5.46	238 nm	339 nm	2.9
3	4.87	229 nm	319 nm	2.7

3.2.2 PMAA-based microgel particles

In this study we have also prepared microgels based on PMAA. In order to obtain the PMAA-based microgels, *t*-BuMA which is a protected form of MAA was used. The *t*-BuMA microgels were deprotected by acid hydrolysis using trifluoroacetic acid in dichloromethane and were subsequently transferred in water. The aqueous solution behaviour of the microgel particles before and after deprotection was investigated as a function of solution pH by potentiometric titrations at a microgel concentration c=0.1 wt % while their swelling behaviour was studied by DLS at c=0.005 wt %.

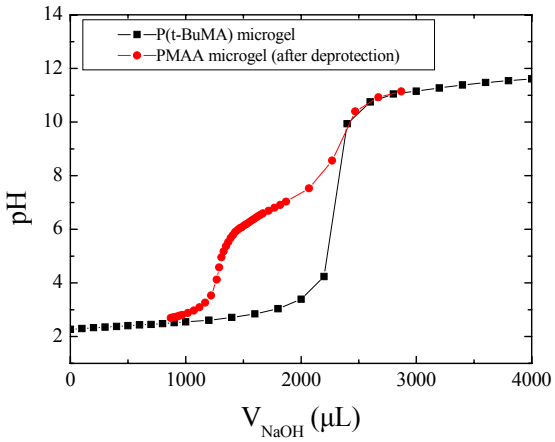

Figure 3.8: Potentiometric titration curves for the P(*t*-BuMA) microgels with 1 wt % cross-linker before (black squares) and after (red circles) deprotection.

Figure 3.8 shows the potentiometric titration curves for the P(*t*-BuMA) microgels prepared using 1 wt % EGDMA before and after the acid hydrolysis of the ester groups. Before deprotection the *t*-BuMA moieties are not affected by the changes in the solution pH and thus the titration curve is very similar to that obtained for water brought to pH 2 with the addition of HCl. However, after deprotection a plateau region is observed in the titration curve of the microgel at around pH 7 signifying the presence of the methacrylic acid groups which possess a weak acid character and thus participate in an acid-base equilibrium. The presence of the plateau region verifies the successful deprotection of the ester groups and the formation of the PMAA microgel particles. The effective pK_α value for the acidic microgel particles was calculated from this plateau region as the pH at 50% ionization and was found to be 7.2. This value is significantly higher than the effective dissociation constant of PMAA homopolymer (pK_α ~ 5.5) and this is again attributed to the polyelectrolyte effect and the Donnan equilibrium which hinder the neutralization of the MAA units within the gel phase, as discussed above for the PDEA microgels.

Figure 3.9a shows the intensity autocorrelation functions for a 0.005 wt % P(*t*-BuMA) microgel sample at different scattering angles. The insets show the distribution of the relaxation times for the different angles. A single process with very strong intensity and diffusive dynamics dominates the autocorrelation functions. From the wavevector dependence of the rates of this process (**Figure 3.9b**), the diffusion coefficient D was calculated $D=1.24\times10^{-8}$ cm^2/sec corresponding to hydrodynamic radius, R_h = 177 nm which was attributed to the hydrophobic P(*t*-BuMA) latex particles.After the deprotection the hydrodynamic radius of the PMAA microgel particles was also determined by DLS. **Figure 3.10a** shows the intensity autocorrelation functions for a 0.005 wt % PMAA microgel sample at different scattering angles. Again a single process with very strong intensity and dynamics is observed with diffusivity $D=1.10\times10^{-8}$ cm^2/sec (**Figure 3.10b**) corresponding to hydrodynamic radius, R_h = 200 nm attributed to the deprotected PMAA microgel particles.

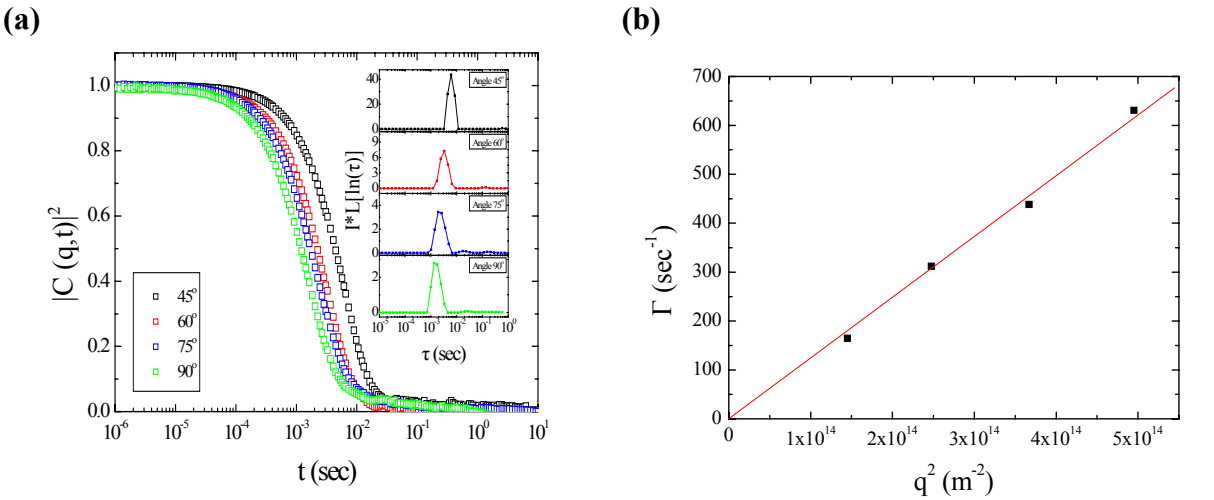

Figure 3.9: Intensity autocorrelation functions for a 0.005 wt % P(*t*-BuMA) microgel sample at different scattering angles. Inset: distribution of relaxation times multiplied by the total scattering intensity (normalized to that of toluene) for the respective angles (a), Wavevector dependence of the rate of the process (b).

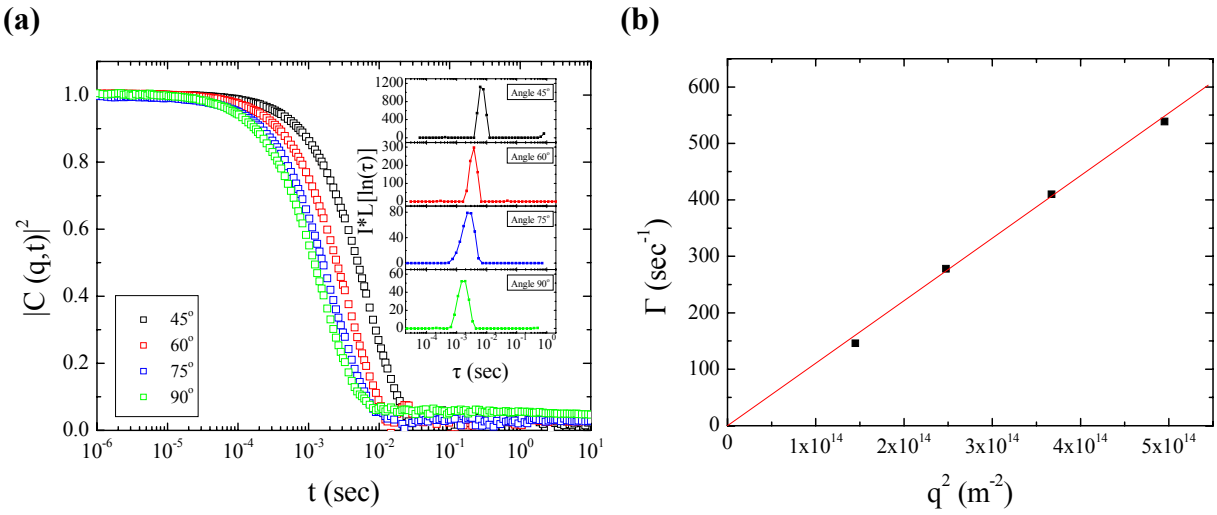

Figure 3.10: Intensity autocorrelation functions for a 0.005 wt % PMAA microgel sample after deprotection. Inset: distribution of relaxation times multiplied by the total scattering intensity (normalized to that of toluene) for the respective angles (a), Wavevector dependence of the rate of the process (b).

The 23 nm increase in size from the hydrophobic P(*t*-BuMA) latex particles to the PMAA microgels is attributed to the hydrophilic nature of MAA, even in its neutral form, which causes the particles to swell. The volumetric swelling factor was calculated to be 1.44 suggesting a 44 % increase in the particle volume upon deprotection. However, hydrogen

bonding interactions among the protonated MAA units prohibit extensive swelling and result in the small particle size increase found for the neutral PMAA microgels.

Following acid hydrolysis of the ester groups, the PMAA microgels formed were characterized in terms of their swelling behavior as a function of the degree of neutralization of the acidic moieties by the addition of base (0.1 M NaOH). **Figure 3.11** shows the hydrodynamic radii and the scattering intensities at 45^o versus the effective degree of ionization of the MAA units obtained by DLS for the PMAA microgels.

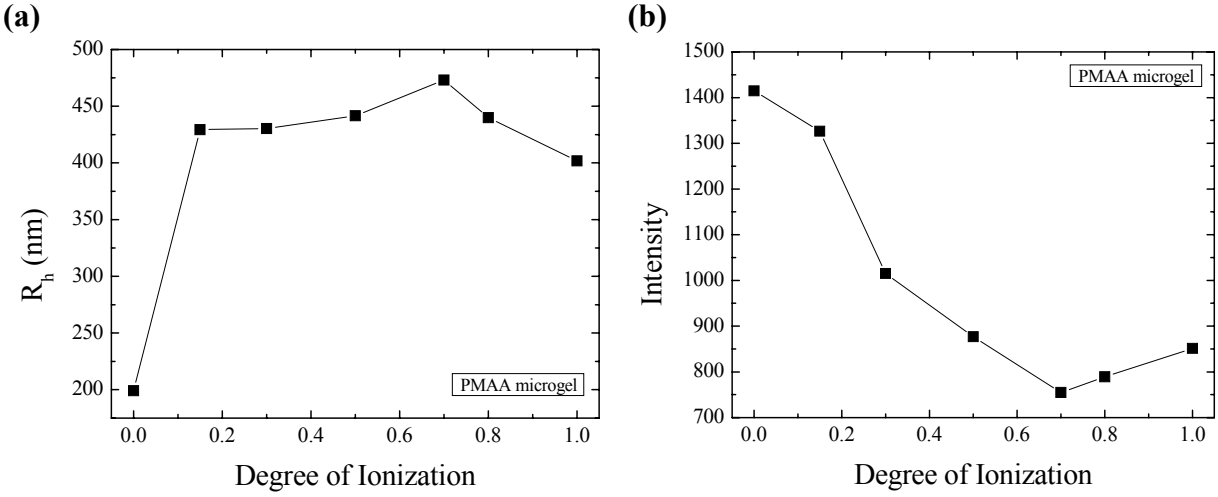

Figure 3.11: Hydrodynamic radii (a) and scattering intensities at 45^o scattering angle (b), for a 0.005wt % PMAA microgel dispersion as a function of the degree of ionization of the monomer units.

When the microgel becomes ionized the particle size increases abruptly upon neutralization of the MAA units. This is due to the electrostatic repulsive forces among the charged monomer units and the increase in the osmotic pressure created within the microgels due to the counterions to the charged monomer units as discussed above for the PDEA microgel particles. The observed decrease in the hydrodynamic size at high degrees of ionization is attributed again to the increase in the ionic strength of the solution which screens the electrostatic repulsions and causes the microgels to shrink. The maximum volumetric swelling factor, calculated as the cube of the ratio of the microgel radius at maximum swelling to that in the collapsed state at degree of ionization equal to zero, was found to be 13.4 which is more than twice the value calculated for the respective PDEA microgel particles prepared with 1 wt % EGDMA. This is attributed to the more hydrophilic nature of the neutralized MAA units compared to that of the ionized DEA moieties. Moreover, the PMAA

microgels exhibit a much sharper swelling transition at lower degrees of ionization compared to the PDEA microgels.

The scattering intensity shown in **Figure 3.11b** was found to decrease as the degree of ionization of the microgels increased and reached a minimum at $\alpha = 0.7$ after which it increased again slightly. In order to explain the observed changes in the scattering intensity, which at first glance seem anomalous considering the increase in the particle (scatterer) size with the degree of ionization, a second effect should be considered. This is the decrease in the refractive index mismatch between the solvent and the water swollen polymer particles as solvent molecules enter the microgels upon swelling. The results suggested that the refractive index matching upon ionization dominated the scattering intensity and prevailed over the effect of the particle size on the scattering intensity. This is also consistent with the optical observation of the change in the turbidity of the sample from milky-white in the collapsed state to clear-transparent for the swollen microgel, discussed above for the PDEA microgels and observed again here for the PMAA particles.

3.3 Ionization and swelling behaviour of the mix microgel particles

Polyampholyte mix microgel particles comprising DEA basic and MAA acidic monomer units randomly distributed within the gel phase were prepared. *t*-BuMA was used again as the protected form of MAA which after acid hydrolysis using trifluoroacetic acid in dichloromethane gave the MAA units, as described above. The composition of the two monomers in the feed was 56 - 44 mole % *t*-BuMA-DEA. The aqueous solution behaviour of the mix microgel particles was investigated as a function of solution pH by potentiometric titrations at a microgel concentration c=0.1 wt % while their swelling behaviour was studied by DLS, as described above for the homopolymer microgels.

Figure 3.12a shows the intensity autocorrelation functions for a 0.005 wt % mix PDEA-P(*t*-BuMA) microgel sample at different scattering angles. The inset shows the distribution of relaxation times for the different angles. A single process with very strong intensity and diffusive dynamics dominates the autocorrelation functions. The diffusion coefficient for this process was found $D=1.29 \times 10^{-8}$ cm^2/sec corresponding to a hydrodynamic radius, R_h = 170 nm which is attributed to the diffusion of the hydrophobic mix PDEA-P(*t*-BuMA) latex particles. **Figure 3.12b** shows the intensity autocorrelation functions for a 0.005 wt % mix PDEA-PMAA microgel sample, after deprotection, at different scattering angles. The inset shows the distribution of relaxation times for the different angles. A single process with very strong intensity and diffusive dynamics dominates the autocorrelation functions.

The diffusion coefficient for this process was found D=1.18x10^{-8} cm^2/sec corresponding to a hydrodynamic radius, R_h = 185 nm. The increase in the size of the microgel after deprotection is attributed to the more hydrophilic nature of MAA compared to *t*-BuMA similar to the discussion above for the homopolymer PMAA microgel. However, the volumetric swelling factor of the mix microgel due to hydrolysis of the hydrophobic *t*-BuMA units cannot be compared to that found for the P(*t*-BuMA) homopolymer microgel upon hydrolysis because the mix microgel exhibits a complex ionization behaviour, discussed below, and cannot be found in the neutral form.

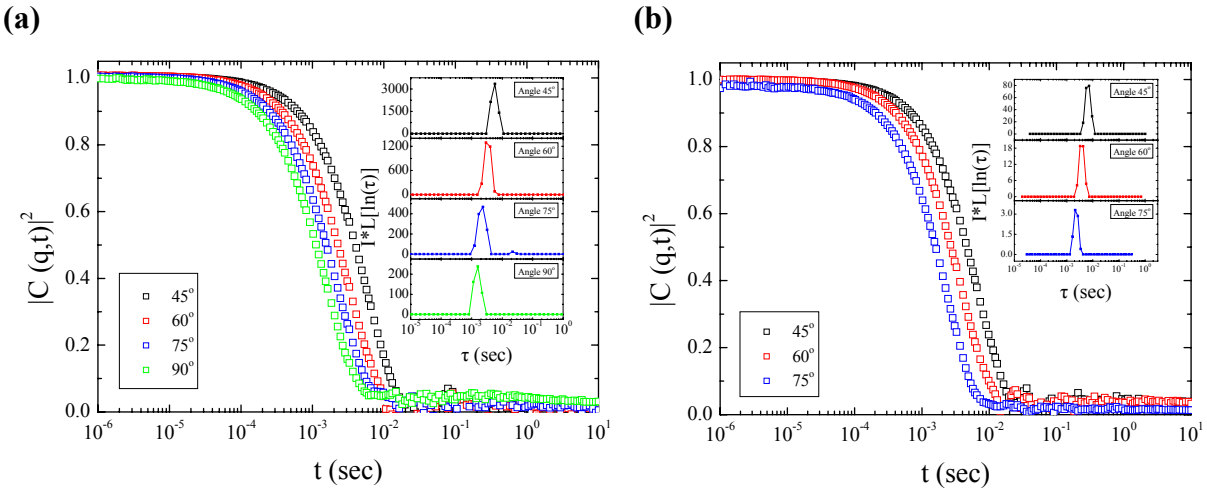

Figure 3.12: Intensity autocorrelation functions of a 0.005 wt % mix PDEA-P(*t*-BuMA) microgel sample before (a) and after (b) deprotection. Insets: distribution of relaxation times multiplied by the total scattering intensity (normalized to that of toluene) for the respective angles.

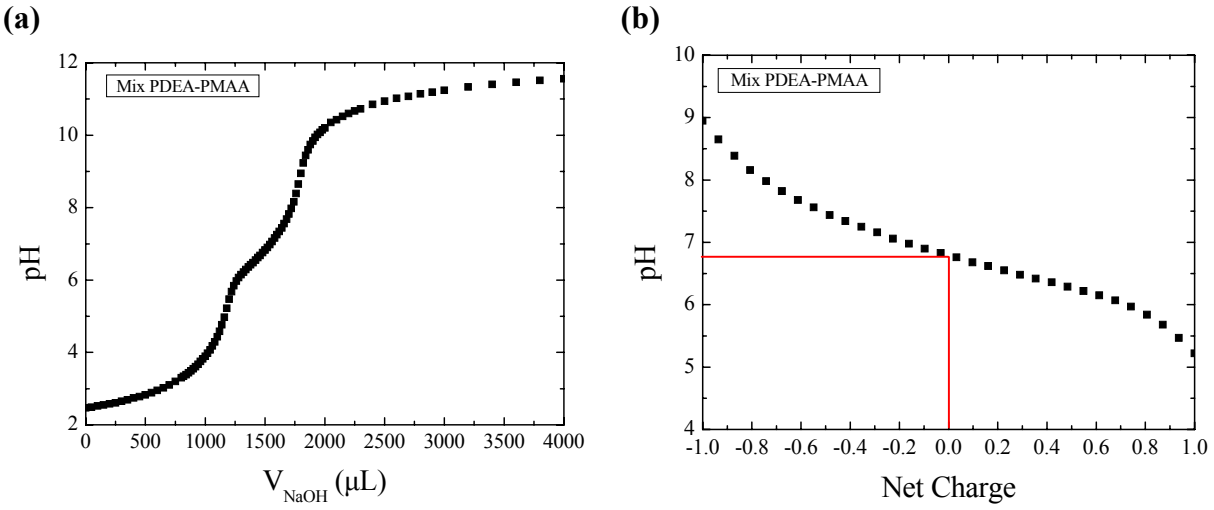

Figure 3.13: Potentiometric titration curve for the mix PDEA-PMAA microgel with 1 wt % cross-linker (a) and the plateau region plotted as the pH versus the net charge of the microgel (b).

Figure 3.13a shows the potentiometric titration curve for the mix PDEA-PMAA microgel prepared using 1 wt % EGDMA and after the acid hydrolysis of the ester groups. A plateau region is observed in the titration curve of the microgel at around pH 7 signifying the presence of the tertiary amine and the methacrylic acid groups which behave as weak base and weak acid respectively and participate in an acid-base equilibrium. It is important to note that a single plateau region is observed in the titration curve signifying the deprotonation of both ionizable groups, DEA and MAA, simultaneously. This is attributed to the similar pK_α values obtained for the two respective homopolymer microgels, pK_α = 5.9 for the PDEA and pK_α = 7.2 for the PMAA particles. In **Figure 3.13b** the plateau region of **Figure 3.13a** is plotted as the pH versus the net charge of the microgel. It is assumed that the added base is all used to either deprotonated the DEA units or neutralize the MAA groups. Thus a net charge of +1 (low pH) signifies that all DEA units in the microgel are protonated and positively charged and all MAA residues are also protonated and neutral. The decrease in the net charge signifies that either the DEA units become deprotonated and neutral or the MAA moieties become neutralized and thus negatively charged resulting in a lower overall net charge. At net equal to zero (pH = 6.8) the number of protonated DEA units is equal to that of the neutralized MAA groups. After this point (higher pH) the number of negatively charged MAA units is higher compared to the positively charged DEA groups resulting in an excess of negative charge in the microgel. Finally, a net charge equal to -1 signifies fully neutralized MAA units and deprotonated neutral DEA groups.

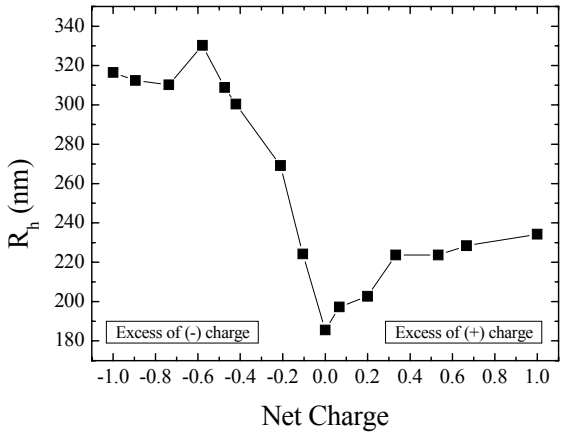

Figure 3.14: Hydrodynamic radii for a 0.005 wt % mix PDEA-PMAA microgel dispersion as a function of the microgel net charge.

Figure 3.14 shows the hydrodynamic radii obtained by DLS, for the PDEA-PMAA mix microgel, as a function of the microgel net charge. The left part corresponds to the

ionization of MAA units at high pH values and thus to a negative net charge while the right part represents the protonation of the DEA units at low pH values where the net charge is positive. The net charge is zero at the isoelectric point, where the number of positively charged DEA units is equal to the number of negatively charged MAA units as discussed above. As seen in **Figure 3.14** the microgel swells at both high and low pH when the particle net charge is different than zero and thus possesses an excess of either positive or negative charge. This swelling is due to the electrostatic repulsions and the osmotic pressure created within the microgel as discussed above for the ionized homopolymer microgels. Moreover, a minimum in the size of the microgel is observed at net charge equal to zero, the isoelectric point, which is attributed to charge neutralization resulting in the collapse of the microgel in the aqueous medium similar to the behavior of protein molecules at their isoelectric point. From **Figure 3.14** we can also observe that the microgel swells more for negative net charge compared to its swelling at positive net charge. This is attributed partially to the higher mole fraction of MAA in the microgel (56 mole %) compared to DEA (44 mole %) and to the more hydrophilic nature of the ionized MAA units compared to the protonated DEA moieties as discussed above for the homopolymer microgels.

The calculated volumetric swelling factors for this microgel were found 5.6 and 2.1 for a negative and positive net charge, respectively. These values are more than two times lower than the respective values calculated for the homopolymer microgels discussed above (13.4 for the PMAA and 5.8 for the PDEA microgel). This result can be explained by the mix character of the microgel. Thus at high pH values (negative net charge) the microgels comprise an excess of ionized MAA units which cause its swelling and also positive and neutral (hydrophobic) DEA units which lead to the microgel collapse. On the other hand, at low pH (positive net charge) the excess of ionized DEA units result in swelling while the charged and neutral MAA units hinder extensive swelling of the microgel. It is thus the interplay between swelling (due to ionization) and deswelling (due to charge neutralization and hydrophobic interactions) which determines the overall swelling of these mix microgel particles. This complex ionization behavior and the overall charge of the mix microgels as a function of solution pH will be investigated in a future study.

3.4 Core-shell microgel particles

Finally, we have also prepared two microgels of a core-shell topology with the core of the particle consisting of DEA or MAA units and shell comprising MAA or DEA moieties, respectively. The synthesis of the core-shell particles involved a two step polymerization

method: the core of the particles is formed in the first step while in the second step these core particles are used as the seeds for the formation of the shell. As already mentioned before, in both cases the MAA moieties were obtained by the acid hydrolysis of the protected *t*-BuMA monomer used for the microgel synthesis. The composition of the microgels from the monomer feed ratio was 56 mole % *t*-BuMA and 44 mole % DEA.

3.4.1 Core PDEA-shell PMAA microgel

The growth of the core-shell particles was followed by DLS. A sample of the microgel core was extracted from the reaction flask, after the completion of the first step, and was measured by DLS. Its size was compared to that of the final core-shell particles after the second step of the synthesis. **Figure 3.15a** shows the autocorrelation functions for the PDEA core and the core PDEA-shell P(*t*-BuMA) microgel particles at c=0.005 wt % and 60° scattering angle. The wavevector dependence of the rates of the processes are shown in **Figure 3.15b**.

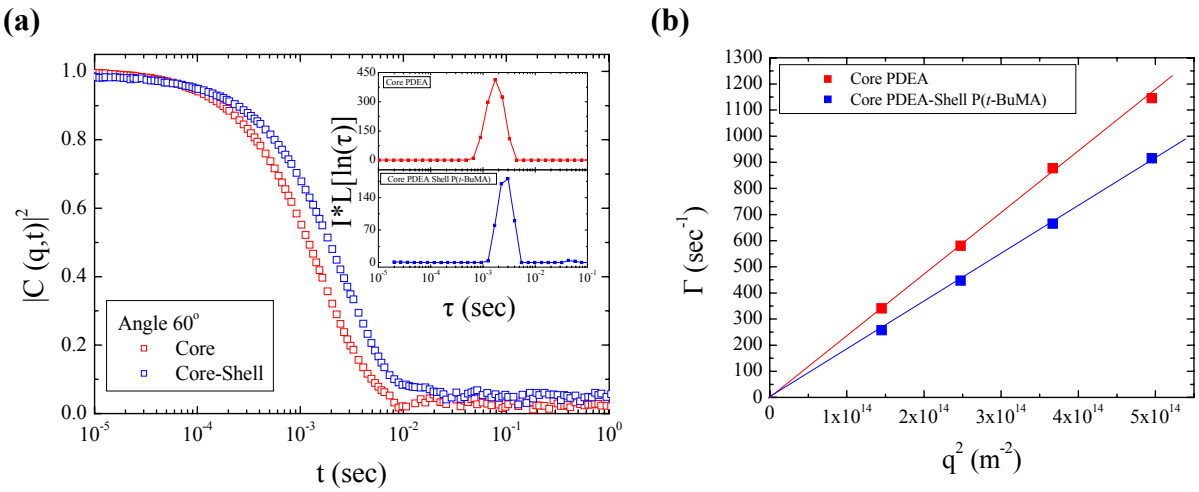

Figure 3.15: Intensity autocorrelation functions of the PDEA core and core PDEA-shell P(*t*-BuMA) microgels at c=0.005 wt % and 60° scattering angle (a). Inset: distribution of relaxation times multiplied by the total scattering intensity (normalized to that of toluene). Wavevector dependence of the rates of the processes for the PDEA core and the core PDEA-shell P(*t*-BuMA) microgels (b).

A single process with diffusive dynamics dominates the autocorrelation functions for both the core and the core-shell microgel particles. The diffusion coefficient of the process for the core particle sample was found D=2.43x10^{-8} cm^2/sec (**Figure 3.15** red symbols)

corresponding to a hydrodynamic radius, R_h = 90 nm which is attributed to the hydrophobic PDEA latex particles. Similarly, the diffusivity of the process for the core-shell particles was D=1.82x10^{-8} cm^2/sec (**Figure 3.15** blue symbols) corresponding to a hydrodynamic radius, R_h = 120 nm. The increase in hydrodynamic size from 90 nm for the core particles to 120 nm for the core-shell microgel suggests the successful synthesis of the core-shell structure. We have also calculated the expected increase in size for a 90 nm sphere upon addition of the shell using the monomer volume ratio in the feed and assuming full conversion. A radius R = 114 nm was calculated for the core-shell particles which is in good agreement with the 120 nm radius found by DLS. Of course, one should be careful when comparing geometrically calculated sizes with hydrodynamic radii obtained by DLS. The aim of our calculation is only to exclude the possibility of the formation of microgel particles incorporating two or more core particles, upon the formation of the shell, which would result in much larger entities found by DLS compared to those expected by the monomer volume ratio in the feed.

After acid hydrolysis of the ester groups, the core PDEA-shell PMAA microgels were formed and the aqueous solution behaviour of the particles was investigated as a function of the solution pH by potentiometric titrations at a microgel concentration c=0.2 wt %, while their swelling behaviour was studied by DLS at c=0.005 wt %. **Figure 3.16** illustrates the potentiometric titration curve for the core PDEA-shell PMAA microgel.

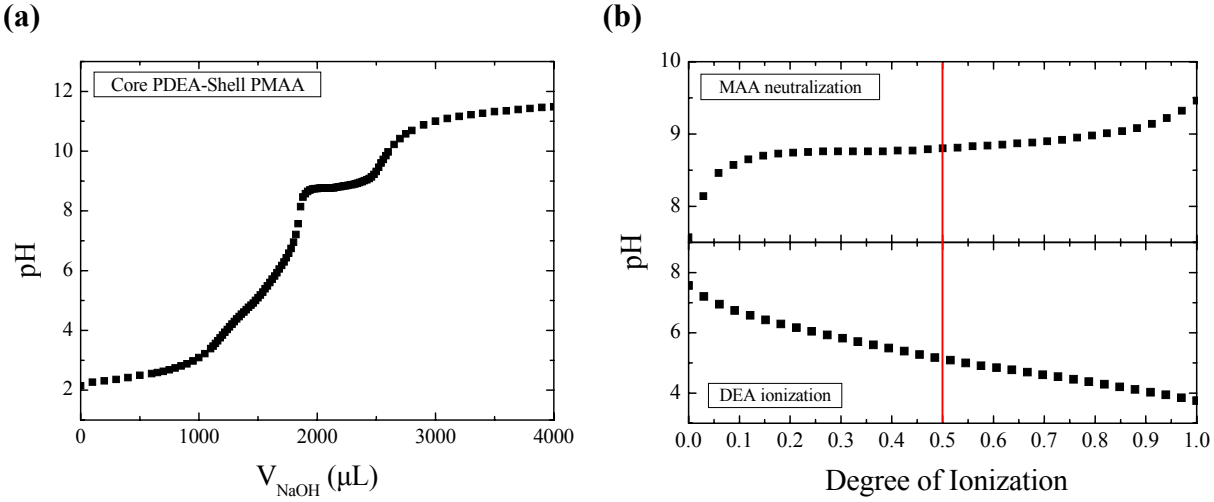

Figure 3.16: Potentiometric titration curve for the core PDEA-shell PMAA microgel with 1 wt % cross-linker (a) and the plateau regions for the PMAA neutralization (top) and the PDEA ionization (bottom) plotted as the pH versus the effective degree of ionization (b).

It is interesting to note that two plateau regions are observed in the titration curve of the core-shell microgels. The first plateau, at pH ~ 5 is less sharp and is attributed to the ionization of the tertiary amine moieties in the core of the microgel while the second plateau, at pH ~ 9, is more sharp and is due to the neutralization of the methacrylic acid groups in the microgel shell. This result is in contrast to the mix PDEA-PMAA microgel particles for which a single plateau region was obtained suggesting the simultaneous ionization of the basic and acidic groups. In the core-shell particles the two types of ionizable groups are spatially separated leading to their independent ionization at a different pH range. This is a very interesting feature, which in a first instance can be used to distinguish the mix and core-shell particles, while on the other hand, it suggests the formation of core-shell particles with novel attractive solution properties. Thus, from the discussion above we can conclude that at the point of maximum deflection in the titration curve, pH ~ 7.6, the particles are uncharged comprising a hydrophobic PDEA core and a neutral PMAA shell. Below this pH value the DEA groups in the core become protonated and thus positively charged, with the MAA groups in the shell being protonated and neutral. Above pH 7.6 the MAA groups in the shell become neutralized and negatively charged, while the PDEA core is deprotonated and hydrophobic. From the two plateau regions, the two effective pK_α values for the PMAA shell and the PDEA core were calculated as the pH at 50% ionization (**Figure 3.16b**) A pK_α = 8.8 was found for the MAA units (**Figure 3.16b**(top)) and a pK_α = 5.3 for the DEA moieties (**Figure 3.16b**(bottom)). The difference of these pK_α values from those for the two respective homopolymer microgels, pK_α = 5.9 for PDEA and pK_α = 7.2 for PMAA, suggests the hindering of the ionization of both the DEA and MAA groups in the core-shell particles. Although, this is understood for the DEA units located in the core of the microgel it remains unclear for the ionization of the MAA groups in the microgel shell since the latter are more accessible to the added base. Finally from the relative width of the two plateau regions the composition of the microgel was calculated, as the moles of DEA over the moles of MAA. The experimentally determined composition was found 49 mole % DEA which is in good agreement with the theoretical composition calculated from the monomer feed ratio (43 mole % DEA).

Next, the swelling behavior of the core-shell particles as a function of the solution pH and thus the ionization of the basic and acidic moieties was studied by DLS. **Figure 3.17** shows the hydrodynamic radii of the core PDEA-shell PMAA microgel as a function of the

microgel net charge. In the second Y-axis the measured solution pH as a function of the microgel net charge is also plotted for a direct comparison with **Figure 3.16b**.

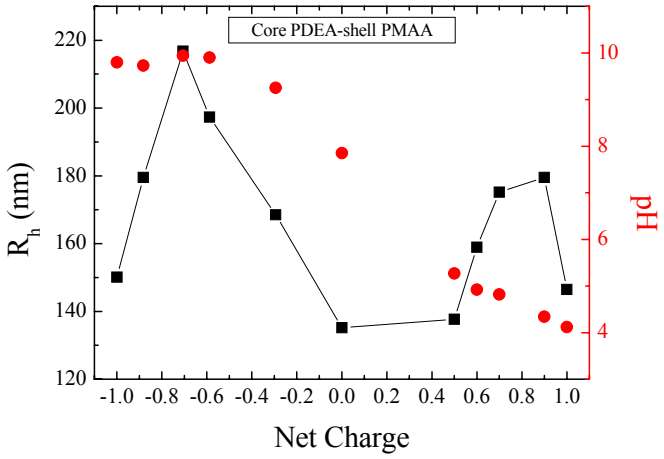

Figure 3.17: Hydrodynamic radii of the core PDEA-shell PMAA microgel and solution pH as a function of the microgel net charge.

The left part of the plot (negative x values) corresponds to the ionization of the MAA units at high pH values (above the pH of maximum deflection) and thus to a negative net charge, while the right part (positive x values) represents the protonation of the DEA units at low pH (below the pH of maximum deflection) and thus corresponds to a positive net charge. The point at pH 7.85 is very close to the pH at maximum deflection and thus corresponds to a microgel charge equal to zero because neither the DEA nor the MAA moieties are charged, as discussed above. As seen in **Figure 3.17** the microgels swell at both high and low pH when the particle net charge is different than zero and thus either the shell or the core of the microgel is swollen, while they exhibit a minimum size at zero charge when both the core and the shell are neutral and collapsed. It should be noted that the driving force for the collapse of the particles at zero net charge is different for the mix and the core-shell particles. Thus, in the mix particles, discussed above, the collapse occurred at the isoelectric point when there were an equal number of positive and negative charges within the particle, while in the core-shell particles the collapse occurs when there is no charge in the shell or the core of the microgel. In the first case we thus have electrostatic interactions between the monomer groups which are expected to depend on the ionic strength of the solution, while in the latter case we have neutral particles which would not be influenced by the presence of salt.

From the minimum size at zero net charge we can calculate the swelling of the particles induced by the hydrolysis of the hydrophobic *t*-BuMA groups. A volumetric

swelling factor of 1.73 was found for the shell of the particles corresponding to a 73 % increase in its volume.

From the maximum hydrodynamic radii obtained at the negative and positive net charge regions and the hydrodynamic radius at zero net charge we have calculated the volumetric swelling factor of the shell and the core of the microgels upon ionization, respectively. These factors were found to be 5.5 for the PDEA core and 5.4 for the PMAA shell. The volumetric swelling factor of the PDEA core is in good agreement to that found for the homopolymer microgel (5.8 for the PDEA homopolymer microgel), suggesting that the swelling of the PDEA cores is not affected by the core-shell topology. On the other hand, the volumetric swelling factor of the PMAA shell is significantly lower than that found for the respective homopolymer microgel (13.4 for the PMAA homopolymer microgel) and suggests that the swelling of the shell of the microgel is hindered in the core-shell topology.

It is interesting to note that although the PDEA core is restricted in the interior of the microgel and thus, one would expect that it cannot swell extensively in the presence of the collapsed shell, it obtains a similar volumetric swelling factor to that found for the homopolymer PDEA microgel. This result suggests that the PDEA swelling is not affected by the neutral PMAA shell possibly because the latter possesses sufficient softness to accommodate the extension required for the unhindered swelling of the core. On the other hand, the swelling of the PMAA shell is hindered by the presence of the hydrophobic PDEA core. The reason for this latter result is believed to be the binding of the swollen shell on the collapsed microgel core. PMAA becomes ionized and thus swells at high pH, however its swelling is restricted by its covalent binding to the hydrophobic PDEA core. This effect has been reported earlier in the literature by Crassous et. al.[8] In this case non-uniform swelling in the inner and the outer part of the shell is expected and this will be investigated in a future study.

3.4.2 Core PMAA-shell PDEA microgel

Next, we prepared microgel particles with a reverse core-shell topology comprising a PMAA core and a PDEA shell. The core of the particles was formed by the emulsion polymerization of *t*-BuMA in the presence of AOT as the stabilizer. SDS was replaced by AOT in this synthesis because it was a more effective stabilizer giving homogeneous, stable emulsions. In our initial experiments we have thus optimized the concentration of AOT in the solution in order to prepare stable core particles with size which would not be significantly different to that obtained for the PDEA core in the core PDEA-shell PMAA microgels.

Figure 3.18 illustrates the dependence of the hydrodynamic radius of the P(*t*-BuMA) core particles on the concentration of AOT stabilizer used in the synthesis.

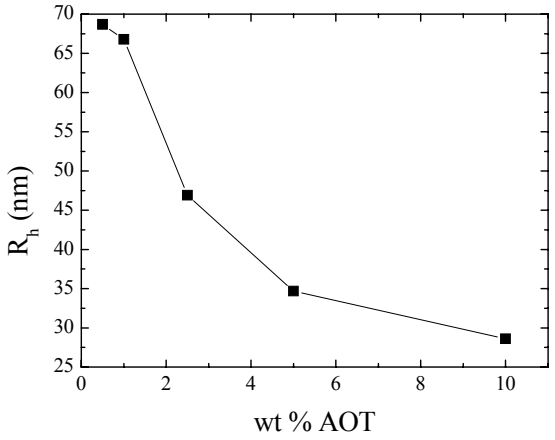

Figure 3.18: Hydrodynamic radii of the P(*t*-BuMA) core particles as a function of the concentration of AOT stabilizer (based on the monomer).

The size of the core particles increased as the concentration of the stabilizer decreases, as expected. For the synthesis of our core-shell particles we chose a 1 wt % AOT which gave core particles with a radius R_h = 67 nm and good colloidal stability. The monomer feed ratio was kept constant, 56 mole % *t*-BuMA and 44 mole % DEA, as for the core PDEA-shell P(*t*-BuMA) microgels. As described above, we followed the synthesis of the core-shell particles by DLS. **Figure 3.19a** shows the autocorrelation functions for the P(*t*-BuMA) core and the core P(*t*-BuMA)-shell PDEA microgel particles at c=0.005 wt % and 90^o scattering angle. The wavevector dependence of the rates of the processes are shown in **Figure 3.19b**.

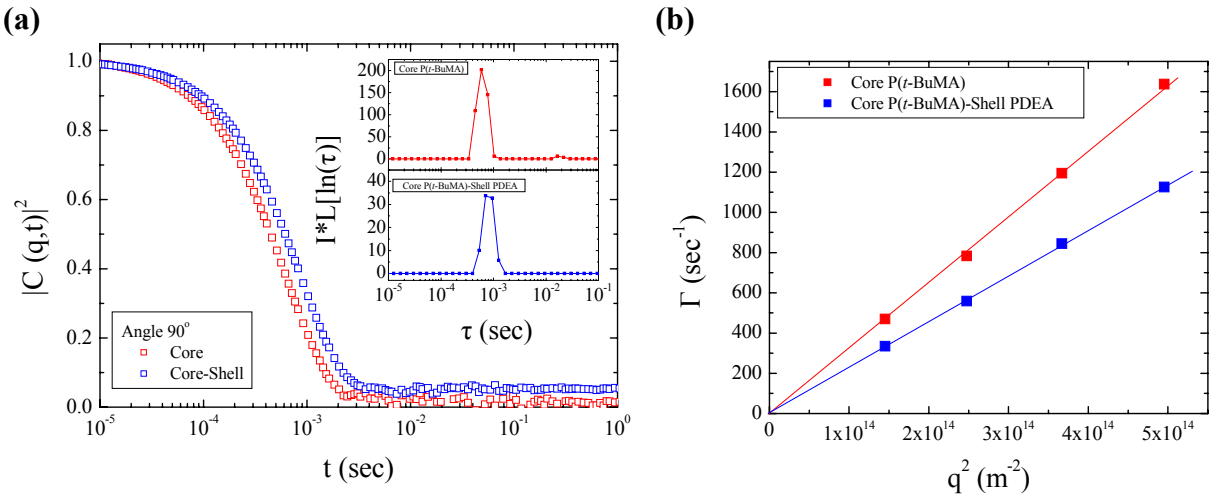

Figure 3.19: Intensity autocorrelation functions of 0.005 wt % P(*t*-BuMA) core and core P(*t*-BuMA) shell PDEA microgels at 90° scattering angle (a). Inset: distribution of relaxation times multiplied by the total scattering intensity (normalized to that of toluene). Wavevector dependence of the rates of the processes for the P(*t*-BuMA) core and the core P(*t*-BuMA) shell PDEA microgels (b).

A single process with diffusive dynamics dominates the autocorrelation functions for both the core and the core-shell microgel particles. The diffusion coefficient of the process for the core sample was found $D=3.28\times10^{-8}$ cm^2/sec (**Figure 3.19** red symbols) corresponding to a hydrodynamic radius, R_h = 67 nm which is attributed to the hydrophobic P(*t*-BuMA) latex particles. Similarly, the diffusivity for the core-shell particles was $D=2.38\times10^{-8}$ cm^2/sec (**Figure 3.19** blue symbols) corresponding to a hydrodynamic radius, R_h = 92 nm. As discussed above, the increase in the hydrodynamic size after the formation of the shell suggests the successful synthesis of the core-shell structures. The theoretically calculated increase in size for a 67 nm sphere based on the monomer feed ratio was found 85 nm for the core-shell particles which is in good agreement with the 92 nm hydrodynamic size found by DLS and verifies the incorporation of a single core in each core-shell particle.

Following acid hydrolysis of the ester groups, the core PMAA-shell PDEA microgels were formed and the aqueous solution behaviour of the particles was investigated as a function of the solution pH by potentiometric titrations at a microgel concentration c=0.2 wt % while their swelling behaviour was studied by DLS at c=0.005 wt %. **Figure 3.20** illustrates the potentiometric titration curve for the core PMAA-shell PDEA microgel prepared using 1 wt % EGDMA.

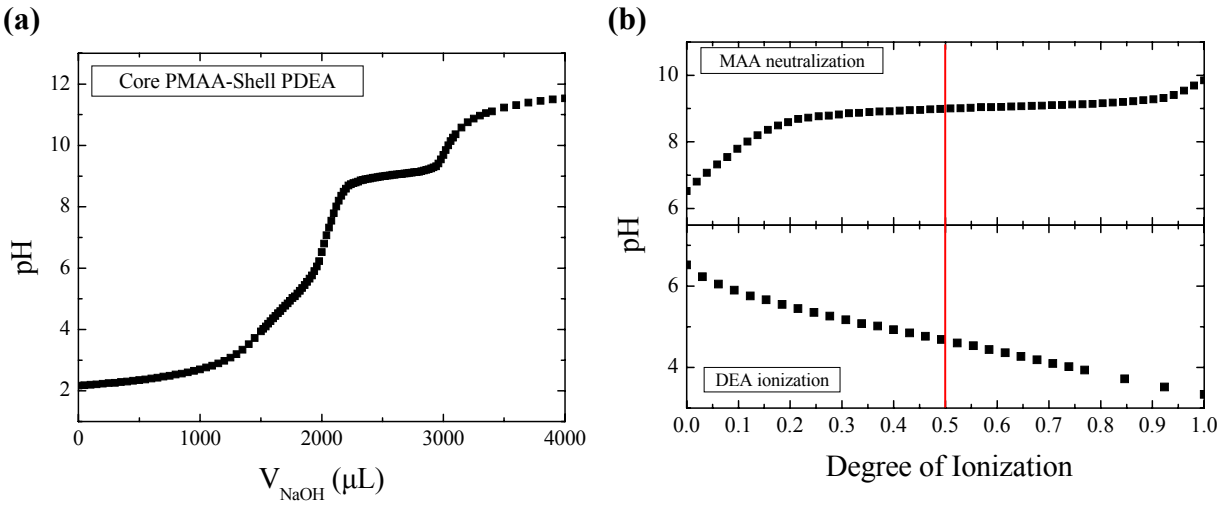

Figure 3.20: Potentiometric titration curve for the core PMAA-shell PDEA microgel with 1 wt % cross-linker (a) and the plateau regions for the PMAA neutralization (top) and the PDEA ionization (bottom) plotted as the pH versus the effective degree of ionization (b).

Two plateau regions are again observed in the titration curve of the core-shell microgels, similar to the core PDEA-shell PMAA microgel particles. The first less sharp plateau, at pH ~ 5, corresponds to the ionization of the tertiary amine moieties in the shell of the microgel, while the second sharp plateau, at pH ~ 9 corresponds to the neutralization of the methacrylic acid groups in the microgel core. This is consistent with the discussion above where the ionization of the basic and acidic units in the core-shell particles was found to be independent in contrast to the common ionization region observed for the mix microgel particles. Thus, again here at the point of maximum deflection in the titration curve, pH ~ 7.6, the MAA units are protonated and the DEA groups deprotonated and the particles are uncharged. Below this pH value and in the pH range 3-7 the DEA groups in the shell are protonated and the shell swells, while above this pH value and in the pH range 6-10 the MAA groups in the microgel core become neutralized and the core of the microgel swells. The effective pK_α values for the core and the shell of the microgel particles were calculated from the two plateau regions as the pH at 50% ionization. A pK_α = 9.0 was found (**Figure 3.2b**(top)) for the PMAA core and a pK_α = 4.7 (**Figure 3.20b**(bottom)) for the PDEA shell. These values are similar to those found for the core PDEA-shell PMAA microgel particles and different from the respective homopolymer microgels, which suggests that the ionization of both the core and the shell of the microgel is hindered in the core-shell structures. The small differences of the pK_α values found for the two core-shell microgels are consistent with

the special location of the ionizable units in the core and the shell of the particles and thus being less and more accessible to the added base respectively. Finally from the relative width of the two plateau regions the composition of the microgel was calculated, as the moles of DEA over the moles of MAA. The experimentally determined composition was found 39 mole % DEA which is in good agreement with the theoretical composition calculated from the monomer feed ratio used in the feed (43 mole % DEA).

The size of the core-shell microgels was investigated as a function of the ionization of the DEA and MAA units by DLS. **Figure 3.21** shows the hydrodynamic radii of the microgels and the respective solution pH as a function of the microgel net charge.

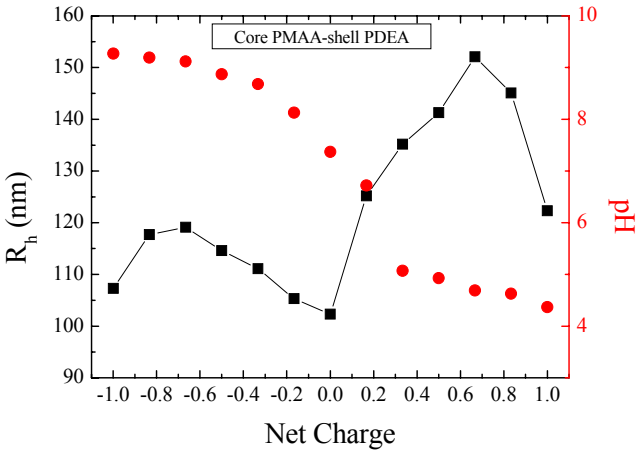

Figure 3.21: Hydrodynamic radii of the core PMAA-shell PDEA microgel and solution pH as a function of the microgel net charge.

Similar to the core PDEA-shell PMAA microgels the left part of the plot corresponds to the ionization of the MAA units at high pH values (above the pH of maximum deflection) and thus to a negatively charged core, while the right part represents the protonation of the DEA units at low pH (below the pH of maximum deflection) and thus a positively charged shell. The point at pH 7.42 corresponds to net charge zero where neither the DEA nor the MAA moieties are charged (**Figure 3.20a**). As seen in **Figure 3.21** the microgels swell at both high and low pH when the particle net charge is different than zero while they exhibit a minimum size at zero net charge as discussed above for the reverse core-shell particles. Again the minimum size for the core shell microgel is due to the electroneutrality of both the core and the shell of the particles, and not an isoelectric point as in the case of the mix microgels.

From the minimum size at zero net charge we can calculate the swelling of the particles induced by the hydrolysis of the hydrophobic *t*-BuMA groups. A volumetric

swelling factor of 1.52 was found for the core of the particles corresponding to a 52 % increase in its volume.

From the maximum hydrodynamic radii obtained at the negative and positive net charges and the hydrodynamic radius at zero net charge we have calculated the volumetric swelling factor of the core and the shell of the microgels, respectively. These factors were found to be 2.4 for the PMAA core and 5.1 for the PDEA shell. The value of the volumetric swelling factor of the PDEA shell is in good agreement to that found for the homopolymer and for the PDEA core in the core PDEA-shell PMAA microgels (5.8 for PDEA homopolymer microgel and 5.5 for the PDEA core in the core PDEA-shell PMAA microgel, respectively) suggesting that PDEA exhibits similar volumetric swelling factors and is not affected by the core-shell topology, as discussed above. On the other hand, the volumetric swelling factor of the PMAA core is significantly lower than that found for the respective homopolymer microgel and even the PMAA shell in the core PDEA-shell PMAA microgel (13.4 for PMAA homopolymer microgel and 5.4 for the PMAA shell in the core PDEA-shell PMAA microgel) and suggests that the swelling of the core of the microgel is hindered in the core-shell topology. Thus, although PMAA becomes ionized and swells at high pH it is restricted in the core of the microgel and thus cannot swell extensively in the presence of the collapsed hydrophobic PDEA shell. It is worth noting that the PMAA swelling is even lower when the acidic groups are located in the core of the microgel compared to its hindered swelling when being in the shell of the particles.

Overall, we have found that the swelling of PDEA is not significantly affected by PMAA either when located in the core or the shell of the microgels and this was attributed to the hydrophylicity of PMAA which allows its deformation and extension upon swelling of the PDEA. On the other hand, the hydrophobic PDEA domains hinder the swelling of PMAA when located either in the core or the shell of the particles and this was attributed to the more rigid character of the bulk PDEA. The hard PDEA domain hinders the swelling of the PMAA shell bound onto the hydrophobic core but is even more effective when surrounding the PMAA core in the form of a hydrophobic shell, as expected. These materials are expected to exhibit interesting rheological properties.

3.5 SEM characterization of the microgel particles

3.5.1 PDEA and PMAA homopolymer microgel particles

The morphology of the microgel particles was investigated by SEM. **Figure 3.22** shows SEM images of the PDEA microgel particles prepared at different cross-link densities, 0.5, 1, 2 and 3 wt % EGDMA, at degree of ionization equal to zero.

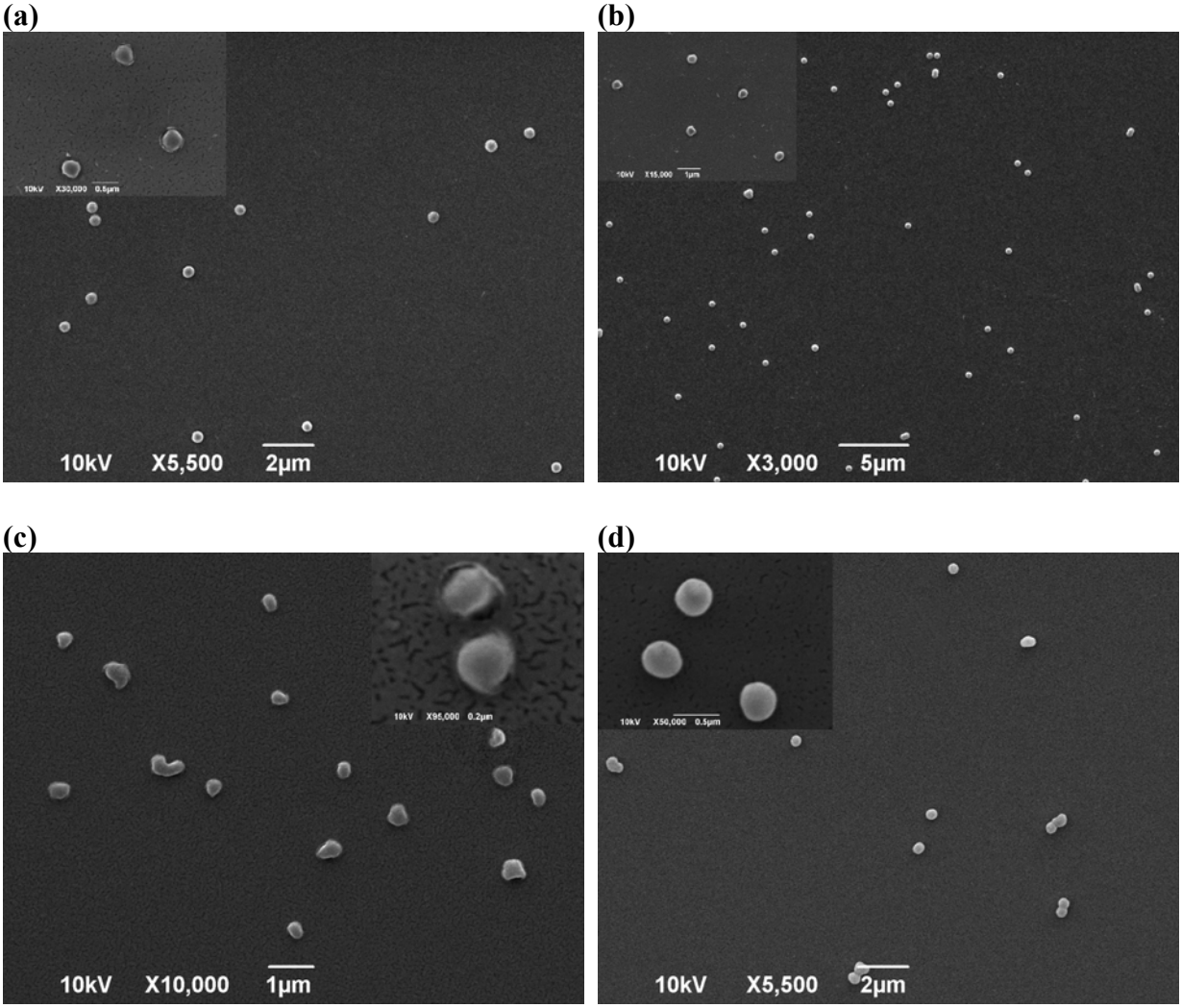

Figure 3.22: SEM images of the PDEA microgel particles with 0.5 wt % EGDMA (a), 1 wt % EGDMA (b), 2 wt % EGDMA (c) and 3 wt % EGDMA (d) at degree of ionization equal to zero.

From the SEM images we observe particles of a spherical shape with a diameter: D=413 ± 28 nm for the microgels with 0.5 wt % EGDMA (**Figure 3.22a**), D=413 ± 6 nm for the microgels with 1 wt % EGDMA (**Figure 3.22b**), D=388 ± 70 nm for the microgels with 2 wt % EGDMA (**Figure 3.22c**) and D=428 ± 24 nm for the microgels with 3 wt % EGDMA (**Figure 3.22d**). The size of the microgel particles with 1 wt % EGDMA is in good agreement

to that found by TEM (D = 383 nm), and is discussed below and verifies the formation of uniform spherical PDEA microgel particles. The slight deformation of the particle shape and their coalescence (**Figure 3.22c**) is attributed to the low T_g of PDEA which results in particle flattening and film forming formation.

(a) **(b)**

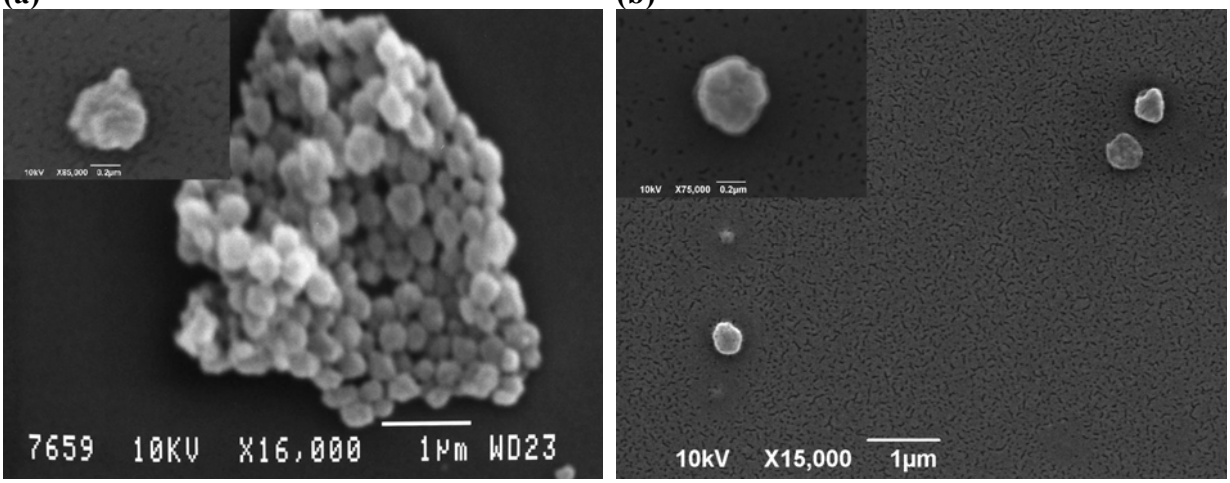

Figure 3.23: SEM images of the P(*t*-BuMA) microgel particles with 1 wt % EGDMA before deprotection (a) and the PMAA microgel particles after acid hydrolysis of the ester groups at degree of ionization equal to zero (b).

Figure 3.23a shows a SEM image of the P(*t*-BuMA) microgel particles before deprotection. Particles of a spherical shape with a diameter of 340 ± 34 nm which is in good agreement with the DLS results (D_h = 354 nm) are obtained. After deprotection (**Figure 3.23b**) the PMAA microgel particles have a diameter of 427 ± 54 nm which is consistent with the increase in size found DLS.

3.5.2 Mix PDEA-PMAA microgel particles

Figure 3.24 shows the SEM images for the hydrophobic mix microgel particles before deprotection (mix PDEA-P(*t*-BuMA)) and the polyampholyte PDEA-PMAA microgel particles, after hydrolysis of the ester groups.

From the SEM images before deprotection (**Figure 3.24a**) we observe particles of a spherical shape with a diameter D=340 ± 13 nm which is in good agreement with the DLS results (D_h = 360 nm), while after the deprotection (**Figure 3.24b**) the particles maintain their spherical shape and very narrow size distribution and their diameter is 347 ± 27 nm which agrees with the DLS results (D_h = 370 nm). It should be noted that the mix microgel particles are particularly uniform in size and retain their uniformity even after deprotection thus giving

well-defined polyampholyte microgels. The slightly deformation of the shape of the particles is attributed to the soft nature of PMAA.

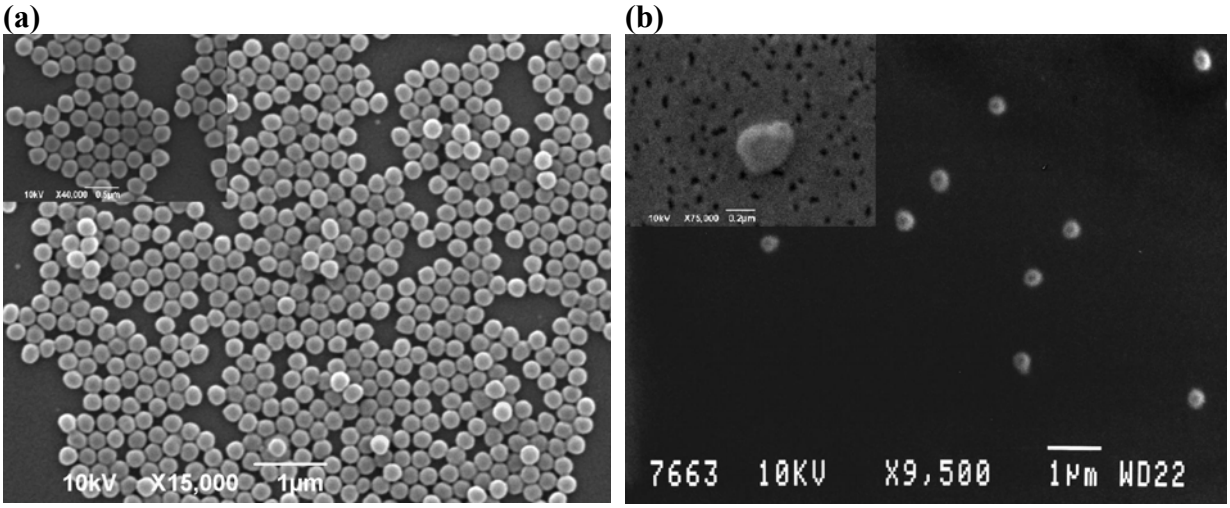

Figure 3.24: SEM images of the mix PDEA-P(*t*-BuMA) latex particles (a) and the mix PDEA-PMAA microgel particles after deprotection at degree of ionization equal to zero (b).

3.5.3 Core-shell microgel particles

Finally, we investigated the morphology of the core-shell microgel particles by SEM. **Figure 3.25** shows the SEM images for the core P(*t*-BuMA)-shell PDEA microgel particles before deprotection and the same sample after hydrolysis which gave core PMAA-shell PDEA microgel particles.

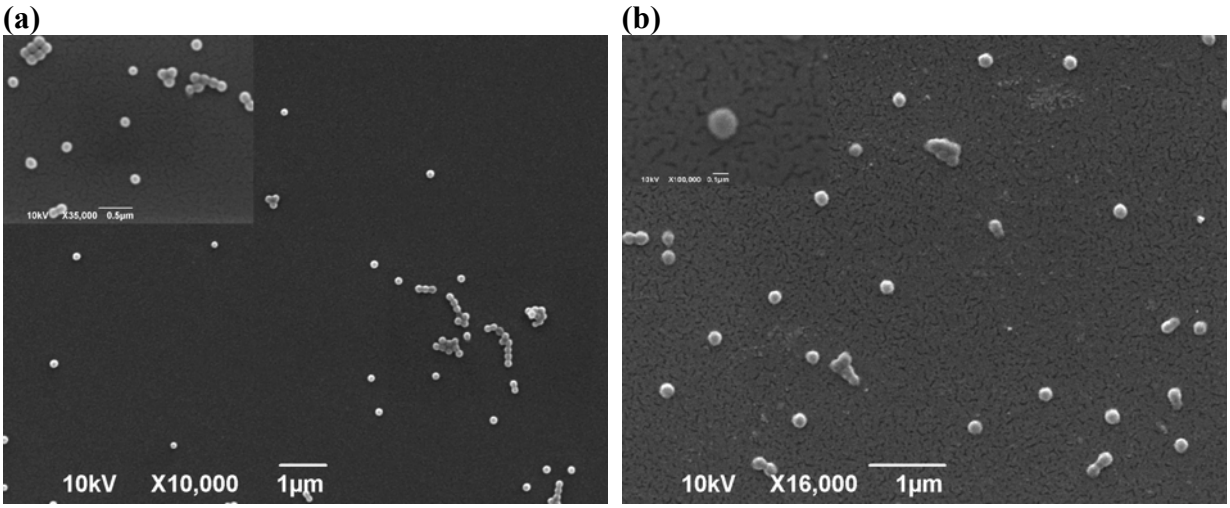

Figure 3.25: SEM images of the core P(*t*-BuMA)-shell PDEA latex particles (a) and the core PMAA-shell PDEA microgel particles, after deprotection at degree of ionization equal to zero (b).

From the SEM images before deprotection (**Figure 3.25a**) we observe particles of a spherical shape and a uniform size distribution with a diameter D=170 ± 10 nm which is very in good agreement with the DLS and TEM results discussed below (D_h = 184 nm and D_{TEM} = 200 nm). After deprotection (**Figure 3.25b**) the particles maintain their spherical shape and narrow size distribution and their diameter is 177 ± 18 nm which agrees well with the DLS results (D_h = 204). The minimal particle coalescent observed in the images is attributed to the soft nature of the PDEA shell and its film forming properties, as discussed above.

3.6 TEM characterization of the microgel particles

3.6.1 PDEA and PMAA homopolymer microgel particles

The shape and the size of the microgel particles were also investigated by TEM. **Figure 3.26** shows TEM images for the homopolymer PDEA microgel particles with 1 wt % EGDMA, stained with potassium hexachloroplatinate (K_2PtCl_6) (**Figure 3.26a)** and the PMAA microgel particles with 1 wt % EGDMA stained with iron(II) chloride ($FeCl_2$) (**Figure 3.26b**). The metal species incorporated within the ionized microgels (α=1) at a monomer / metal = 2 / 1 molar ratio, cause their collapse[9] and provide the necessary contrast for the TEM imaging.

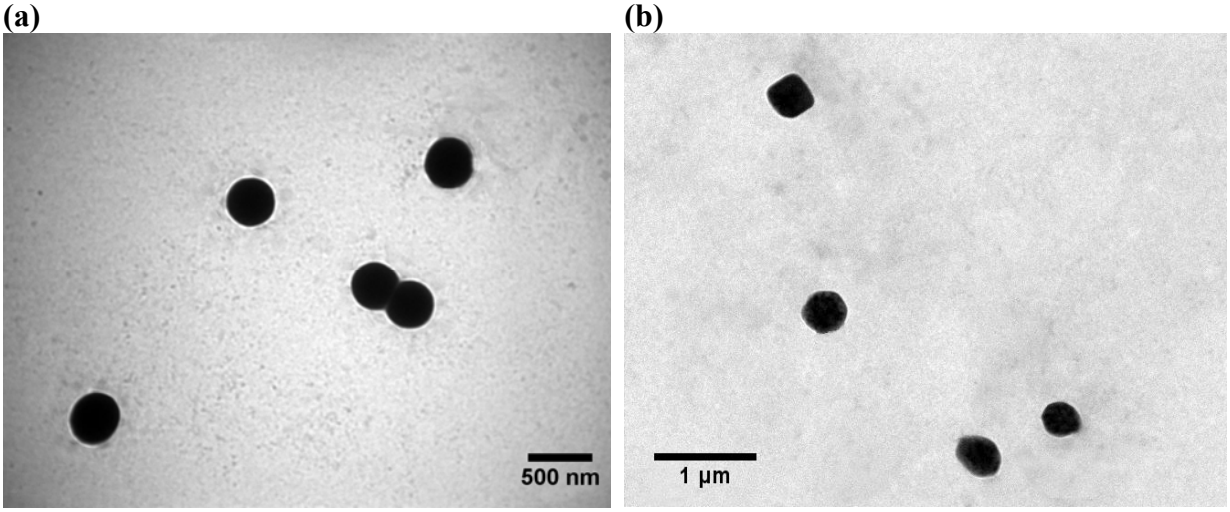

Figure 3.26: TEM images of the PDEA (a) and PMAA (b) microgel particles stained with potassium hexachloplatinate and iron(II) chloride, respectively.

The PDEA microgel particles are spherical in shape with a mean TEM diameter of 383 ± 7 nm and have a very narrow size distribution as seen in **Figure 3.26a**. The diameter calculated by TEM is smaller than that found by DLS (D_h = 528 nm for α = 0). This

difference is attributed to the fact that dynamic light scattering estimates a hydrodynamic size of the microgel in solution while TEM deals with the dried sample. The former technique reports a hydrodynamic diameter that includes the thickness of the stabilizing layer and possible hydrodynamic interactions between the particles and thus tends to oversize relative to electron microscopy. Moreover, particle coalescence is minimal and individual PDEA particles are observed by TEM despite the low T_g of PDEA.[10] This is attributed to the ionization and the subsequent metallation of the microgel particles which is expected to increase the T_g of the polymeric material and thus prevent particle flattening and film formation. On the other hand, the PMAA microgel particles are also spherical in shape and have a quite uniform size distribution as shown in **Figure 3.26b**. Their TEM diameter was calculated around 440 ± 20 nm which is in good agreement to that found by DLS (D_h = 400 nm at $\alpha = 0$).

3.6.2 Mix PDEA-PMAA microgel particles

Figure 3.27 shows TEM images for the mix PDEA-PMAA microgel particles stained with K_2PtCl_6 (**Figure 3.27a**) and cadmium nitrate ($Cd(NO_3)_2$) (**Figure 3.27b**), respectively. The successful staining of the microgels with both positively and negatively charged metal containing species verifies the presence of both the DEA and MAA moieties within the microgel. The metal species were incorporated at a monomer / metal = 2 / 1 mole ratio, within the ionized microgels at low and high pH at which the positively charged DEA units interacted with the negatively charged $PtCl_6^{2-}$ anion and the negatively charged MAA units with the positive Cd^{2+} cations, respectively.

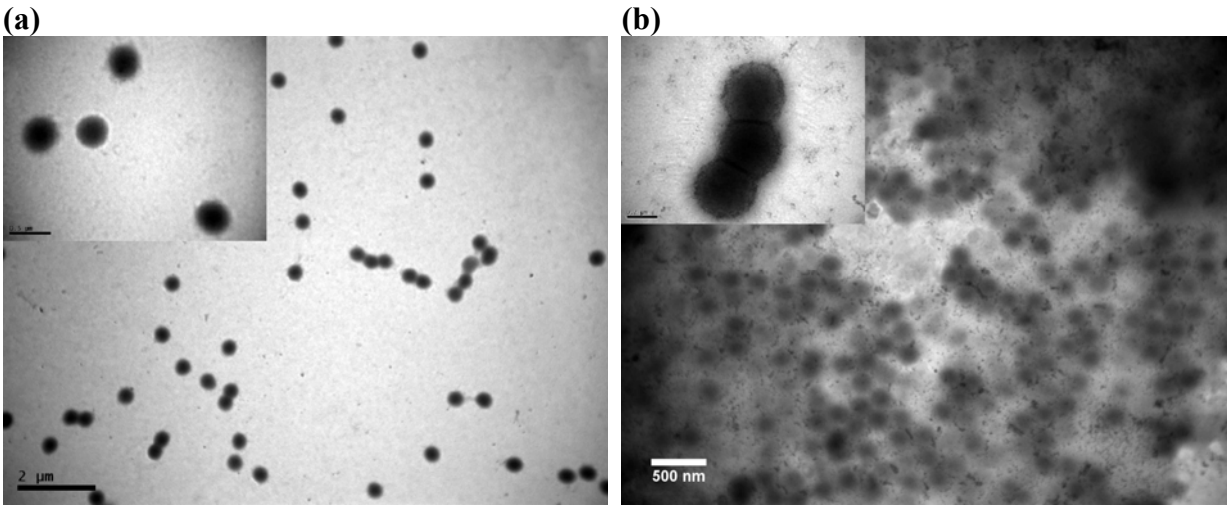

Figure 3.27: TEM images of the mix PDEA-PMAA microgel particles stained with potassium hexachloroplatinate (a) and cadmium nitrate (b).

In both images the mix PDEA-PMAA microgel particles are spherical in shape with a mean TEM diameter of 380 ± 20 nm and have a very narrow size distribution. The diameter calculated by TEM is in good agreement with that found by DLS (D_h = 370 nm at a microgel net charge equal to zero).

3.6.3 Core-shell microgel particles

Next, the core-shell particles were characterized by TEM before and after deprotection of the *t*-BuMA units to MAA. **Figure 3.28** shows the core P(*t*-BuMA)-shell PDEA microgel particles before deprotection stained with K_2PtCl_6 which selectively stains the PDEA shell of the microgel. The metal species were incorporated at a monomer / metal = 2 / 1 mole ratio at low pH (α_{DEA} = 1).

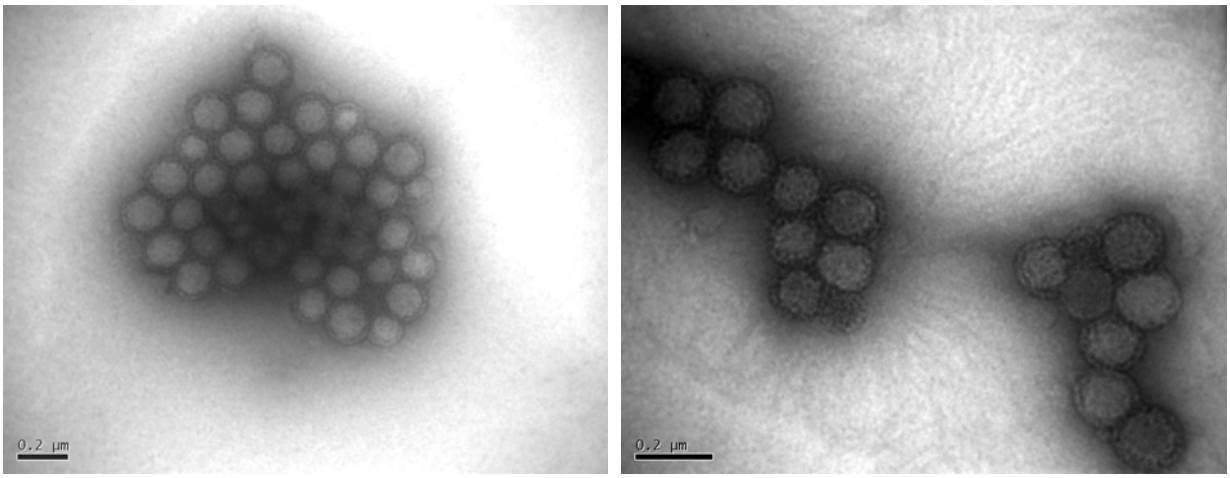

Figure 3.28: TEM images of the core P(*t*-BuMA)-shell PDEA microgel particles stained with potassium hexachloroplatinate.

The TEM images verify the core-shell topology of the microgel particles. Spherical particles with a lighter color core attributed to the P(*t*-BuMA) which in not stained and a dark ring, due to the stained PDEA shell are clearly observed in **Figure 3.28**. A mean TEM diameter of 120 ± 11 nm for the P(*t*-BuMA) core and a total diameter of 175 ± 15 nm are measured and are in good agreement with the respective values found by DLS ($D_{h,core}$= 134 nm and $D_{h,core\text{-}shell}$ = 184 nm).

Moreover, the microgel particles after deprotection were also investigated by TEM. **Figure 3.29** shows TEM images of the core PMAA-shell PDEA microgel particles stained with cadmium nitrate ($Cd(NO_3)_2$) (**Figure 3.29a**) and potassium hexachloroplatinate (K_2PtCl_6) (**Figure 3.29b**). The metal species were incorporated within the ionized microgels

at a monomer / metal = 2 / 1 mole ratio, and provided the necessary contrast for the TEM imaging.

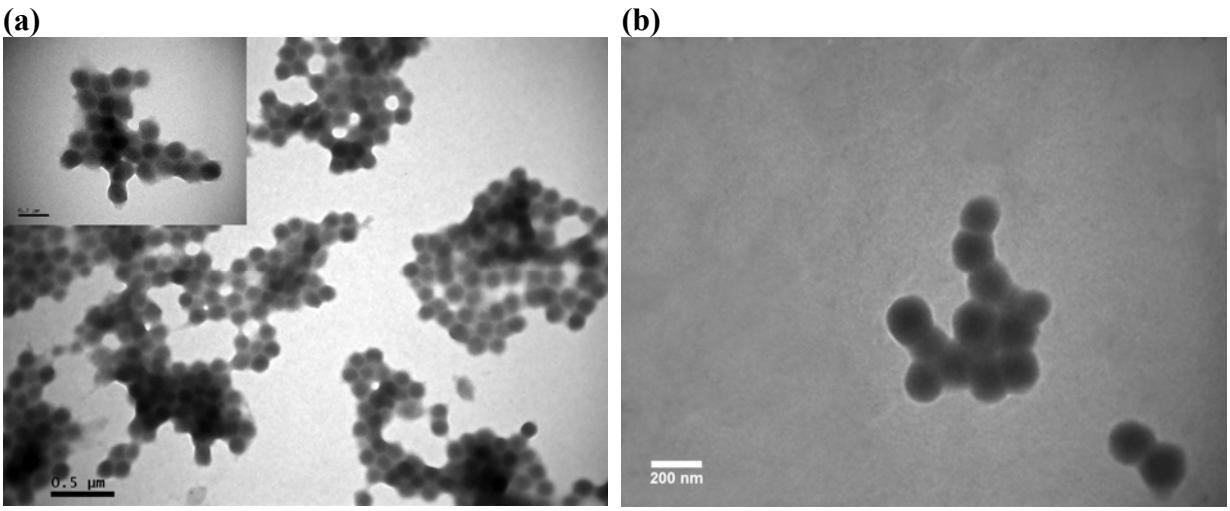

Figure 3.29: TEM images of the core PMAA-shell PDEA microgel particles stained with cadmium nitrate (a) and potassium hexachloroplatinate (b).

The successful staining of the particles with both $PtCl_6^{2-}$ and Cd^{2+} is an indirect indication of the presence of both basic and acidic residues within the microgel particles. In both images the core PMAA-shell PDEA microgel particles are spherical in shape with a mean TEM diameter of around 171 ± 15 nm and a very narrow size distribution. The diameter calculated by TEM is in good agreement to that found by DLS (D_h = 204 nm at a microgel net charge equal to zero). In **Figure 3.29a** where the core of the particle is stained we observe higher contrast due to the metal in the center of the particle and lighter colour shell which not stained. This result verifies that the core-shell topology is maintained after the deprotection of the *t*-BuMA units into MAA and that the deprotection does not affect the shell of the particles. In **Figure 3.29b** where the shell of the particle is stained we can not observe the core-shell topology, possibly due to metal diffusion in the hydrophilic PMAA core of the microgel.

Table 3.3 summarizes the characteristics of the microgels prepared for this study.

Table 3.3: Characteristics of the microgels prepared in this study.

Microgel	pK_{α} PDEA	pK_{α} PMAA	Iso electric point	R_h (before deprotection)	R_h (minimum)	R_h (maximum)		R_{SEM}	R_{TEM}
						Low pH	High pH		
5 wt% PDEA 0.5 wt% EGDMA	6.0	-	-	-	250 nm	535 nm	-	207 nm	-
5 wt% PDEA 1 wt% EGDMA	5.9	-	-	-	264 nm	440 nm	-	207 nm	192 nm
5 wt% PDEA 2 wt% EGDMA	5.5	-	-	-	238 nm	339 nm	-	195 nm	-
5 wt% PDEA 3 wt% EGDMA	4.9	-	-	-	229 nm	319 nm	-	215 nm	-
8.33 wt% PMAA	-	7.2	-	177 nm	200 nm	-	474 nm	170 nm	220 nm
Mix PDEA-PMAA	-	-	6.8	170 nm	185 nm	234 nm	330 nm	170 nm	190 nm
Core PDEA Shell PMAA	5.3	8.8	-	120 nm	135 nm	179 nm	216 nm	-	-
Core PMAA Shell PDEA	4.7	9.0	-	92 nm	102 nm	152 nm	119 nm	90 nm	90 nm

3.7 References

[1] Lee, S. A.; Gast, P. A.; Butun, V.; Armes, S. P. *Macromolecules* **1999**, *32*, 4302.

[2] Zhang, J.; Peppas, A. N. *Macromolecules* **2000**, *33*, 102.

[3] Dai, S.; Ravi, P.; Tam, K. C.; Mao, B. W.; Gan, L. H. *Langmuir* **2003**, *19*, 5175.

[4] Bradley, M.; Vincent, B.; Burnett, G. *Aust. J. Chem.* **2007**, *60*, 646.

[5] Fernadez-Nieves, A.; Fernadez-Barbero, A.; de la Nieves F. J. *Journal of Chemical Physics* **2001**, *115*, 7644.

[6] Seigel, R. A.; Firestone, B. A. *Macromolecules* **1988**, *21*, 3254.

[7] Philippova, O. E.; Hourdet, D.; Audebert, R.; Khokhlov, A. R. *Macromolecules* **1997**, *30*, 8278.

[8] Crassous, J. J.; Ballauff, M.; Drechsler, M.; Schmidt, J.; Talmon, Y. *Langmuir* **2006**, *22*, 2403.

[9] Palioura, D.; Armes, S. P.; Anastasiadis, S. H.; Vamvakaki, M. *Langmuir* **2007**, *23*, 5761.

[10] Amalvy, J. I.; Wanless, E. J.; Li, Y.; Michailidou, V.; Armes, S. P.; Duccini, Y. *Langmuir* **2004**, *20*, 8992.

Chapter 4

4.1 Conclusions

pH-responsive microgels particles have been synthesized by emulsion polymerization and their aqueous solution behavior was investigated by potentiometric titrations and DLS.

In the first part of our study, homopolymer microgel particles comprising basic or acid monomer units have been prepared. DEA was used as the basic monomer, while MAA was employed for the acidic microgels. Good control of the latex particle nucleation and growth was achieved which allowed the control of the microgel size by the monomer concentration in the feed. All homopolymer microgels were shown to swell as the degree of ionization of the monomer units increased, due to electrostatic repulsions and the osmotic pressure within the gel phase. It is interesting to note that the maximum degree of swelling was observed at degree of ionization 0.7, suggesting that at this ionization value the swelling due to ionization is counterbalanced by the ionic strength of the solution which causes the shrinkage of the microgels at high degrees of ionization. Furthermore, the influence of the microgel cross-link density on its ionization behaviour and its degree of swelling was investigated. The effective pK_α values determined by potentiometric titration curves were found to decrease as the cross-link density of the microgels increased, suggesting that the ionization of the monomer units is progressively hindered by the increase of the cross-link density of the microgel. This is attributed to the polyelectrolyte effect and the Donnan equilibrium which become more important as the cross-link density increases. On the other hand the volumetric swelling factor of the microgels was found to decrease as the cross-link density of the microgels increased, as expected. Anionic microgel particles based on PMAA were also prepared by acid hydrolysis of the protected ester groups of P(*t*-BuMA)-based microgels. The aqueous solution behaviour of the microgel particles

before and after hydrolysis was investigated as a function of solution pH by potentiometric titrations and DLS. Before deprotection the *t*-BuMA moieties are not affected by the changes in the solution pH and thus the titration curve is very similar to that obtained for water. However, after deprotection a plateau region observed in the titration curve of the microgel at around pH 7 signifies the presence of the methacrylic acid groups and verifies the successful deprotection of the ester groups and the formation of the PMAA microgel particles. The effective pK_α value for the acidic microgel particles was calculated from this plateau region to be 7.2. DLS also showed a 44 % increase of the initial volume of the particles after deprotection. This increase is attributed to the more hydrophilic nature of MAA, even in its neutral form, which causes the particle to swell. Upon ionization the PMAA microgels also swell similar to the PDEA microgels. The maximum volumetric swelling factor was calculated to be more than twice the value calculated for the respective PDEA particles. This is attributed to the more hydrophilic nature of the neutralized MAA units compared to that of the ionized DEA moieties. Scanning and Transmission Electron Microscopy studies verified the spherical shape and the uniform size distribution of the particles.

In the second part of our study mixed polyampholyte microgel particles comprising both DEA and MAA units randomly distributed within the particle were prepared. Potentiometric titrations were used to determine the ionization range of the microgels. One plateau region was found for the mixed microgel particles signifying the ionization of the basic and acidic moieties. The size of the mixed microgels particles was found to increase at both high and low pH when the particle net charge is negative or positive, respectively while collapsed microgel particles were found at the isoelectric point at zero net charge when the hydrophobic interactions dominate. Scanning and Transmission Electron Microscopy studies verified the spherical shape and the uniform size distribution of the particles.

Finally, we have also synthesized microgel particles with a core-shell topology comprising either a PDEA core and a PMAA shell or a PMAA core and a PDEA shell. Both particles were characterized by potentiometric titrations and DLS. The titration curves showed two plateau regions for the core-shell particles, one corresponding to the ionization of the DEA units and the second to the neutralization of the MAA moieties. This result is significantly different than the mix polyampholyte microgel particles discussed above which exhibit a common ionization region for the basic and acidic monomer units. The calculated effective pK_α values for the DEA and MAA

units were similar for the two microgels. A pK_α of 8.8 was found for PMAA when located in the shell of the microgel compared to the pK_α value of 9.0 for PMAA found in the core. Similarly PDEA exhibited pK_α values of 4.7 and 5.3 when located in the shell and the core of the microgels respectively. This difference is attributed to the hindered deprotonation of the DEA in the core of the particles relative to that in the shell but also to the possible less accurate pK_α determination for DEA due to its broad ionization region. The swelling properties of the core-shell microgel particles as a function of the solution pH were examined by DLS. The particles were found to swell at both high and low pH due to the ionization of either the core or the shell of the particle. Moreover, we have found that the hydrophilic PMAA does not influence the swelling of the PDEA domains while hydrophobic PDEA hinders significantly the swelling of PMAA in particular when the PMAA core is surrounded by a rigid hydrophobic PDEA shell. In the intermediate pH range the microgels are collapsed and exhibit a minimum in size because they are neutral comprising hydrophobic DEA units and protonated MAA moieties. SEM showed spherical particles of a narrow size distribution, while TEM verified their core-shell topology by selectively staining the core or the shell of the microgels.

The microgel particles discussed above carry both positively and negatively charged moieties. The hydrophilicity, the softness, the size and the charge of the particles can be tuned by simply adjusting the solution pH. Moreover, these properties can be tuned independently for the core and the shell of the particles in the sore-shell microgels, resulting in particles with a soft hydrophilic core and a hard shell or the opposite. Such tunable particles are very attractive colloidal systems and can find numerous applications in many different fields.

Future work will involve the detailed study of the overall charge, phase and rheological behavior of these microgel particles. Moreover, the interaction of the microgels with metal compounds and the formation of nanoparticles with optical, catalytic and magnetic properties, within the microgel particles, will be investigated.